Advancing Clinical Gait Analysis Through Technology and Policy

by
Junjay Tan
B.S., Mechanical Engineering and B.A., Plan II Liberal Arts
The University of Texas at Austin, 2006

Submitted to the Engineering Systems Division and the Department of Mechanical Engineering
in Partial Fulfillment of the Requirements for the Degrees of

MASTER OF SCIENCE IN TECHNOLOGY AND POLICY and
MASTER OF SCIENCE IN MECHANICAL ENGINEERING

at the
MASSACHUSETTS INSTITUTE OF TECHNOLOGY

June 2009

Signature of Author: ______________________________
Engineering Systems Division and Dept. of Mechanical Engineering
April 20, 2009

Certified by: ______________________________
Dava J. Newman
Professor of Aeronautics and Astronautics and Engineering Systems
Thesis Supervisor

Certified by: ______________________________
C. Forbes Dewey, Jr.
Professor of Mechanical Engineering and Biological Engineering
Thesis Reader

Accepted by: ______________________________
Dava J. Newman
Professor of Aeronautics and Astronautics and Engineering Systems
Director, Technology and Policy Program

Accepted by: ______________________________
David E. Hardt
Chairman, Committee on Graduate Students
Department of Mechanical Engineering

Advancing Clinical Gait Analysis Through Technology and Policy

by

Junjay Tan

Submitted to the Engineering Systems Division and the Department of Mechanical Engineering on April 20, 2009 in Partial Fulfillment of the Requirements for the Degree of Master of Science in Technology and Policy and the Degree of Master of Science in Mechanical Engineering.

Abstract

Quantitatively analyzing human gait biomechanics will improve our ability to diagnose and treat disability and to measure the effectiveness of assistive devices. Gait analysis is one technology used to analyze walking, but technical as well as economic, social, and policy issues hinder its clinical adoption. This thesis is divided into two parts that address some of these issues.

Part I focuses on the role public policies have in advancing gait analysis. Through an analysis of gait analysis technologies, case studies of MRI and CT Angiography, and a high-level analysis of data standards used in gait analysis, it concludes that policies cannot directly create the institutional structures and the data standards required to advance gait analysis as a clinical diagnostic tool. Only through indirect means, such as research funding, can policies support the development of organizations to take ownership of gait analysis technologies. Part I also concludes that policies should not fund development of gait technologies but instead should fund research units working on data standards and accurate human body models.

Part II focuses on a technical issue in gait analysis, namely, how to address uncertainties in joint moment calculations that occur from using different body segment inertial parameter estimation models. This is identified as a technical issue needing attention from our broader policy analysis in Part I. Using sensitivity studies of forward dynamics computer simulations coupled with an analysis of the dynamical equations of motion, Part II shows that joint moment variations resulting from different segment inertial parameters are significant at some parts of the gait cycle, particularly heel strike and leg swing. It provides recommendations about which segment inertial parameters one should estimate more accurately depending on which joints and phases of the gait cycle one is interested in analyzing.

Thesis Supervisor:
Dava J. Newman, Professor of Aeronautics and Astronautics and Engineering Systems

Thesis Reader:
C. Forbes Dewey, Jr., Professor of Mechanical Engineering and Biological Engineering

Acknowledgements

“Oh I get by with a little help from my friends/
I get high with a little help from my friends/
Oh I'm gonna try with a little help from my friends/”
--The Beatles

First and foremost, thanks to my parents and my sister Lilian for their love, support, and confidence in my abilities through the years. I would not be where I am today without them.

Thanks to Dava for her creative spirit, generosity, support, and broad perspective on life. She has taught me much throughout my years at MIT. Thanks also to Forbes for his insights and advice in graduate school, as well as for introducing me to many aspects of bioengineering and biomedical informatics I had not known about before coming to MIT.

A big thanks to all my good friends at MIT who have kept me smiling through hard times, provided heart-to-heart talks, and reminded me of the beauty of life when things were down, especially Kyle (Mr. “Buddy Lee”), Tim, Rob (“Dr. Love”), Megan, Valerie, Shan, Decker, Monica, Zoe, Romain Levy, Travis, and Jesse. Also, thanks to other members of the MIT community who have taken time to mentor me in various ways, including Gari Clifford and Ken Zolot.

Thanks to all the other student, faculty, and staff members of the Man-Vehicle Lab who have made my graduate experience enjoyable—especially Thaddeus, Jessicas (both of them), Jaime, Chris, and Zakiya. I especially thank my officemate Roedolph for making our office the most fun office in the world, even if we didn’t have sunlight and had to battle roaches at times. Good thing we had our Nerf gun!

A special “thanks, mate” to James Waldie for his help and moral support. The lab could not ask for a better (and more fun) postdoc. Thanks also to Alan Natapoff for ideas and help with statistical analysis. Thanks to Sydney, Ed, and Sally for helping me with various administrative issues that have arisen (as well as great conversations).

I gratefully acknowledge the MIT-Portugal Program for funding much of this research. Thanks to Frank Field for his funding through a TA position in ESD.10, and to Profs. Pierre Lermusiaux, Evelyn Wang, and Alexander Mitsos for their funding through a TA position in 2.005, as well as Martin Segado, who was a great 2.005 co-TA. It was a great joy to work with you all!

Table of Contents

List of Figures

List of Tables

1 Introduction

Upright movement permeates American aphorisms, connoting independence, autonomy, perseverance, strength, achievement—'standing on your own two feet,' 'walking tall,' 'standing up for yourself,' 'taking things in stride,' 'climbing the ladder of success,' 'one small step for a man, one giant leap for mankind.'

--Lisa Iezzoni, *When Walking Fails*

1.1 Problem

Quantitatively analyzing human gait biomechanics will improve our ability to diagnose and treat disability and to measure the effectiveness of assistive devices. Of the many types of human movement, this thesis focuses on walking, which is a fundamental movement associated with social independence and many health benefits. Gait analysis is one technology used to study walking, but technical as well as economic, social, and policy issues hinder its clinical adoption.

This thesis is divided into two parts, both of which focus on clinical gait analysis. The first part focuses on the role public policies have in advancing gait analysis. The second part focuses on a technical issue in gait analysis, namely, how to address uncertainties in joint moment calculations that occur from using different body segment inertial parameter estimation models. This is identified as a technical issue that needs attention based on our broader policy analysis. The specific health technology and technical problems are explained in greater detail below.

1.1.1 Health Technology Policy

Health technology policy faces a tension between a desire for stricter cost-effectiveness scrutiny and the fear that overly strict standards will prevent promising technologies from being used, after which their effectiveness are often discovered. The latter fear is cited to justify implementing public policies, such as Medicare reimbursement, to support the development or use of an untested medical technology.

This tension means that costly technologies with unclear benefits are sometimes supported, while at other times promising technologies are stalled. Gait analysis fits in the latter category, though public policies to directly support its development and use may not be required because its technologies have non-medical applications as well. Technologies that have medical and non-medical applications may not require federal support if regulatory barriers to entry into medical markets are low.

At the same time, just because a technology is transferable from commercial to medical applications and has low regulatory barriers does not mean that its clinical promise can be fully realized without policies that create appropriate institutional structures and technology standards. Part I analyzes these issues to determine what role public policies have in advancing gait analysis.

1.1.2 Gait Analysis Technical Issue

An important output calculated from gait analysis is joint moments (or torques). Joint moments are important to know for two reasons. First, they can be correlated to poor biomechanics that may lead to degenerative processes. Second, they can be used to compute other variables, such as joint powers and individual muscle and tendon forces (Challis & Kerwin, 1996). But difficulty arises because joint moments are not directly measured variables and must be calculated from experimental data based on additional assumptions, one of these being body segment inertial parameters (BSIPs). BSIPs consist of body segment masses, center-of-mass locations, and inertias. This technical issue limits the use of gait analysis in clinical decision-making. An analysis of uncertainties in joint moment calculations due to differing BSIP values is therefore important for understanding how joint moment calculations may vary for the same subject, which relates to gait analysis's variability and accuracy.

Although we can take more accurate measurements of the entire body to try to achieve better BSIP estimates, this is an inefficient method. The research in Part II aims to provide guidelines regarding which specific body parts to measure more accurately depending on which cycle of the gait cycle one is interested in examining.

1.2 Research Overview

This section presents an overview of the research questions, hypotheses, methodology, conclusions, and limitations of this thesis.

1.2.1 Research Questions

To address the problems discussed in Section 1.1, this thesis is divided into two parts focusing on the following research questions:

- Part I: What public policies are appropriate for advancing clinical gait analysis?
- Part II: How can we better interpret joint moment results from gait analysis in light of large uncertainties in body segment inertial parameter estimates?

1.2.2 Hypotheses

In Part I, we hypothesized that the technologies required for gait analysis can be developed through commercial (non-medical) markets and that policies should focus on fostering the professional institutions and data standards required for clinical gait analysis to be a practical diagnostic tool.

In Part II, we hypothesized the following about joint moment results:

- Joint moment estimates will be significantly different during periods of high force impact, i.e., during heel strike, but similar at other periods of the gait cycle
- Joint moment variations will be different for different joints.
- Joint variations will be significant at some phases of the gait cycle and less so at others

1.2.3 Methodology

The methodology used in Part I involves an analysis of gait analysis technologies, case studies of MRI and CT Angiography to draw lessons for advancing clinical gait analysis, and a high-level analysis of data standards used in gait analysis for improving data sharing.

The methodology used in Part II of this thesis involves sensitivity studies of forward dynamics computer simulations as well as analyses of the dynamical equations of motion. 3D forward dynamic simulations are physical simulations that track experimental gait data in order to capture data from instrumented “virtual humans.” It is an increasingly popular method for studying human locomotion.

1.2.4 Conclusions

Part I concludes that policies cannot directly create the professional institutional structures and the data standards required to advance gait analysis as a clinical diagnostic tool. Only through indirect means, such as research funding, can policies support the development of organizations to take ownership of gait analysis technologies and data standards. Part I also concludes that policies should not fund development of gait technologies, but instead should fund research units working on data standards and accurate human body models.

Part II of this thesis concludes that joint moment variations resulting from different segment inertial parameters are significant at some parts of the gait cycle, particularly heel strike and leg swing. It provides recommendations about which segment inertial parameters one should estimate more accurately depending on which joints and which phases of the gait cycle one is interested in analyzing.

1.2.5 Contributions

This thesis presents several contributions. First, it provides recommendations on how public policies can advance gait analysis as a clinical tool. Though much literature exists regarding public policies for other diagnostics, such as medical imaging, there is a dearth of literature regarding gait analysis. Second, this thesis analyzes how body segment inertial parameter (BSIP) values affect joint torque estimates in gait analysis and provides recommendations on which BSIPs to measure more accurately depending on the joints and gait phases of interest.

1.2.6 Limitations and Future Work

Part I could analyze other related diagnostic modalities, both inside and outside the imaging field, as well as expand the standards analysis beyond data sharing to encompass clinical protocols. Also, Part I could analyze wearable sensor technologies, which hold promise as a technology for mobile gait analysis and for which regulations are still emerging.

The major limitations of Part II are that it analyzes one subject at one walking speed and analyzes only one body model.

1.3 Motivation

Physical disability is a significant national health problem that will only worsen as the population ages, a trend highlighted in Figure 1. In 2000, close to one fifth of community dwelling persons age five and older in the U.S. reported disabilities, while 41.9% of adults age 64 and older reported disabilities.

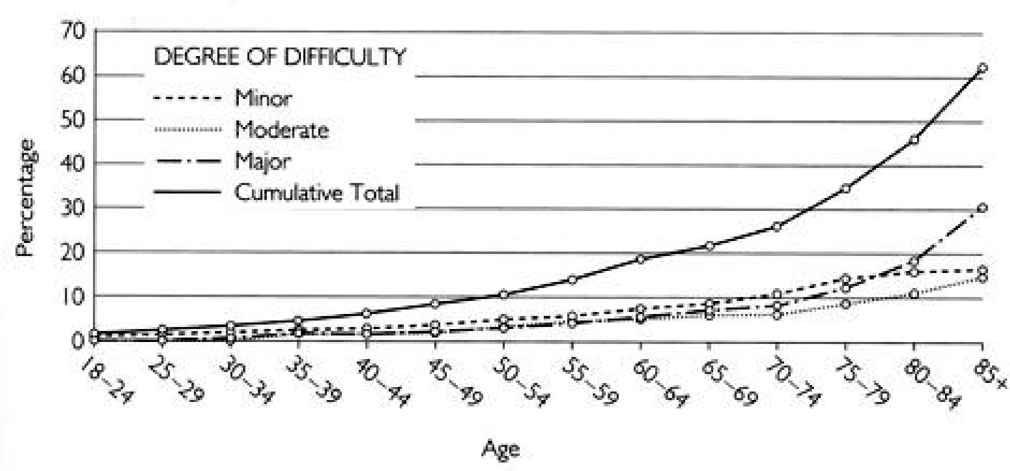

Figure 1: Percentage of adults with mobility difficulties by age (Iezzoni, 2003)

Further, the U.S. census bureau projects that the number of elderly will rise from 34.7 million in 2000 to 69.4 million in 2030. Of these elderly, 39.5 million reported sensory and physical disabilities in 2001. People with significant physical disabilities also live longer today due to advances in medicine, further compounding the costs of disability (Iezzoni & O'Day, 2006). Treating and diagnosing physical disability through improved medical technologies is therefore important. Table 1 highlights some disability statistics from 2001.

Table 1: Adults Reporting Mobility Difficulty in 2001 (Iezzoni, 2003)

*Difficulty**	Estimated Number (millions)	Percentage
None	168.32	90
Minor	7.93	4
Moderate	5.23	3
Major	5.82	3
TOTAL REPORTING DIFFICULTY	18.98	10

*None = persons who report no difficulty with walking *and* climbing stairs *and* standing *and* use no mobility aid; minor = persons who report some difficulty with walking *or* climbing stairs *or* standing *or* who use a cane or crutches; moderate = persons who report a lot of difficulty with walking *or* climbing stairs *or* standing *or* who use a walker; major = persons who report being unable to perform walking *or* climbing stairs *or* standing *or* who use a manual or power wheelchair or scooter

Of the many types of physical disabilities, walking disability is one of the most crippling and is therefore the focus of this research. Walking disability can come about through a variety of causes, some of which are summarized in Table 2. A key issue in addressing walking disability is how to best quantify and measure locomotion disability. This issue remains unresolved, as no definitive theories of walking have been accepted. Further, technologies such as powered orthoses and functional electrical stimulators are being introduced to address locomotion disability, yet these technologies are expensive and of unclear efficacy. The ability to assess, diagnose, and measure the effectiveness of new therapies to address walking disability is critical, both from a science perspective and from a health policy perspective.

Table 2: Common Causes of Mobility Difficulties (Iezzoni, 2003)

	Mobility Difficulty (%)		
Causes	*Minor*	*Moderate*	*Major*
Arthritis and musculoskeletal problems	25	26	24
Intervertebral disk and other back problems and sciatica	14	16	8
Accidental falls	6	7	6
Ischemic heart disease and other heart conditions	5	5	6
Motor vehicle traffic accidents	4	5	4
Chronic bronchitis, emphysema, asthma, and other lung conditions	4	4	4
Cerebrovascular disease, including stroke	1	2	5
Overexertion and strenuous movements	2	3	1
Unspecified accidents	2	2	1
Machinery, firearm, and other specified accidents	1	2	2
Osteoporosis and bone or cartilage disorders	1	1	2
Diabetes	1	1	1
Multiple sclerosis	< 1	< 1	2

1.4 Definitions

This section defines the major terms used in this document.

1. Physical Disability: an impairment that prevents one from performing functions of daily living that healthy people can perform.

> This definition is based on the World Health Organization's (WHO) *International Classification of Functioning, Disability, and Health* (ICF), which defines disability as an "umbrella term for impairments, activity limitations or participation restrictions," categorizing "a person's functioning and disability…as a dynamic interaction between health conditions (disease, disorders, injuries, traumas, etc.) and contextual factors." (Iezzoni & O'Day, 2006).

2. Gait Analysis: a diagnostic method that records human body kinematics and dynamics during some sort of gait movement, where gait implies that the body is supported on the legs. Kinematics refers to the motion of objects without consideration of the forces that cause that motion, while dynamics is concerned with forces as well as properties of the moving bodies, such as their masses and inertias. The focus is on whole-body movements, such as limbs, torso, and head, rather than smaller bodies such as cells or even fingers. Additionally, muscle EMG signals may be recorded as well.

This definition follows that of Rose (1983), who suggested that the term "gait assessment" be applied to the whole process of examining a patient's gait and suggesting treatment, while the term "gait analysis" be used for the technical side of gait assessment, which includes making objective measurements such as walking speed, joint angles, forces, and EMG muscle recordings (Whittle, 1996). This thesis focuses on gait analysis and its application to gait assessment as a clinical diagnostic.

3. Movement Analysis: measurement and analysis of the body as a whole. Thus, gait analysis is a subset of motion analysis.

***4. Forward Dynamic Simulations*:** computer models that simulate movement of physical objects by numerically integrating dynamic equations of motion in time, subject to gravity, inertial and velocity-dependent forces, and muscle forces. In forward dynamic simulations, forces produce motions, whereas traditional analysis of gait data involves inverse dynamic analysis, where experimentally measured ground forces and torques are cascaded through rigid body linkages representing the body segments in order to estimate joint torques (Piazza, 2006).

5. Body Segment Inertial Parameters (BSIPs): the mass, center of mass location, and moments of inertia of human body segments.

6. *Gait Cycle:* the time required for a leg to undergo both a stance and a swing phase. This is typically the time axis presented in gait analysis result plots.

1.5 Overview of the Following Chapters

Part I encompasses chapters 2 through 5. Chapter 2 presents background on gait analysis and health policies related to gait analysis. Chapter 3 presents our technology analysis to answer key question one. Chapter 4 presents the case studies of MRI and CT Angiography, while Chapter 5 analyzes data standards in gait analysis and presents policy conclusions.

Part II encompasses chapters 6 through 8. Chapter 6 reviews the biomechanics of human walking, while Chapter 7 presents our research methodology in detail. Finally, Chapter 8 presents results and conclusions.

PART I: Public Policies for Advancing Gait Analysis

As explained in Section 1.1.1, Part I addresses how public policies can advance gait analysis. Specifically, this part aims to answer the following three key questions:

- Is the technology required for clinical gait analysis different from that required for commercial applications of motion capture and analysis? If so, how, and what role do regulatory requirements play in effecting technology transfer into the medical field for gait analysis?

- How does gait analysis compare to imaging—a widely-used (and therefore, in our view, successful) clinical diagnostic—in terms of its political, economical, and social structure, and what lessons can be learned from examining the medical imaging field's development?

- What is the state of data standards in gait analysis, and how might policies address the deficiencies?

These three questions cover a range of technology, social science, and standards issues central to the advancement of gait analysis as an accepted clinical diagnostic. After answering these questions, we provide recommendations on whether and how public policies can advance clinical gait analysis. The hypothesis, scope, and methodology of Part I are summarized below in the next sections

Hypothesis

A key issue in health policy is whether appropriate medical technologies will be developed by industry alone. In other words, do appropriate incentives exist without additional federal encouragement, or must government create incentives for development of appropriate technologies through such means as university research? This question is significant for gait analysis because many of its technologies have applications in other markets such as entertainment, engineering, and sports, and therefore the market may already pursue appropriate technological advancements without public funding.

For gait analysis, we hypothesize that the desired technologies can be developed through commercial markets without significant publicly funded development of these technologies and that policies should instead focus on fostering the professional institutions and data standards required for clinical gait analysis to become a practical diagnostic tool.

Scope

This research focuses only on public policies for the U.S. healthcare environment. By public policies, we mean policies enacted at the federal level, such as Medicare reimbursement decisions, statutes, and research funding initiatives. In other countries—especially those with national healthcare systems— medical regulations and reimbursement policies are different, which means our analysis and recommendations may not be applicable. Further, we focus only on lab-based gait analysis as a diagnostic tool. Some research has focused on using wearable sensors for mobile gait analysis (e.g., (Bonato, 2005)), but these technologies are still developing and policies regarding mobile health devices are still emerging, even for standard measurements such as blood pressure (Olson, 2008). We believe that general acceptance of gait analysis as a lab-based tool must emerge prior to its use in mobile or home-based diagnostic devices, and therefore focus only on the former. Finally, although this study focuses on gait analysis, our conclusions will likely be generalizable to advancing clinical movement analysis as a whole.

Methodology

The methodologies used to answer the three questions are as follows. The first question is answered through an analysis of the technologies used in gait analysis and related applications. The second question is answered through case studies of medical imaging—which, like gait analysis, is a multidimensional diagnostic that relies heavily on operator interpretation of results— to glean insights into relevant policy issues for gait analysis. Specifically, we analyze the cases of MRI and CT Angiography, for reasons to be detailed in Chapter 4. The third question is answered by performing a high-level analysis of standards used to store and communicate gait analysis data and comparing them to DICOM, the standard used for medical images.

Conclusions

Part I concludes that policies cannot directly create the professional institutional structures and the data standards required to advance gait analysis as a clinical diagnostic tool. Only through indirect means, such as research funding, can policies support the development of organizations to take ownership of gait analysis and its data standards. Part I also concludes that policies should not fund development of gait technologies, but rather should fund research units working on data standards and accurate human body models.

Overview of Proceeding Chapters in Part I

Chapter 2 presents background on gait analysis and health policies related to gait analysis. Chapter 3 presents our technology analysis to answer key question one. Chapter 4 presents the case studies of MRI and CT Angiography, while Chapter 5 analyzes data standards in gait analysis and concludes with overall policy recommendations.

2 Gait Analysis and Related Policies

This chapter is divided into two sections. Section 1 presents an overview of the regulatory, reimbursement, and policy issues relevant to clinical diagnostic technologies. Section 2 then presents a brief history of modern gait analysis and explains its medical potential.

2.1 Health Technology Policy

This section provides an overview of why government intervention is often required to promote and develop medical technologies, the U.S. regulatory environment for diagnostics, how reimbursement decisions for diagnostics are made, and the evidence-based medicine approach.

2.1.1 Rationale for Government Intervention

It may first be helpful to define why public policies are needed regarding medical technologies. One reason is because the medical industry differs from most other industries in two ways: (1) providers rather than purchasers or beneficiaries generally determine the services provided, and (2) health providers are generally reimbursed for services by third parties rather than beneficiaries. The health care market therefore does not fulfill the criteria of efficient markets, which means we may require government intervention to protect the public welfare and to promote effective use of healthcare and related technologies (Hillman, 1986).

2.1.2 Regulation of Diagnostic Technologies

Any device advertised for use in medical applications must be approved by the U.S. Food and Drug Administration (FDA), which regulates medical devices according to the Food, Drug and Cosmetic Act (FD&C). Specifically, gait analysis systems to be used for diagnostic purposes are considered medical devices according to section 201(h) of the FD&C, which defines a medical device as any device "intended for the use in the diagnosis of disease or other conditions, or in the cure, mitigation, treatment, or prevention of disease, in man or other animals" (21 U.S.C. § 321 (2004)).

Medical devices are classified into three classes that determine regulatory scrutiny. Section 513 (21 U.S.C. § 360c (2004)) of the FD&C Act divides them as follows:

- *Class I devices*: these devices do not require pre-market approval or clearance and are considered the safest. They therefore have the least controls, i.e., the FDA's "general controls." Ground force plates are considered Class I devices (21CFR890.1575 (2007)).

- *Class II devices:* These devices require "special controls," such as performance standards, post-market surveillance, and dissemination of guidelines. Many diagnostic tests are considered class II devices. These devices are cleared using the 510K process, which is discussed below.

- *Class III devices*: These devices require pre-market approval because general and special controls are not satisfactory to ensure their safety or effectiveness. They include devices used to support human life, such as pacemakers.

Further, section 510(k) of the FD&C Act requires device manufacturers to notify the FDA at least 90 days in advance of their intent to market a medical device (21 U.S.C. § 360 (2004)). This allows the FDA to determine whether the device is equivalent to a device it has already classified. 510(k) is known as the “pre-market notification,” and is meant to ensure that the device to be marketed is “at least as safe and effective” as a “legally marketed device” (U.S. Food and Drug Administration, 2006). Devices cleared through the 510(k) process are not considered approved by the FDA but are considered “cleared” devices and can be marketed in the U.S.

2.1.3 Reimbursement

After the FDA approves a medical technology, insurers such as Medicare decide on coverage. Private insurers make their own coverage decisions but often follow the lead of Medicare.

Medicare is a social insurance program for people age 65 and over administered by the Centers for Medicare and Medicaid Services (CMS). It is grounded in the Social Security Act. Section 1862(a)(1)(A) of the Social Security Act states that Medicare explicitly covers only diagnostics that are “reasonable and necessary for the prevention of illness” (42 U.S.C. § 1395y (2008)). However, no statutory definition of this phrase is provided, leading to vigorous debates about specific technologies (Redberg, 2007).

Private insurers decide what to insure in two stages: (1) what services are covered by particular plans, and (2) case-by-case decisions about the “medical necessity” of covered services. Coverage generally follows the precedents set by Medicare, making Medicare coverage the key step in gaining private insurance coverage.

There are no established protocols for deciding coverage, both at the Medicare and at the private insurance level. Although Medicare espouses evidence-based approaches (discussed in the next section) for making coverage decisions, it does not always follow them. Berensen and Abelson write that “inadequate study is especially serious for medical devices and imaging equipment,” and that once a procedure gains FDA approval, “Medicare rarely demands evidence that it benefits patients before agreeing to pay for it” (Berenson & Abelson, 2008). Iezzoni & Day emphasize that coverage standards are subjective, and the lack of data supporting effectiveness of many procedures allows insurers and Medicare to deny coverage easily (Iezzoni & O'Day, 2005). And unlike pharmaceuticals, which undergo periodic review by the FDA after approval, few systematic criteria are applied to ensure patient benefit in the case of medical devices after formal requirements for FDA approval and insurance coverage are met (Redberg, 2007)

2.1.4 Evidence-based medicine

Rising costs in medicine have prompted policymakers, insurers, and some physicians to advocate evidence-based medicine. The most common definition from Sackett states that EBM is "the conscientious, explicit and judicious use of current best evidence in making decisions about the care of the individual patient. It means integrating individual clinical expertise with the best available external clinical evidence from systematic research." (Sackett, 1996).

The movement towards evidence-based medicine became widely accepted in the 1990s. Areas of EBM include coverage policies, performance measures, disease management, quality improvement, regulations, and public policies. All these areas share four common features: (1) analysis of evidence and development of guidelines and policies is done by small groups of experts, (2) they all use explicit, rigorous review processes, (3) the product is generic, meaning the guidelines are intended to apply to a class or group of patients defined by some clinical criteria, rather than to an individual patient, and (4) their effects on care are indirect, i.e., they are intended to enable, guide, motivate, or sometimes force physicians and other providers to deliver certain types of care to people, but they do not directly determine the care provided to a particular patient (Eddy, 2005).

Associated with the movement toward evidence-based medicine is the movement to evaluate cost-effectiveness of medical procedures by bodies such as Medicare. Cost-effectiveness analysis aims to evaluate health outcomes and costs of different procedures relative to one another so that decision makers can select the “best” alternative. However, it neglects many factors that may be equally or more important in making funding and reimbursement policy decisions, such as justice, equity, and costs and benefits outside the health care system (Gazelle *et al.*, 2005).

Evidence-based medicine involves analysis of many levels of effectiveness, from technical accuracy to impact on societal health outcomes. An example of the many levels of evidence for medical imaging diagnostics and specific metrics by which each may be measured is presented in Table 3.

Table 3: Levels of Evidence in Evaluations of Diagnostic Technologies, with examples taken from the medical imaging field (Pearson *et al.*, 2008)

Level of evidence	Example of Measures
1. Technical	Pixels per millimeter Section thickness
2. Diagnostic accuracy	Sensitivity Specificity Area under the receiver operating characteristic curve
3. Impact of diagnostic thinking	Percentage of cases in which the clinician believes that the test alters the diagnosis
4. Impact on therapeutic actions	Percentage of cases in which the choice of therapies is changed after information from the test is provided
5. Impact on patient outcomes	Differences in mortality, morbidity, or quality of life between patients managed with the test and those managed without it
6. Impact on societal outcomes	Cost-effectiveness of the improvement in patient outcomes, such as cost per life year saved, calculated from a societal perspective

2.2 Gait Analysis Overview

This section summarizes the potential of gait analysis as a diagnostic tool for musculoskeletal disorders, the modern history of gait analysis, and the process and economics of gait analysis.

2.2.1 Diagnostic Potential

Technologies for gait analysis measure the dynamics (forces) and kinematics (motion) of movement, providing a quantitative basis by which to analyze and diagnose movement disorders. Advantages of gait analysis over unaided clinical observation include identifying problems at multiple levels, identifying dynamic movement patterns not evident otherwise, and comparing range of motion curves of normal ranges to tested subjects (Finch, 2001).

Gait analysis has potential as a diagnostic tool for assessing the severity of pathology, predicting better treatments, and assessing the effects of interventions. It has been used and studied most extensively on altering treatment procedures in cerebral palsy (CP) patients. Accordingly, many (but not all) insurers cover its application to CP. Gait analysis supplemented with EMG recordings is particularly useful for determining which muscles are activated during poor gait, which can inform surgical procedures. Research also suggests that gait analysis holds potential for diagnosing multiple joint diseases such as osteoarthritis, anterior cruciate ligament (ACL) rupture in the knee, hemiplegia, and muscular dystrophy (Whittle, 2002).

2.2.2 History of Modern Gait Analysis

The history of modern gait analysis systems can be traced to the late 1970s and early 1980s. During the late 1970s, gait analysis was introduced into clinical settings largely due to the efforts of four orthopedic surgeons: Jaquelin Perry, David Sutherland, and Jim Gage in the U.S., and Gordon Rose, in the UK (Whittle, 1996).

Sutherland provides a published personal account of the historical development of and applications of gait analysis technologies, which we briefly summarize below. More detailed information about each technology is presented in Chapter 3.

2.2.2.1 Motion Capture

Much work in the 1950s focused on recording joint angles using electrogoniometers because such systems could collect information quickly and analog graphs of motion could be displayed without extensive data processing. These were important features since powerful computers were unavailable. The introduction of the Vanguard Motion Analyzer in the 1960s brought forth film-based techniques using passive marker systems. This system used high-speed cameras to track markers in space, but manual calculations were needed to convert image data into coordinate data. Research work during the 1960s and 1970s focused on automating this process of acquiring marker coordinates from images. During the late 1970s, a technical director at Oxford Medical Systems—a company focusing mainly on cardiology products—thought that a commercial market for an automatic 3D gait analysis system existed. Oxford Medical Systems therefore licensed technologies from the Universities of Strathclyde and Dundee and spent two years developing a system called VICON, whose name was derived from “video-converter.” The first VICON system was shipped in 1980.

Although the VICON system was effective for extracting 2D coordinate data, its software could not calculate 3D coordinates. Michael Whittle, who had worked with NASA to make 3D measurements of astronaut body forms in a Skylab experiment, became the director of the Oxford University Motion Laboratory after its former director left to found Oxford Metrics, a spin-off of Oxford Medical Systems focusing on the VICON system. To fulfill his research needs, Whittle likely wrote the 3D motion capture software. After Oxford Metrics, Motion Analysis Corporation was the next major motion-capture company to emerge. After Motion Analysis came Bioengineering Technology Systems (BTS), which was founded in Milan, Italy, in 1986. BTS developed the ELITE motion capture system (Sutherland, 2002).

The advent of MEMS (microelectromechanical systems) sensors in the late 1990s reduced the price, size, and power consumption of traditional sensors while improving their accuracy. This led to increased attention on using wearable sensors for motion capture applications. Several companies have emerged marketing such motion capture suits. Additionally, Organic Motion presented the first commercial markerless motion capture system in 2007, although the accuracy is still inadequate for biomechanical applications (Bonato, 2009).

2.2.2.2 Kinesiological EMG

EMG (electromyography) systems measure the electrical activity of muscles to provide information about muscle excitations. These can involve surface (non-invasive) EMG, or fine-wire (invasive) EMG. Most of the developments in EMG technology and application occurred prior to the 1980s. (Sutherland, 2001).

2.2.2.3 Ground Force Measurement

In the mid-1960s, Sutherland requested the development of a force plate for the Shriners Hospital San Francisco Gait Laboratory because no commercial force places existed. The lab hired engineers to produce a clinically useful force plate, which appeared in 1975. Similarly, other gait labs contracted to have custom force plates built as well. Several years later, the Kistler Corporation, a respected Swiss company, produced a commercial model. This was followed by those of other companies, such as Advanced Mechanical Technology, Inc. (AMTI) and Bertec, ushering in the market a variety of reliable, commercially available force plates (Sutherland, 2005).

2.2.3 Gait Analysis Process

Gait analysis consists of three main steps: taking a patient’s history, performing a physical examination, and performing “special investigations,” such as X-rays or oxygen consumption analysis. A gait analysis team generally consists of a physician, a physical therapist, and a biomedical engineer, though different centers may have different team sizes and team members with different skills (Simon, 2004; Whittle, 1996). Only the physical therapist and engineer are required to conduct the study, with the physician performing the initial clinical examination and assisting in interpreting results (Bonato, 2009).

Referrals to gait labs are often made by patients’ physicians, though physical therapists might do so in some cases as well. These physicians are generally orthopedic surgeons. The patient stays at the gait lab for 2-3 hours, and her stay there consists of the physician taking a patient history, then performing various gait analysis tests (Whittle, 1996).

Specifically, taking the history and performing the clinical exam of a patient requires 20-30 minutes, placing markers on the subject and calibrating devices for motion detection and muscle activity monitoring takes 30-60 minutes, and testing itself lasts 5-30min depending on the number of conditions examined. Post-processing the data then takes additional time. While gait analysis results can be processed and returned quickly by computers, they must still be read and interpreted by humans. Gait reports can number in the hundreds of pages, and in contrast to medical images, they are not presented as appealing 3D images. Instead, reports are a jumble of plots and figures that require much technical expertise to understand. Simon and many others propose that computer assisted gait data analysis and report generation can address this issue, though such methods still have not been developed (Simon, 2004).

As a point of comparison, the Motion Analysis Laboratory at Spaulding Rehabilitation Hospital in Boston takes about 2 hours to perform a gait study and can test up to three child subjects a day (Bonato, 2009).

2.2.4 Coverage

Controversy over gait analysis's clinical relevance is reflected in most U.S. private insurance policies, such as those of Blue Cross & Blue Shield and Aetna, which regard it as "research" and therefore not reimbursable (Aetna, 2008; Blue Cross & Blue Shield of Mississippi, 2008). This suggests that more efficacy studies are needed before gait analysis will be covered as a normal diagnostic procedure.

However, gait analysis is sometimes covered for cerebral palsy applications. Children with cerebral palsy are treated with a variety of medications, physical therapy sessions, bracing, assistive devices, and orthopedic or neurosurgical procedures to prevent deformity and improve mobility. While in the past many orthopedic procedures were performed at separate times, today physicians attempt to perform multiple procedures in one surgical session. Gait analysis provides greater confidence over clinical examination that proper surgical procedures will be chosen, has been shown in various research studies (Simon, 2004).

2.2.5 Economics

3D gait analysis typically ranges from $600 to $1000, although it can cost up to $2,000. The average reimbursement is $500 or less. (Roan, 2007; Simon, 2004; Stanford School of Medicine Human Performance Lab, 2008). Despite these costs to patients, Simon (2004) writes that in the U.S. it is rare for a gait lab to have revenue balance expenses. He cites the main reason being the time and expense of performing gait studies. Specifically, establishing a gait lab requires purchasing equipment that averages around $300,000, excluding facility renovations and rental cost of the lab space. Maintenance contracts for hardware and software add another $30,000 to $50,000 a year. Full-time lab personnel consist of a bioengineer, a physical therapist, and a secretary receptionist, for whom salary and benefits add up to about $250,000 annually. To balance expenses, a gait lab would have to perform at least 15 studies a week for 50 weeks at $500 per study, or $375,000 in revenue. Since, as mentioned earlier, each test takes about three to four hours, few labs are capable of testing 600 subjects per year (Simon, 2004).

2.2.6 Criticisms of Gait Analysis

This section highlights the main criticisms directed at gait analysis regarding why gait analysis is not widely used by clinicians or eligible for reimbursement. These are the issues we will focus on when performing analyses.

Little literature exists that attempts to analyze the non-technical issues hindering clinical gait-analysis. Simon (2004) analyzed some institutional issues that have hampered gait analysis's advancement in the clinic. However, he proposes largely technological or organizational fixes to the problems, without delving into whether or how public policies can address these. For example, to speed up gait analysis testing time, he proposes replacing skilled the professionals who currently perform the tests (i.e., biomedical engineers and physical therapists) with technicians such as those used in radiology. He also suggests that markerless motion analysis systems can reduce patient preparation time. Regarding the complex reports, he suggests using machine learning algorithms to analyze the data and provide recommendations—a situation that still appears far in the future, as such techniques are rare even in medical imaging. Finally, he also suggests creating integrated databases and networks to link gait labs with referring clinicians.

In 1995, the National Center for Medical Rehabilitation Research (NCMRR) within the National Institutes of Health (NIH) sponsored a workshop to develop and prioritize a set of recommendations regarding the role of gait analysis in enhancing the function of people with locomotor disabilities. The workshop resulted in 37 prioritized recommendations. However, little was done in the proceeding decade. From 2004-2008, the research committee of the Gait & Clinical Movement Analysis Society (GCMAS), a professional organization interested in human movement, convened to revise the recommendations in light of new developments. The members reevaluated and prioritized the eight main objectives to be achieved. Based on Simon (2004) and the NIH/GCMAS recommendations, this research synthesizes the main criticisms of gait analysis.

The first major criticism involves proving the diagnostic effectiveness of gait. Specifically, interpretation of data varies from clinician to clinician and from institution to institution (Simon, 2004). This is exacerbated by many physicians' and therapists' lack of understanding about gait analysis' capabilities, benefits, and limitations. Lack of efficacy data showing that functional outcomes are improved due to gait analysis contributes to this. Also, the act of processing raw data and transforming it into data valuable to the gait analyst may lead to errors, since few studies analyze these artifacts. Finally, because of these issues, the cost-effectiveness of gait analysis as a clinical tool cannot be established (Gait & Clinical Movement Analysis Society, 2008).

The next criticism focuses on gait analysis economics. Gait labs are economically inefficient, largely due to their personnel costs and the time it takes to perform a gait study (Simon, 2004). This is exacerbated by the fact that gait labs may lack the business structures needed to promote and sustain the field (Gait & Clinical Movement Analysis Society, 2008).

Related to cost and effectiveness, another criticism is that gait analysis provides insufficient advantages over simpler methods to justify the costs. Physicians must be convinced that it offers significant advantages over questionnaires, observation of gait with the naked eye, and 2D video recordings. Historically, most orthopedic surgeons and rehabilitation specialists relied on static examinations and observational gait analysis, with questionnaires being added in recent years. Cultural and institutional barriers therefore exist in converting these professionals to accept clinical gait analysis (Gait & Clinical Movement Analysis Society, 2008).

Others also criticize gait analysis as not being representative of real-world conditions, since it is limited to testing in controlled lab environments, such as walking through an empty room or moving on a treadmill. Such critics are often researchers working on mobile gait analysis systems (Bonato, 2005)

Also, gait analysis data are difficult to share. This is due to differences in methods used by different labs, and little work has focused on developing procedures for sharing (Gait & Clinical Movement Analysis Society, 2008). Related to this problem is the lack of standards for testing inter-laboratory reliability, which means there are no processes to certify that a gait lab meets some accepted standard for accuracy (Sutherland, 2002).

Finally, there is a lack of cohesion within the field. This makes it hard to advance its standing “within business markets and political arenas.” (Gait & Clinical Movement Analysis Society, 2008).

These criticisms are summarized in Table 4, along with the method we use to analyze the issues regarding each of them.

Table 4: Main criticisms of gait analysis

Criticism	Specific issues	Method used to gain insight into issues
Clinical effectiveness	• Interpretation of data varies from lab to lab and clinician to clinician • Physicians and therapists don't understand the capabilities, benefits, and limitations of gait analysis • Lack of efficacy data showing that functional outcomes are improved directly due to gait analysis • Processing and transforming raw data to data valuable to gait analyst may lead to errors	Case study of MRI/CTA
Cost-effectiveness	• Gait labs are economically inefficient • Gait labs lack business structures needed to promote and sustain the field	Case study of MRI/CTA
Provides few advantages over simpler methods	• Gait analysis must offer significant advantages over questionnaires or observational gait analysis, which historical bias causes physicians to stick to	Case study of MRI/CTA
Complex results are hard to interpret	• Gait reports consist of "too many pages of text, graphs, and figures in a format not easily understood or useful to the average clinician."	Case study of MRI/CTA
Lab conditions are not representative of real-world conditions	• Gait tests may not accurately represent how clinical interventions affect patients' lives	Not addressed in this research
Heterogeneous data standards	• Gait/motion analysis data are difficult to share • Different labs use different protocols, systems, and data processing methods	Analysis of Protocols and Standards in gait analysis and DICOM
Lack of cohesion within the field	• Lack of professional cohesion within the field.	Case study of MRI/CTA

The next chapter analyzes the technologies used in gait analysis to determine whether and how commercial markets address the technology advancements needed for clinical gait analysis.

3 Gait Analysis Technology Transferability

As mentioned in Chapter 2, one reason that advancement of gait analysis into clinical applications is stalled might be because appropriate technologies are not being developed by private industry without policies to drive their development for clinical applications. Therefore, one question we aim to answer is whether and how the technology required for clinical gait analysis differs from that desired in related commercial applications. This would determine whether public policies are required to develop such technologies specifically for clinical gait use.

To answer this question, this chapter analyzes the technologies used in clinical gait analysis and that used in other similar applications. Many of the companies that produce gait analysis systems also produce motion capture systems for other commercial markets (sports, entertainment, etc.), and much of the technology is similar. This chapter then analyzes how directly transferable the commercial technology is to the medical field and whether high regulatory barriers exist.

3.1 Gait Analysis Technologies

As mentioned in Chapter 2, gait analysis involves acquiring quantitative measurements of human body kinematics and dynamics during gait movement. Two separate measurement devices are used for this: a motion capture device for measuring kinematics, and a force measurement device for measuring dynamics. EMG sensors are also sometimes used to record muscle activity.

The most widely used gait analysis system combines an optical (camera-based) marker system with force plates (Figure 2), which is interfaced to a computer for data processing. However, a variety of other setups are used as well.

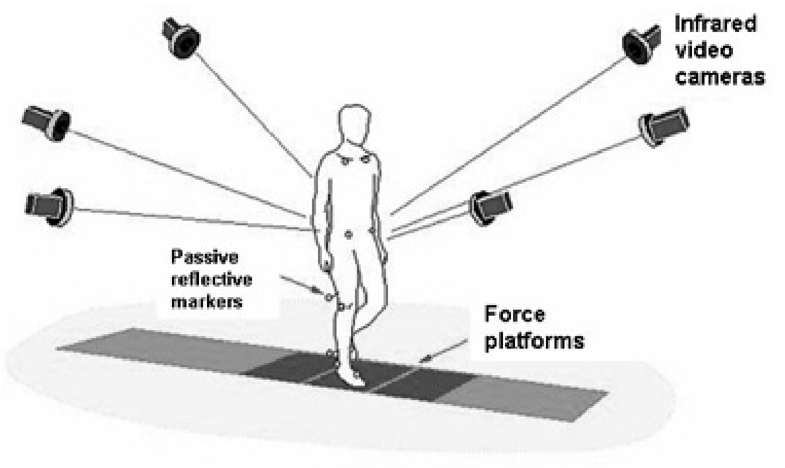

Figure 2: Typical gait analysis setup (Medscape.com)

3.1.1 Motion Capture Technologies

A variety of motion capture technologies exist for use in recording movement kinematics. These include magnetic systems, mechanical systems, optical systems, and sensor-based systems.

3.1.1.1 Magnetic Systems

These systems locate position and orientation of sensors in space using a magnetic field, offering good accuracy and update rates. Each sensor contains three orthogonal sets of coils, which allows the sensor to be located when the transmitter produces an electromagnetic field of three frequencies inside the test space. A downside of magnetic motion capture systems is their sensitivity to magnetic objects inside the tracking space. One example of such systems is Ascension Technology’s MotionStar, shown in Figure 3. Magnetic systems range in cost from about $5,000 to $150,000 (Ruiz, 2002).

Figure 3: Ascension Technology’s MotionStar magnetic motion capture system (Ascension Technology, 2009)

3.1.1.2 Mechanical Systems

Mechanical motion capture systems are comprised of electrogoniometers, which are hinges strapped at joints that record joint angles. A potentiometer or some other transducer transforms joint rotations into electrical signals. Although the hardware used in mechanical systems are cheaper than in other systems, mechanical systems are often heavy and restrictive. Potentiometers also degrade in performance with age. Mechanical systems generally cost between $5,000 and $10,000. An example of such a system is Meta Motion’s Gypsy exoskeleton-based system, shown in Figure 4.

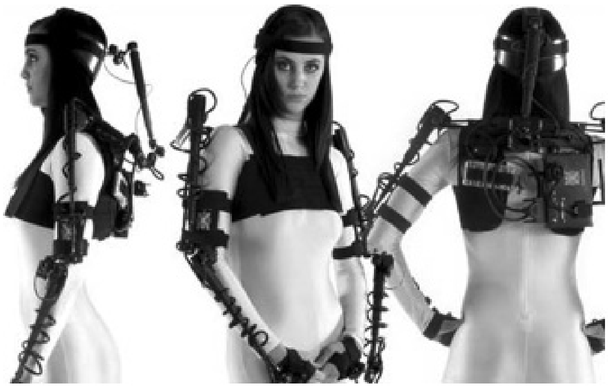

Figure 4: Meta Motion's Gypsy mechanical motion capture system

3.1.1.3 Image-based systems

Optical systems include those that track passive or active (e.g., LED-lit) markers in video frames, as well as markerless systems.

Marker-based systems

Marker-based systems were developed to automate motion capture. Such systems track passive reflective markers or active light-emitting diodes (LEDs) on the body and determine the 3D marker locations using triangulation methods from multiple cameras (generally 4 to 32) around the subject. They are favored in the computer animation and film industries because of their high accuracy and fast update rates (Vlasic *et al.*, 2007); however, they are also expensive, typically costing between $100,000 and $250,000 (Ruiz, 2002). Additionally, they can run into problems if the markers are occluded from view.

The location of markers in world coordinates is generally determined by finding the centroid of each marker in each camera frame. From these 2D locations, the positions of the cameras are then factored in to triangulate each marker's location in 3D space. Major manufacturers of such systems include Vicon and Motion Analysis Corporation.

Markerless systems

Markerless systems have been the holy grail of optical motion capture technology since marker-based systems were introduced. This is due to the time-intensive nature of marker-based systems as well as their accuracy problems in locating joints due to skin marker movement. The first commercial system by Organic Motion was introduced at SIGGRAPH in 2007, which featured real-time rapid calibration and extraction (Figure 5). Although technical specifications and reviews have not been provided of the technology, a clear restriction available from publicity videos is that a specialized curtained stage must be used to ensure clear contrast between subject and background. Organic Motion's system costs $80,000. The Motion Analysis Lab at Spaulding Rehabilitation Hospital has been working with Organic Motion on gait analysis applications of the system, but it is still not accurate enough for biomechanical applications (Bonato, 2009).

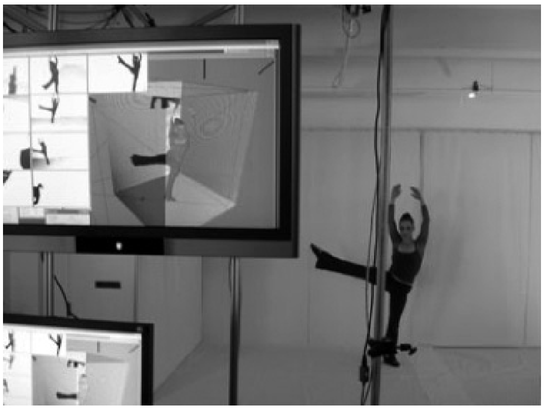

Figure 5: Markerless motion capture system (Organic Motion)

3.1.1.4 Inertial Motion Capture Systems

Such systems were sparked by the rise of MEMS sensors and involve placing accelerometers or gyroscopes on body suits to measure joint angle rotation. Although such systems are very portable and relatively cheap—on the order of $25,000 to $80,000—they do not measure positions and distances directly and measurements drift significantly over several minutes because the noisy measurements must be integrated twice to provide position data (Vlasic et al., 2007). These systems perform especially poor for fast, high acceleration movements. An example of such a system is Xsen's Moven suit, shown in Figure 6.

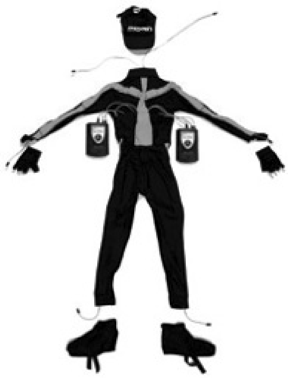

Figure 6: Xsen's Moven sensor-based motion capture suit

3.1.1.5 Hybrid Sensor Systems

Such systems use two motion capture systems in tandem to address shortcomings of using each system alone. An example is Hy-BIRD by Ascension Technology, which combines optical and inertial technologies to handle conditions when the image is blocked from view.

3.1.2 Force Measurement Technologies

The two main types of force measurement technologies used are force plates and pressure mapping systems.

3.1.2.1 Force Plates

The most commonly used device to measure forces is a force plate (Figure 7). Force plates comprise a large number of force sensors to improve the spatial resolution of forces. A difficulty traditionally encountered in using force plates is requiring proper foot placement. Often, this requires having only one foot touch the plate, which is difficult for patients with cross-walking pattern disabilities (Edginton *et al.*, 2007).

Figure 7: Force Plate for Gait Analysis (Noraxon U.S.A. Inc., 2009)

3.1.2.2 Pressure Mapping Systems

A less common system is shoe-based pressure mapping. Such systems involve thin, flexible force sensors that have relatively high spatial resolution for force measurements. An example is Tekscan's F-scan system (www.tekscan.com).

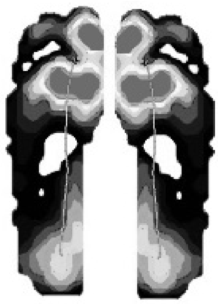

Figure 8: image from Tekscan's pressure mapping system
(Motion Analysis Laboratory, Children's Hospital, San Diego, CA)

3.1.3 Instrumented Treadmills

Instrumented treadmills integrate force plates inside a treadmill and are specially designed for gait analysis. The main advantage of such systems is to eliminate the need for proper foot placement on ground force plates (Edginton et al., 2007). This can speed up gait analysis sessions.

3.1.4 EMG Measurement Systems

EMG systems measure the electrical activity of muscles to provide information about muscle excitations. Such systems may be invasive, where sensors are pricked into specific muscles to provide data with less cross-talk from adjacent muscles, or noninvasive, where surface electrodes are placed on top of skin. Noninvasive sensors are generally used for gait analysis applications. Figure 9 shows these two types of EMG systems.

Figure 9: Invasive (left) and noninvasive (right) EMG systems (drbezner.com, www.health.utah.edu)

3.1.5 Software

Additionally, to calculate joint moments, a human body model is required. This model involves physical properties of the limbs (masses, inertias, center-of-mass locations), as described in Part I. Motion analysis companies often sell software consisting of customizable human body models with their systems, though other software besides the manufacturer's, such as the free open-source software OpenSim, can be used as well. An example is Vicon's BodyBuilder softwar. Such software typically includes many other functionalities as well, such as 3D visualization capabilities.

3.2 Major Commercial Markets

Besides clinical and research markets, other markets exist for the technologies used in gait analysis. These markets are often catered to by the exact companies marketing clinical gait analysis systems (e.g., Vicon and Motion Analysis Corporation). This section analyzes to what extent gait analysis technologies are used in these markets.

Motion capture for entertainment
Movement analysis is widely used in the entertainment industry to create life-like animation in movies and video games. The large size of this market means that advancements desired by entertainment companies will drive the technology. Only kinematics data is required for entertainment purposes.

Sports performance analysis
Movement analysis is widely used in professional sports to optimize movement. Recently, it has seeped into amateur athletics as well, such as high school runners (Roan,

2007). Video analysis is commonly used for most applications. Dynamic (force) data as well as kinematics (motion) data are often used for sports applications, although kinematics data alone is widely used as well. Muscle EMG data is rarely collected. The sports analysis market is relatively small, catering mainly to professional athletes and teams, but may grow in the future if the price of such services goes down.

Ergonomics/Industrial Design

The ergonomics and industrial design markets use motion capture and force measurement technologies (especially pressure mapping systems) to analyze ergonomics of product designs. This market size is potentially large, catering to product design firms and manufacturers of consumer goods.

3.3 Technology Transferability Between Markets

This section analyzes how transferable technologies developed for commercial applications are to gait analysis in the medical market.

3.3.1 Market Overlaps

The entertainment market (motion capture for video games and films) is the largest market for these technologies, so any gait analysis technology applicable to this market will likely be advanced through industry alone. Motion capture systems, but not force plates or EMG, are used in the entertainment market.

Force plates are used in engineering as a whole, which likely drives their advancements. Similarly, pressure mapping systems technologies are used in the ergonomics/industrial design field as well as in general engineering applications, such as single sensor elements in consumer electronics, consumer peripherals, and automotive applications (Ashruf, 2002). These are all large markets that drive advancements.

EMG systems are driven by other applications in the biomedical market, and these systems have matured through decades of use. Instrumented treadmills may have market applications to sports analysis, but this is unclear.

Biomechanical software is driven by applications in sports analysis, ergonomics, and engineering design generally.

These market overlaps are summarized in Table 5.

Table 5: Gait Analysis Technologies Used In Commercial Markets

Technology	Commercial Markets
Motion Capture	Entertainment (video games, film, animation)
Force Measurement: Force plates	General engineering/science Sports analysis
Force Measurement: Pressure Mapping Systems	Ergonomics/Industrial Design General engineering/science
EMG	None, but used for other biomedical applications
Instrumented treadmills	Limited use in sports analysis
Biomechanics software	Sports analysis Ergonomics General engineering/science

3.3.2 Performance requirements

After determining which gait analysis technologies are used by other industries, we now analyze the general performance requirements of these other industries to see whether the advancements they drive will be appropriate for gait analysis applications as well. This will highlight whether public policies are needed to support development of such technologies for medical applications.

As explained in Chapter 2, the main objectives of gait analyses are to *record kinematics* and to *calculate joint moments*. Additionally, a system should be easy to set-up and quick to use. These characteristics improve throughput (and therefore revenue) of gait labs. Future applications might also aim to predict muscle/tendon forces and muscle activations.

3.3.2.1 Motion Capture

Motion capture systems contribute to recording kinematics and to calculating joint moments. Regarding kinematics, the technical requirements for gait analysis are to (1) track body kinematics accurately and (2) to record the subject quickly. Regarding joint moments, the technical requirements for gait analysis are to be able to locate joint center-of-rotations accurately.

For motion capture in the entertainment market, driving applications include facial motion capture (high accuracy), movement, and digital puppetry (real-time applications). The selling points of Organic Motion's markerless system to the entertainment industry, which has drawn much attention in the animation industry, shows that accurate tracking, quick set-up, and fast calibration are desired characteristics (Organic Motion website, 2009). Thus, it appears that advancements in industry are in line with advancements needed by the gait analysis community, and public policies are not required to develop the technologies specifically for clinical gait analysis.

3.3.2.1 Force Measurement

Force measurement relates to the calculating of joint moments. Specifically, to daisy chain ground forces through the joints via inverse kinematics to determine moments, we need to know how forces are applied to the foot. High spatial resolution and accuracy are therefore desirable performance characteristics. As these are general performance characteristics, engineering and ergonomics/ID applications must have similar requirements, so again, commercial advancements are in line with the needs of the gait analysis community. Further, Sutherland (2005) writes that such systems are reliable and accurate already, suggesting that only incremental improvements are required.

3.3.2.2 EMG

As with force plates, the EMG systems market appears to be a mature market (Section 2.2.2.2), and the developments needed to make it better are the same as that required for all other biomedical applications, so public policies are not needed to develop this technology specifically for gait analysis. However, a detailed S-curve analysis could strengthen this conclusion.

3.3.2.3 Instrumented Treadmills

Instrumented treadmills have no commercial markets outside of the limited sports analysis market, but it seems reasonable to believe that improvements are not hard to come by, since instrumented treadmills combine a treadmill with a force plate. Its advancement is therefore tied to advancements in force plate technology.

3.3.2.4 Biomechanics Software

As discussed in Part I, the human body model is an integral part of accurate joint moment calculation. Also, visualization capabilities have improved rapidly with increasing computing power since the 1980s. Biomechanical software developed for the engineering, ergonomics, and sports analysis markets are interested in the same things as the gait analysis market, namely, accurately predicting forces and torques in the body. However, better methods to create accurate models used in these software do not seem to be pursued by commercial manufacturers. Rather, their focus seems to be on providing flexibility and ease-of-use to users for inputting parameters and creating models.

3.3.3 Regulatory Hurdles

Regulation of gait analysis devices is light because they are noninvasive and pose no risk of bodily harm. For example, both force measurement platforms and goniometers are classified as Class I devices (U.S. Food and Drug Administration, 2009), which do not require FDA pre-market approval or clearance, as explained in Chapter 2.

This shows that regulatory barriers are very low for manufacturers in motion capture or force measurement systems to transfer their commercial technology to the medical market. EMG systems are already marketed to biomedical markets, so the commercial to medical application barrier will already be achieved by other medical applications.

3.4 Conclusions

This analysis shows that the technical and performance requirements for gait analysis technologies are the same in commercial applications as for the clinical gait analysis market.

However, the advancement of human body models used in biomechanics software depends on improvements in our ability to acquire data for these models, which is not pursued by any gait analysis technology companies. This might involve advancements in other fields, such as medical imaging of body parts, which suggests a place where policies on research funding initiatives could advance gait analysis.

This analysis suggests that advancements driven by commercial markets are in line with advancements desired in clinical gait analysis, and public policies should therefore not be used to reimburse gait analysis solely to create a market for further technology development, nor to support development of such technologies. Public policies should, however, focus on improving the accuracy of biomechanical models used in gait analysis by funding research in this area. One technique that might address this issue is explored in Part II of this thesis.

The next chapter analyses case studies of MRI and CT Angiography to draw lessons about social, economic, and political issues relevant to clinical gait analysis. This addresses the part of our hypothesis about whether and how public policies can promote the appropriate social structures for advancing gait analysis.

4 MRI and CT Angiography Case Studies

This chapter aims to understand what political, economic, and social issues may be hindering the advancement of clinical gait analysis. It does so by analyzing two case studies from the medical imaging field: the development of MRI and the widespread reimbursement of CT Angiography. Medical imaging is a widely used, clinically accepted diagnostic. It is similar to gait analysis in its multidimensional nature, as well as its dependence on a reader's ability to interpret the data for effectiveness in affecting treatment outcomes positively. Comparing these imaging case studies to the status of gait analysis, we then draw lessons for how public policies can advance clinical gait analysis.

4.1 Methodology

This chapter analyzes case studies of two medical imaging modalities to draw lessons for gait analysis. We now justify our method and the cases selected, and define our areas of focus for the case studies.

4.1.1 Justification for Case Study Method

The case study method is a general research strategy that takes into account contextual factors and may use a variety of evidence, such as documents, artifacts, interviews, and observations. We believe that contextual variables regarding the clinical acceptance of MRI and CTA are important for understanding why clinical gait analysis has stalled and how public policies might help it fulfill its diagnostic potential. The case study method is therefore chosen because it is the preferred method for analyzing "how" and "why" questions about contemporary events when behavioral events cannot be controlled (Yin, 2003).

4.1.2 Justification of Cases

MRI and CTA are used as case studies because, like gait analysis, both these modalities are multidimensional diagnostics, as opposed to binary diagnostics such as pregnancy test strips. For binary diagnostics, analytical tools such as Receiver Operating Characteristic curves—which plot sensitivity vs. specificity— have been established to analyze effectiveness, while multidimensional diagnostics are more complex and the interpretation of results depends largely on readers. Also, diagnostic results can present signs of pathologies different from those initially suspected (Gazelle et al., 2005). But unlike gait analysis, MRI and CTA has been accepted and insured within the clinical community. Besides imaging's strong selling point of noninvasive anatomical examination, we seek to understand the social, economic, and political factors that brought this situation about, and what policy lessons might be applied to advancing gait analysis.

The case of MRI shows the factors that led to acceptance of this imaging modality in a wide variety of clinical applications. However, MRI arose before the evidence-based medicine movement became standard in the 1990s. The case of CTA provides a contemporary complement to the MRI case by showing how a new technology rose to become a widely reimbursed diagnostic.

4.1.3 Propositions

A case study is driven by propositions, which direct attention to issues that should be examined. This study's propositions are driven by the criticisms of gait analysis identified in Chapter 2, which are reproduced in Table 6.

Table 6: Main criticisms of gait analysis (trimmed version of Table 4)

Criticism	Specific issues	Method used to gain insight into issues
Clinical effectiveness	• Interpretation of data varies from lab to lab and clinician to clinician • Physicians and therapists don't understand the capabilities, benefits, and limitations of gait analysis • Lack of efficacy data showing that functional outcomes are improved directly due to gait analysis • Processing and transforming raw data to data valuable to gait analyst may lead to errors	Case study of MRI/CTA
Cost-effectiveness	• Gait labs are economically inefficient • Gait labs lack business structures needed to promote and sustain the field	Case study of MRI/CTA
Provides few advantages over simpler methods	• Gait analysis must offer significant advantages over questionnaires or observational gait analysis, which historical bias causes physicians to stick to	Case study of MRI/CTA
Complex results are hard to interpret	• Gait reports consist of "too many pages of text, graphs, and figures in a format not easily understood or useful to the average clinician."	Case study of MRI/CTA
Lack of cohesion within the field	• Lack of professional cohesion within the field.	Case study of MRI/CTA

Based on these criticisms, we focus on five propositions in our case studies:

(1) Clinical effectiveness may be hard or impossible to gauge for multidimensional diagnostics and so is not always held up as a barrier for acceptance and coverage of a clinical diagnostic technology.

(2) Cost-efficient workflows are necessary to promote offering of the diagnostic, and for keeping costs to payers manageable.
(3) New diagnostics must have significant advantages over previous established methods.
(4) The relevant clinical data to be examined by physicians must be presented appropriately.
(5) There must be professional cohesion around the technology.

4.2 Case Study 1: MRI

MRI, introduced in the 1980s, is one of the most recognizable medical technologies in the world and revolutionized noninvasive soft-tissue diagnosis. It provided a good complement to X-rays and CT, which imaged hard objects such as calcium in bones. However, its use has expanded to the extent where it is a default diagnostic tool. This means it may be used in cases where it provides no additional useful information, compared to simpler methods such as a physical exam. As such, the growing use of MRI has come under closer scrutiny by health assessors.

4.2.1 Technology

MRI works on the principles of nuclear magnetic resonance, wherein atom nuclei absorb energy and then relax by emitting energy in response to excitation by different frequencies. The different relaxation rates of different atoms can be used to identify molecule compositions. MRI focuses on hydrogen nuclei, which can provide knowledge about the placement of hydrogen atoms in the body, which in turn provides knowledge about anatomy in the body. The architecture of a common MRI machine is shown in Figure 10. Because of its effects on water molecules, MRI is particularly suited for visualizing soft tissues in the body.

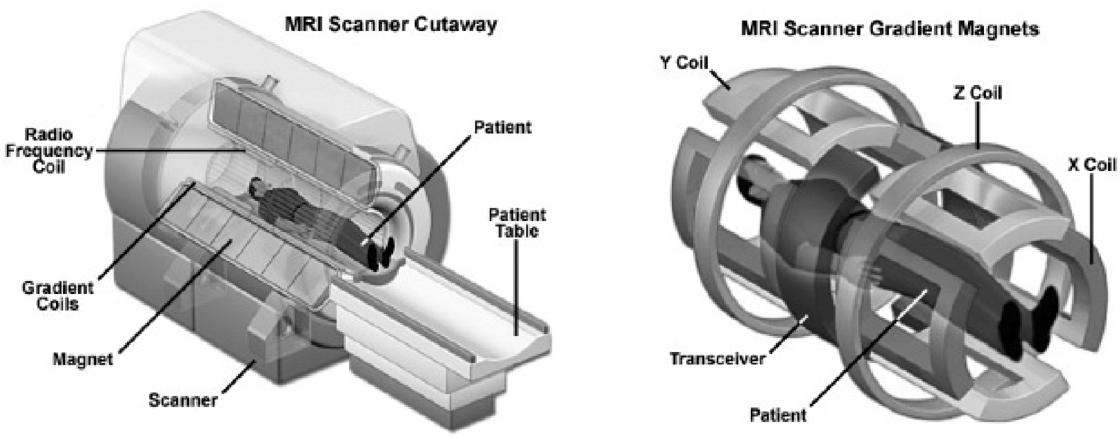

Figure 10: MRI scanner architecture (left) and magnetic coil design (right) (Coyne, 2009)

4.2.2 Social, Political, and Economic history

Joyce (2008) chronicles the rise of MRI from a social science perspective, providing a detailed account of the social, political, and economic environment from which the MRI grew to what it is today. This case study is taken mostly from her work.

MRI technology grew largely from the work of American physician Raymond Damadian, American chemist Paul Lautenbur, and British physicist Peter Mansfield in the 1970's. Damadian experimented with using NMR to diagnose cancer, publishing a paper in *Science* and filing a patent issued in 1974 that described a full-body NMR scanner based on his findings. Damadian's article interested many researchers, including Leon Saryan at NMR Specialties in New Kensington, Pennsylvania. Chemist Paul Lautenbur, who also worked at NMR Specialties, observed Saryan's research and imagined different uses for the information produced by NMR. He was particularly interested in how normal tissue relaxation times differed and thought that this information could be used to produce anatomical pictures, which he called "maps" of the inner body. Lautenbur's innovation was to propose using a gradient, which was a coil that created a second magnetic field in addition to a large magnet. Lautenbur's 1973 paper in *Nature* advocated using anatomical pictorial representations of NMR data. During the same time, UK physicist Peter Mansfield also proposed using NMR to provide spatial information of inert matter such as crystals. Mansfield and a colleague, Peter Grannel, published their ideas in *The Journal of Physics C*. While presenting his ideas at a conference, Mansfield heard about Lautenbur's work.

The work of Damadian, Lautenbur, Mansfield, and colleagues sparked a drive in the 1970s to create a viable medical technology. Two areas of contention existed, however: what to name the technology, and whether to produce only pictorial information from NMR data or to include numerical data as well. Many scientists, particularly those working in physics and chemistry, thought numerical values were as or more important than the graphical information produced, so they included these in their publications as well. A related problem was how to present the graphical information. Some researchers--influenced by the colorful pop art of the time—used bright colors that mimicked Warhol paintings. By the end of the 1970s, research teams had settled on naming the technology "NMR imaging."

NMR imaging entered clinical practice in the 1980s, but there was controversy over which medical specialty should control the technology. It could have been placed in nuclear medicine departments, where experts were trained to read detailed numerical information. But at the same time, NMR also produced anatomical pictures, so it could be placed in radiology departments as well. Radiologists specialize in anatomical image interpretation. Although many people had reservations about placing it into radiologists' hands (because radiologists were biased towards images and so would ignore the biochemical information), NMR eventually became part of radiology in many countries.

Institutional changes in radiology and medicine contributed to this outcome. Professional radiology organizations, such as the Radiological Society of North America (RSNA) and the American College of Radiology (ACR), grew rapidly in the 1970s. These organizations took advantage of their growing membership and actively lobbied for control over imaging interpretation. Further, radiologists in the U.S. were gaining greater independence in the early 1970s. The ACR, for example, urged radiologists to "gain independent practice status in their hospitals," which allowed them control over their fees and income. After some resistance, the American Hospital Association (AHA) accepted this demand and, due partly to ACR's lobbying efforts, gave up trying to pass legislature allowing the AHA to regain control over radiology.

During the same period, the appearance in medicine of many other new imaging modalities such as CT and ultrasound also increased the range and expertise of radiologists in image interpretation. Economics also played a role, as the high cost and large size of NMR machines meant that private physicians would not purchase the machines, leaving it up to hospital radiology departments to purchase and utilize them.

The placement of NMR into radiology departments shaped development of the technology in several ways. First, data presentation became entirely image-based, meaning that numerical NMR values were ignored. Second, data appearance was changed to grayscale, since radiologists were used to such images from x-rays and CAT scanning. Third, the word "nuclear" was dropped from the name, and NMR was renamed MRI. This came about because of the anti-nuclear power plant and nuclear weapon movements of the 1970s and the Three Mile Island incident, which biased public opinion against anything associated with nuclear.

4.2.3 Effectiveness and Advantages

FDA requires MRI equipment manufacturers to show that their machines visualize body parts to a certain degree of accuracy (i.e., resolution). Manufacturers also provide detailed information of the algorithms used and other technical information as part of the approval process. MRI devices are classified by the FDA as Class II devices. Manufacturers do not have to compare their techniques to preexisting ones in clinical studies to prove that they produce better results in order to gain FDA approval. After FDA approval, no other government agencies require efficacy studies. However, the Agency for Healthcare Research and Quality (AHRQ) does fund research to examine health care costs, quality, and outcomes. Other agencies and NIH also provide grants for efficacy and outcomes research, but none of these evaluations are required as is done with pharmaceuticals.

Proponents who argue that MRI is used extensively because it's the "best technology" suggest that its use leads to better diagnostic accuracy and treatment outcomes. But Joyce points out that studies comparing MRI to other diagnostic techniques show that while imaging improves diagnostic confidence in specific cases, it doesn't always improve diagnostic quality or health outcomes for patients in all its current applications. For example, some studies show that MRI does not produce the most effective or cost-effective information in diagnosis of many common shoulder and knee muscle problems, suggesting that a combination of patient histories and physical exam techniques provide more accurate information in these cases. In some cases, MRI appears to at best replicate the information already gained through other means.

This shows that proving effectiveness is not required for the medical community to embrace a diagnostic technology. Related to this issue is that for specific applications, MRI doesn't require significant advantages over other simpler techniques (such as a detailed physical exam or questionnaire) to warrant its use.

4.2.4 Economics

Insurance companies generally pay between $400 and $600 for typical MRI exams without contrast agents, and imaging units can do one to three exams per hour (Joyce, 2008).

4.2.5 Work Practices

The MRI workflow can be divided into two parts: imaging, which is the physical act of acquiring images, and image interpretation, which is the reading of images by radiologists.

4.2.5.1 Imaging

Joyce points out that imaging is structured like many assembly-line occupations in its emphasis on repetition and specialization. Specifically, the process begins with the technologist interviewing the patient to discover if there are any safety or health hazards, then by her positioning the patient in the machine, acquiring images (which typically lasts 20 minutes), releases the patient, and sending the images to a radiologist for review. Faster throughput increases volume and hence revenue, which is especially important for private imaging centers whose sole activity is patient scanning.

The emphasis on throughput permeates other design aspects of the medical imaging room as well. For example, computer screens are often positioned away from patients as they exit the imaging room to prevent them from stopping to view images and thereby slowing the workflow.

4.2.5.2 Image interpretation

The room where radiologists interpret MRI examinations is called the reading room. Here the radiologist reads the image to a transcriber, who edits the radiologist's verbal recording into a written report. Patients never interact with radiologists. Joyce also compares the radiologists' workflow to an assembly line. In large hospitals, they may sit side-by-side in a reading room, speaking into a microphone. In smaller centers, they usually work alone and may sometimes call technologists on site or another physician if unsure about a scan. Radiologists typically specialize on some modality, though they will read images from many anatomical parts. In larger sites, radiologists may specialize on one imaging technique and one anatomical area.

4.2.6 Analysis

We draw several lessons for clinical gait analysis from this case study of MRI.

First, the history of MRI shows that data presentation is tied to ownership of the technology. How information is presented is important, and this in turn relates to interpretation expertise. Specifically, radiologists specialized in reading black and white X-rays and so manufacturers changed their image output to mimic this, even though MRI images could be any color. Related to the movement of MRI machines into radiology departments, the case study shows how technology ownership leads to professional cohesion around it, and how these professional organizations can then push manufacturers to design machines in a ways that suit them better.

Second, we found that new diagnostics don't necessarily need to have significant advantages over previous methods in specific applications to be used widely and reimbursed. This may stem from the fact that multidimensional diagnostics sometimes pick up signs of pathologies besides the one being focused on. Related to this, the case of MRI shows that shows that effectiveness is hard to gauge (e.g., radiologist interpretation of images is often subject to errors as well), so lack of proof of effectiveness is not necessarily a barrier to clinical acceptance and reimbursement.

Third, we found that MRI developed efficient workflows, which has allowed it to handle larger volumes of imaging procedures and retain large profits. The completion of a scan in 20-30 minutes and the assembly-line structure of the MRI exam room and radiologist reading rooms contrast sharply with the practice of gait analysis, which takes 2-3 hours per patient and has the same 2-3 specialists performing the test and interpreting the results.

4.3 Case Study 2: CT Angiograms

CT Angiography (CTA) became practical in the early 2000s due to advances in detector technology and computing power. CTA provides a complementary case study to MRI because it arose in the evidence-based medicine era, is of unclear effectiveness, and poses radiation dangers, yet nevertheless gained wide clinical approval and coverage. Advocates of CTA believe that it reduces the need for more invasive and expensive methods such as conventional angiograms, which involve threading a catheter through arteries. Critics counter that the benefits of CTA are limited and that the costs and safety risks may be significant.

4.3.1 Technology

CT works by synthesizing X-ray images from different angles into a 3D image. Its most basic form, shown in Figure 11, works as follows. A motorized table moves the patient through the imaging system while an x-ray source concurrently rotates within the circular opening, with a set of x-ray detectors rotating in sync at the other end of the patient. The x-ray source produces a narrow, fan-shaped beam that ranges in width from 1 to 20mm. The figure shows only one row of detectors, but current machines have many rows of detectors side-by-side to allow simultaneous imaging of many slices, which reduces scanning time. After scanning, the data are then processed by computer to produce image slices that represent 3D views of the target regions (Brenner & Hall, 2007). Scanning with modern CTA scanners takes about 12 seconds (Berenson & Abelson, 2008).

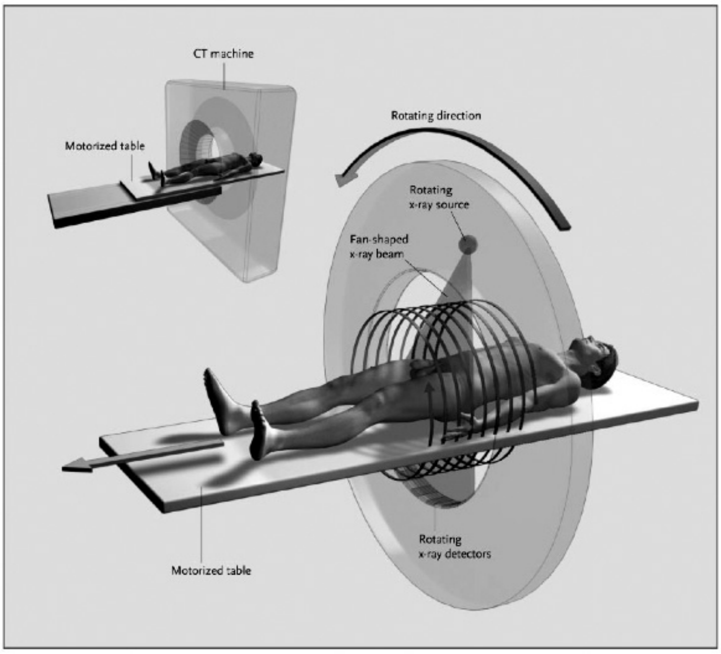

Figure 11: CT Technology (Brenner & Hall, 2007)

4.3.2 History

Although Computed Tomography (CT) was first introduced in 1972 for brain imaging, CTA did not develop until the late 1990s, when scanning and computational technologies had advanced enough to make this feasible for general clinical use.

The first CT scanners required hours of scanning time and days of computation for each slice (a "slice" being a 2D image that represents a certain volume thickness). By the 1980s, scans were still performed slice by slice but computation had become faster. Helical CT scanners were introduced in the early 1990s, consisting of a slip-ring mechanism that allowed the x-ray tube/detector array to rotate continuously while the patient was moved inside the scanner. This sped up scan times, but helical scanners were still too slow for many CTA applications, meaning that with single-detector CT's, one had to use very thick CT slices in order to scan quickly. Such thick slices gave poor resolution. New X-ray tube technology was also introduced during this time that could withstand the heat generated during continuous X-ray production. By the late 1990s, scanners consisting of multiple rows of detectors were introduced that allowed many images to be acquired during one helical revolution. This sped up scan time and also allowed the scanning of long segments of the body using acceptable volumes of intravenous contrast. CTA scanning was now practical, though analyzing and synthesizing the large numbers of images generated still required an expensive workstation solely dedicated to 3D image manipulation. By the early 2000s, workstation technology had further advanced, and the number of detectors per scanner had also increased, finally making CTA a clinical reality (Dolmatch, 2005).

By 2005, 64-row scanners came to market, sparking great enthusiasm for CTA. Larger numbers of physicians began purchasing CTA machines and performing tests in-house. By 2007, Medicare had become concerned about CTA's rapid adoption despite "lack of clinical evidence to demonstrate improved patient outcomes" (Appleby, 2008). Key questions Medicare had about the technology included whether CTA was an advance over cardiac catheterization or simply an add-on test, which patients benefited the most from CTA, and whether CTA saved lives. Under Medicare rules, Medicare has to reach a national coverage decision about a new technology when it receives requests from its own staff or the public that is deemed legitimate. Alternatively, new procedures and technologies can be used without such a coverage decision if Medicare's local contractors allow it and agree to pay for it. By 2007, all local contractors in the U.S. were paying for CTA. This meant that Medicare could only slow adoption of CTA by reaching a national coverage decision to pay for CTA for a limited patient group. Additionally, CMS also proposed that patients receiving CTA be enrolled in clinical trials aimed at determining the procedure's effectiveness relative to catheterization (Appleby, 2008).

CMS's limitations led to protest from physicians, specialist groups, and manufacturers. The Society of Cardiovascular Computed Tomography, an organization of 4,700 specialist physicians, strongly opposed the limitations. It and other specialty societies, such as the American College of Cardiology and the American College of Radiology, began a letter-writing campaign to block CMS's decision. Manufacturers of CT scanners such as GE also urged Medicare not to enact the limitations (Appleby, 2008). The specialist organizations and other prominent medical groups consisting of physicians who performed scans began lobbying CMS and members of Congress. Among the many arguments they made were that CMS ignored some studies showing the benefits of CTA and that Medicare had agreed to pay for other tests such as mammograms without requiring proof that they improved care. They argued that new technologies need time to prove themselves. Eventually, about a dozen senators and 79 representatives supported the opposition of Medicare's limitations (Berenson & Abelson, 2008).

Medicare eventually allowed CTA to remain covered for a wide range of patients under rules set regionally by Medicare's intermediaries and carriers, i.e., the insurance companies that process Medicare claims (Appleby, 2008). Industry consultants believe that since Medicare has agreed to pay for CTA tests, commercial insurers will start doing so as well (Berenson & Abelson, 2008). Additionally, there is reason to believe that media attention may have contributed to enthusiasm for the technology by physicians and patients as well. Such media names as Oprah Winfrey and Matt Lauer of the *Today Show* have promoted the technology, and *Time Magazine* even put CTA on its cover next to the title, "How to stop a heart attack before it happens" (Redberg, 2007).

4.3.3 Regulation

As with MRI machines, under FDA regulations, CTA scanner manufacturers must certify only that they are safe and provide accurate images (technical accuracy). (Berenson & Abelson, 2008)

4.3.4 Economics

CTA scans are billed at $500 to 1,500 (Berenson & Abelson, 2008).

4.3.5 Controversies Regarding CTA

There are several major controversies regarding the use of CTA. First is the economic incentive for physicians to increase the number of scans performed. Since physicians and hospitals own many CTA scanners, they have an incentive to perform scans in order to recoup the costs. For example, industry consultants estimate that about 3,000 CTA tests need to be performed to pay off a scanner. Even ignoring the economic incentives, just having a CTA scanner nearby likely makes physicians more willing to send patients off for a test since it is convenient.

Another controversy is that CTA scans may cause more harm than good because the radiation from CTA scans increases cancer risk. This risk is made greater if scans are done repeatedly, such as on an annual basis in order to track the progression of arterial blockage.

Also, CTA is often used in combination with other diagnostic tests, such as nuclear stress tests, which creates a layering of diagnostic tests, thereby further increasing medical costs with unclear benefit. Critics also argue that if a CTA scan finds plaque that a physician intends to stent, a conventional angiogram (requiring threading of a catheter) will still be necessary to determine how to implant the stent, so CTA does not always eliminate the use of conventional angiograms.

Additionally, some cardiologists believe that by age 50, most patients will have arterial plaque visible on CT scans anyway, so findings of this by a CT scanner aren't particularly useful. To be more useful, these cardiologists believe that CTA must tell whether particularly blockages are likely to rupture or to significantly reduce blow flow to the heart.

So far, various studies have presented mixed results about CTA's effectiveness in diagnosing heart disease, and no conclusive evidence exists that CTA leads to life-saving treatment (Appleby, 2008). However, the technology may one day prove useful—for example, by determining which arterial plaques are stable and which are likely to rupture—and not reimbursing them may stifle growth and innovation (Berenson & Abelson, 2008). Holding back the technology therefore has costs, and Harvard Business School economist Regina Herzlinger remarks that unless a technology is used, ways to improve it are unlikely to be discovered (Appleby, 2008).

4.3.6 Analysis

The case of CTA is significant because CTA emerged in the era of evidence-based medicine, which was supposed to encompass stricter standards for acceptance and reimbursement of a technology, and because of it involves radiation safety risks. Several key issues are highlighted by this case.

First, the case shows how the media, lobbying, and interest groups can affect Medicare's coverage decisions. As discussed earlier, the formation of physician interest groups centered solely around the technology created strong pressure on Medicare to relax its restrictions on CTA use. Further, the media touted CTA as the next big thing, which likely made the public and physicians favorable towards the technology.

Second, it shows how evidence of effectiveness (and maybe even safety) is not required for a diagnostic to be accepted, as long as there is enough physician enthusiasm for a technology.

Third, it reiterates the clinical obsession with visualization, as several physicians quoted in the sources remarked that they were won over on the technology after viewing their first CTA images.

Finally, it emphasizes the importance of ownership of a technology, as well as the creation of efficient workflows.

4.4 Case Study Conclusions

Comparing MRI and CTA to gait analysis shows that gait analysis lacks the visual "wow" factor that physicians get when viewing medical images. Gait analysis results are presented in lengthy reports with many tables and plots. Medical images also come with reports and annotations, but one can also look at the image itself and see many key issues without reading a text.

How this "wow" factor comes about relates in large part to what the stakeholder group that controls the technology is used to seeing. For radiologists, it was black and white images. For the orthopedic surgeons and physical therapists that use gait analysis, it may be 3D models of the body, or it may be something else. For gait analysis to have an impact clinically, it must first impress these experts, and then organizational structures must be set up to make the diagnostic process efficient and for groups that support the technology to have a voice in medical policymaking.

Although public policies cannot directly set up appropriate institutional structures, it can fund further research that links gait analysis technology engineers to clinicians who might find it useful. This latter group might not be limited to physical therapists, physiatrists, and orthopedic surgeons. Specifically, such projects should focus on how such experts want to view the information, and how the technical data could be best presented to them. With greater enthusiasm for the technology and with technological improvements sparked by the commercial markets that allow for faster workflows, gait analysis might become a clinically reimbursed tool, even if rigorous effectiveness data does not exist.

Although gait analysis may appear to be an expensive diagnostic, a simple analysis of its cost to payers shows that it is comparable to medical imaging, despite its inefficiencies. This suggests that future technological and workflow improvements could make it a cheap diagnostic procedure compared to imaging. If it alters treatment at a low price point, it may be a very cost-effective diagnostic. Though imaging procedure costs vary widely depending on body part scanned and where the scanning takes place, average values for each modality are available from National Imaging Associates (Abelson, 2004). Gait analysis costs for 2D video-based without ground force plate and 3D marker-based with ground force plate systems are also compiled (Roan, 2007; Stanford School of Medicine Human Performance Lab, 2008). Figure 12 shows these costs. Note that these values are from payment data and not from charges listed on bills for insurers, which are generally much higher and which are negotiated by insurers to these lower payment amounts. Note also that these values do not include insurance reimbursement, which generally cover all or most of the costs of MRI, CT, and PET scans. For example, Massachusetts insurers generally pay providers between $500 and $1,400 for an MRI scan (Kowalczyk, 2004).

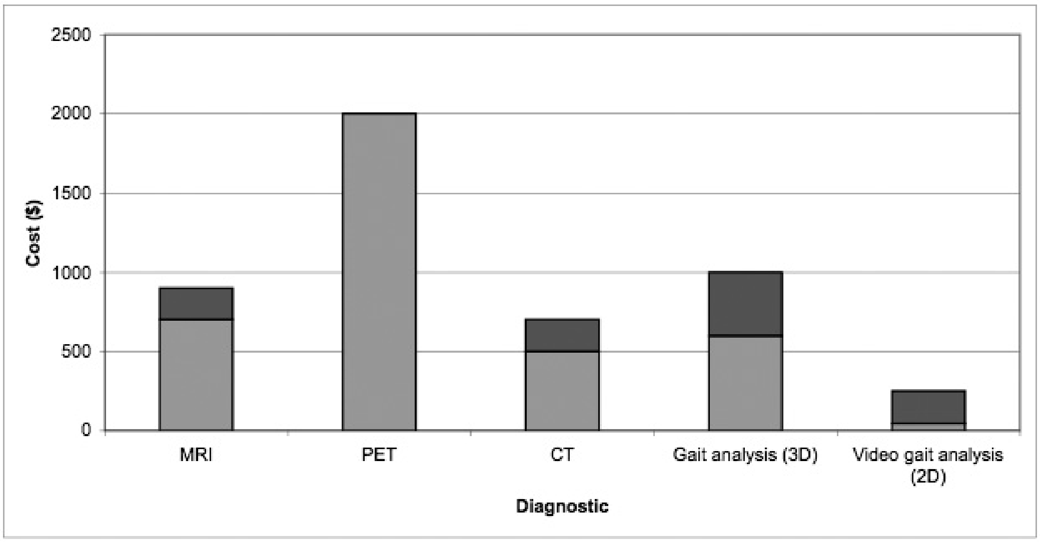

Figure 12: Average range of payment costs for several imaging and gait analysis procedures, not including insurance reimbursement (colors represent range of costs, with darker regions signifying the low to high range)

One can see that 3D gait analysis is about the same price as an MRI or CT scan. However, most insurers do not cover gait analysis, making it much more expensive to the patient than imaging procedures. Even the cost of a simple 2D video gait analysis procedure can cost more than what a patient pays out-of-pocket for an imaging procedure. This cost data suggests that gait analysis may dramatically reduce in price as the technologies and workflows improve, making it a relatively cheap diagnostic and therefore more favorable in Medicare’s view.

The next chapter analyzes data standards used in gait analysis and compares them to DICOM, the standard used in medical imaging to learn whether public policies can improve data sharing. This addresses our hypothesis about whether and how public policies can promote the appropriate data standards for advancing gait analysis.

5 Data Standards and Part I Conclusions

Data standards are vital for the effective interchange of medical information. For example, effective implementation of DICOM standards and protocols in medical imaging helped the field advance rapidly. In gait analysis, sharing of data is often difficult because of differences in data acquisition methods. The Gait and Clinical Movement Analysis Research committee points out that “not enough work has been done to develop procedures for sharing…[which] can limit understanding, interpretation, and presentation of results” (Gait & Clinical Movement Analysis Society, 2008). This chapter presents a high-level examination of data standards used in gait analysis with respect to DICOM and focuses on how public policies can address this issue.

5.1 Scope

This research focuses only on data standards for gait analysis, which addresses the criticism that it is hard for gait labs to share data. It does not focus on protocols used to capture gait data or on other operator workflows.

5.2 Methodology

We perform a high-level examination of current gait analysis data standards to determine their strengths and weaknesses. Then, we compare these standards to the DICOM standard used in medical imaging to draw conclusions on how public policies can improve gait analysis data standards setting.

5.3 Background on Technical Standards and Protocols

Standards are required for efficient exchange of data between labs, clinics, and physicians. The U.S. standards system is unique in the world in two main ways: (1) standards-setting is voluntary and done by the private sector, and (2) the standards-setting environment is diverse, encompassing about 600 organizations and consortia (Mallet, 1998). This contrasts with the government-centralized standards setting processes of the EU and places constraints on how one can use policies for standards setting. One advantage of the U.S. setup is that standards may be set faster and more appropriately for each field. A disadvantage is that appropriate standards may not be set in the case of public goods, such as health care.

Issues that can arise without proper data standards include individual manufacturers investing effort to create unique formats, lack of legacy, and a heavy burden on users to understand a large number of formats and how they interact. Standards allow the testing of similar products to compare performance, and they give users confidence that products conform to a minimum level of performance. Standards benefit manufacturers by providing them greater realization of network effects, and they protect buyers from stranding. However, standards may also constrain variety and innovation. Under incompatible standards, firms will compete for the market, each hoping that its standard will dominate the market. Under compatibility, firms will compete within the market along other dimensions, such as price, product features, and service (Shapiro, 2001). However, proprietary standards can give firms competitive advantages that hinder cooperative standard setting.

5.4 Gait Analysis Data Standards

Gait analysis data includes motion capture data, force data, and sometimes EMG data. Any data standard must store these data types, as well as patient information and settings used in capturing the data.

Two main types of data formats can be considered in gait analysis. The first is raw data captured from devices, which is then processed in some way. The second is the skeletal model file used to calculate joint moments and angles. This skeletal file contains a predefined skeleton (rigid-body linkage) software model with specified joint constraints and ranges of motion that is then scaled to the subject and used to determine joint angles from collected motion-capture position data.

Optical data generally has to processed before data is available, while magnetic and mechanical systems can be analyzed in real-time (Gleicher, 1999). Organic Motion advertises that its markerless system is capable of real-time response as well, though, as mentioned earlier, such systems still have not achieved the accuracy required for gait analysis applications.

5.4.1 Motion Capture Standards

We focus our analysis on motion-capture data formats, since force and EMG measurements are straightforward to analyze and only involve a few measured variables, whereas motion capture data is more complex.

The two main types of motion capture data are translational data and rotational data. Native data captured by different types of system will differ, however, which may require different data processing routines to create another data type—typically joint angles. For example, translational data is captured natively by optical systems, rotational data is captured natively by mechanical systems, and both translational and rotational data are captured natively by magnetic systems. The most commonly used formats for motion capture data are C3D, ASF/AMC, and BVH (Kitagawa & Windsor, 2008).

5.4.1.1 Major formats

The major formats used for motion capture applications are discussed below.

A. Optical Marker Raw Data Formats

A.1 C3D

C3D was originally created to store both raw camera information during tests as well as the marker motion derived from it. Oxford Metrics, now known as Vicon Corporation, chose to use C3D as its file format for marker data (Gleicher, 1999). C3D is designed as a flexible format that can be used to store a variety of data in a single file for gait analysis. This is appropriate because it was designed for gait analysis applications. C3D stores two types of measurement data: positional information (i.e., 3D coordinates) and digital analog information (data from force plates, EMG, etc.), both synchronized by frame. C3D also accepts parameter data, which is other information about the data. These include measurement units and database information such as patient name and diagnosis. To share this data, however, users must agree to use the same names for labeling data, which C3D does not specify (Motion Lab Systems, 2008).

A.2 Adaptive Optics AOA format

The AOA format is a tracker format that describes a set of markers and their position at each sample time. It was developed by Adaptive Optics, a motion capture hardware company (Gleicher, 1999).

A.3 Motion Analysis TRC format

Motion Analysis Corporation developed TRC to store raw data from its full body optical motion capture systems, as well as for use as the output format in its real-time face tracker software. Marker position is stored as global coordinates (Gleicher, 1999).

B. Skeleton model/motion data

The main skeletal model/motion data formats are ASF/AMC, BVH, and HTR. OpenSim, a research consortium funded by NIH and based at Stanford University, has created its own XML-based format as well.

B.1 ASF/AMC

Acclaim—a defunct video game company whose name is now owned by another company—created its own data formats for optical motion capture. The Acclaim format is unique because it separates the skeletal file from the motion file, the rationale being that the same skeleton is often used for many different motions. ASF (Acclaim Skeletal File) contains information about the skeletal model, such as units, documentation, basis pose, bone definitions, and joint degrees of freedom and ranges of motion. AMC (Acclaim Motion Capture) contains the motion data for the skeleton. One advantage of the ASF/AMC format is that files contain both global rotational data as well as local rotational data of all skeletal limb segments. Vicon adopted the format after Acclaim placed it in the public domain (Kitagawa & Windsor, 2008).

B.2 BVH

BVH (BioVision Hiearchical) format was developed by BioVision, a now defunct motion capture service company. It is one of the most popular motion data formats in the animation community. BVH format is a binary file containing skeleton and motion capture data. Advantages of BVH include flexibility and ease of editing. However, it lacks a full definition of the skeleton's basis pose. Further, there are interoperability problems because BVH format is often implemented differently in different motion analysis applications, meaning that BVH format used in one application may not be interpreted in another (Gleicher, 1999).

B.3 HTR

HTR (Hiearchical Translation Rotation) was developed as a native format for the skeleton of Motion Analysis software prior to the introduction of Acclaim's ASF/AMC format. It was created as an alternative to BVH to address BVH's shortcomings. HTR allows much flexibility in data types and ordering and contains a full basis pose specification (Gleicher, 1999).

B.4 OpenSim

OpenSim is an XML (eXtended Markup Language)-based format for storing skeletal information. XML is a specification similar to HTML used in writing web sites, but with much more markup capability and therefore greater flexibility. Each OpenSim model file defines the constraints, joints, and rigid segments of a generic skeleton in a hierarchical manner that is then scaled to the subject being measured. OpenSim was developed by Simbios, which is the National NIH Center for Biomedical Computing focusing on Physics-based Simulation of Biological Structures, housed at Stanford University. OpenSim, encompassing analysis software and standards for data sharing of gait models, is meant to provide a free, open-source platform for researchers to exchange musculoskeletal simulations (models, libraries, and scripts) (simtk.org/home/opensim). More information about OpenSim can be found in Chapter 7.

B.5 Other Raw Data Formats

Raw data formats exist for other motion capture modalities. For example, BRD format was created for Ascension Technologies's Flock of Birds magnetic motion capture system and can store data from any magnetic system. In this format, each magnetic sensor's position and orientation at each sample is stored in world coordinates. Sensors report information independently of one another, so no hierarchical information is stored (Gleicher, 1999).

5.4.2 Recommended Formats: C3D and OpenSim

Although all the formats evaluated here store gait data to some degree, only C3D and OpenSim were developed specifically for gait analysis applications rather than for entertainment applications. Both formats are also open standards, which is important for the medical community, as evidenced by the successful adoption and use in medical imaging of the open DICOM standard. This means that extensive documentation is publicly available.

5.5 DICOM

We now briefly examine the formation and overall structure of the DICOM standard used in medical imaging to see what lessons can be drawn for gait analysis data standards. DICOM can be considered a successful standard because it has been adopted as the standard in radiology.

5.5.1 Brief Overview of DICOM Standard

DICOM (Digital Imaging and COmmunications in Medicine) is a standard that specifies how medical imaging and related data are to be stored, transmitted, and printed. Its use has allowed sharing of medical imaging data captured using many different modalities.

DICOM is maintained by the DICOM Committee, an “independent, international standards development organization administered by NEMA’s (National Electrical Manufacturers Association) Medical Imaging and Technology Alliance” (DICOM PS 3.1). The Committee is divided into many working groups that perform the majority of work regarding upgrades and corrections to the standard. The DICOM Committee has no enforcement authority and manufacturers can choose to comply with however many (or none) of the standards in the 16 DICOM volumes as they please. In that sense DICOM can be considered more a guideline than a mandatory standard (Pianykh, 2008). However, all major manufacturers have incorporated the standard because radiologists demand it (DICOM PS 3.1).

Note that DICOM does not provide procedural standards about how imaging should be performed by technologists and what settings they should use when running imaging equipment; rather, it specifies only the data workflow used by the devices.

5.5.2 Brief History

In the 1970s, most radiological data was stored in analog media such as magnetic tapes. The rise of digital computers—and the fact that imaging machines at the time used proprietary standards that hindered sharing of data—led the American College of Radiology (ACR) and the National Electrical Manufacturers Association (NEMA) in 1983 to form a joint committee for developing a standard to make digital medical imaging independent of device manufacturers. The committee began by studying other standards and was particularly impressed by one used by the American Association of Physicists in Medicine (AAPM) for storing images on magnetic tape. AAPM stored information as sequences of data elements, where each element was identified by a unique name, known as a tag. The committee adopted this idea of representing data as a sequence of tagged data elements.

ACR-NEMA 1.0, the first version of the standard, was presented in 1985 and distributed at the Radiological Society of North America (RSNA) annual meeting. The committee presented ACR-NEMA 1.0 to meeting attendees as a guideline and NEMA assumed no responsibility for its enforcement or interpretation.

As ACR-NEMA 1.0 contained many weaknesses and errors, ACR and NEMA realized that the standard needed more work. To do this, ACR-NEMA created working groups—autonomous subcommittees that worked on specific parts of the standard. In 1988, the committee released ACR-NEMA 2.0, which medical imaging device manufacturers began to adopt. However, ACR-NEMA 2.0 had a major weakness: it provided limited means for communicating imaging data over computer networks. The committee soon realized that fixing this omission required a major revision.

DICOM 3.0 was presented at RSNA in 1992 in prototype form. By the 1993 meeting, a functional form of DICOM 3.0 was available. To this day, the standard is still called DICOM 3.0, and all revisions are made to this standard (Pianykh, 2008).

5.5.4 How It Works (a very high level view)

DICOM defines how devices interface, store, and transfer data within a Picture Archiving and Communication Systems (PACS). PACS are computers or networks dedicated to image storage, retrieval, distribution, and presentation. PACS interface with a Radiology Information System (RIS), which is a database used by radiology departments to handle radiological data. In turn, the RIS connects to a Hospital Information System (HIS), which is the general system (encompassing both paper- and computer-based methods) that manages administrative, financial, and clinical aspects of a hospital. Health Level 7 (HL7), is commonly the standard used in handling HIS data aspects. This workflow is shown in Figure 13.

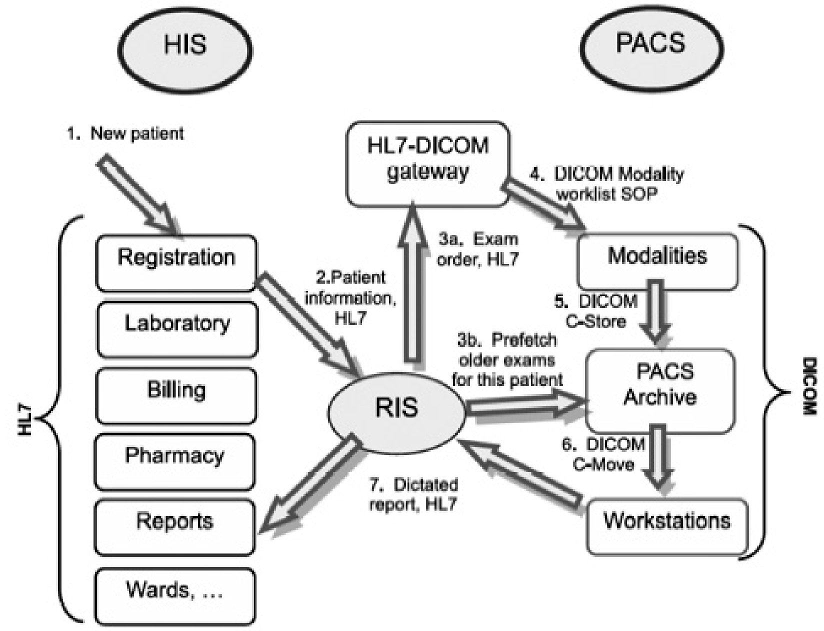

Figure 13: Typical workflow for radiological data in a hospital (Pianykh, 2008)

5.5.4.1 DICOM Information Hierarchy

DICOM can be viewed as a model of real world imaging processes: it attempts to reflect how physicians take and think about images. To do this, it uses the Patient-Study-Series-Image hierarchy (Figure 14).

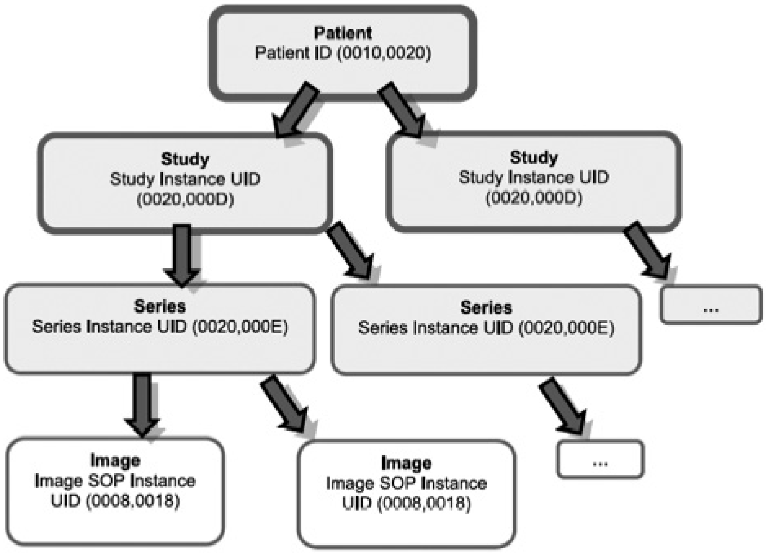

Figure 14: DICOM four level information hierarchy used to uniquely identify data (Pianykh, 2008)

This hierarchy makes sense if we imagine a patient coming to a hospital. At the top level, we want to associate all images with the patient. This patient may then have several studies performed on him (MR, CT, PET, etc.), which brings us to the next lower level. Each study may have multiple images, and these images often go together in a distinct series, such as separate CT slices that must be fused together in a specific configuration to assemble a 3D image. This brings us down to the Series level. At the lowest level, we have data for the individual 2D images. At each level, DICOM assigns universal identifiers. The four hierarchy attributes in this way uniquely identify imaging data.

These attributes used to identify data—such as patient ID, date of birth, etc.—are defined by a dictionary specified in the DICOM standards, as shown in Figure 15. This prevents confusion over naming of data elements.

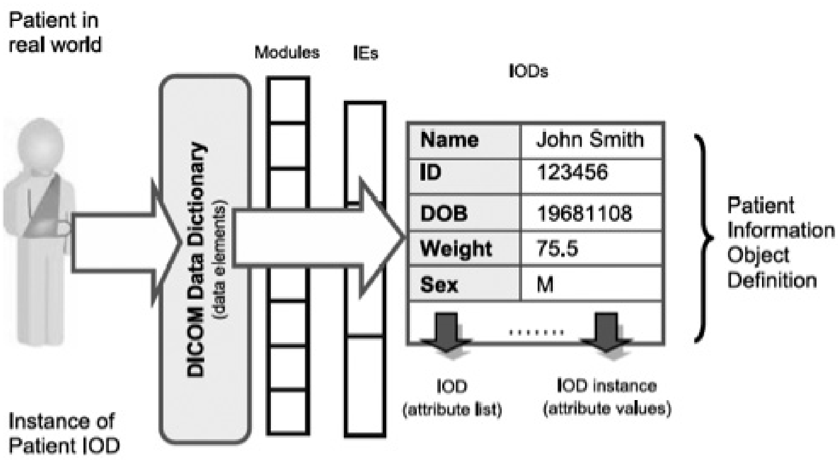

Figure 15: From Patient to Patient Object in DICOM

5.5.5 Lessons for Gait Analysis

Even after examining DICOM from such a high-level, we can see that data standards setting in gait analysis has several major shortcomings.

First, DICOM is updated by DICOM Committee working groups, and the DICOM Committee and NEMA take ownership of the standard. While standards setting by committee tends to be slow and bureaucratic, such steps are necessary to ensure that key stakeholders are represented and in agreement with the standard. As many gait analysis technologies are established, it does not seem crucial to have standards that change rapidly. In fact, the continued use of many standards long after their initial conception (and after the companies that created them had become defunct) suggests relative maturity of gait analysis standards, and current optical motion capture standards are likely applicable to new technologies such as markerless motion capture. Although C3D is an open standard, it is managed by a single company. This is unsustainable, as the standard will not adapt to technology changes, particularly if the company goes out of business. It also means there is insufficient manpower to continually update the standard.

Related to the need for an organization to own the standard is the need to update C3D or replace it if a better standard exists. This would involve studying other standard formats, both in motion capture and in other medical fields. Efforts to create gait analysis standards have been largely ad hoc, based on the needs of one company/research lab or another. In contrast, the DICOM committee used a more structured process and examined other standards of the time to pick best features. This showed much foresight, as DICOM became poised to take advantage of networking technologies when the internet emerged.

Second, C3D or some other gait analysis data standard should specify data labels, as DICOM does with its dictionary. One of C3D's "features" is its flexibility, but this poses problems for researchers who want to share data because different researchers will label different data differently.

5.6 Policy Recommendations

As standards setting is performed by non-governmental bodies in the U.S., public policies cannot directly set standards. However, policies can spur the development of organizations in charge of standards. One example of this is NIH's SIMBIOS center, which produces OpenSim and defines its data standards for skeletal models. The objective of this collaboration is to create software applications and an online community for researchers to share biomechanical models. However, OpenSim doesn't deal with the raw data capture aspects, just the sharing of models and results.

As gait analysis remains largely in researchers' hands, setting data standards through the research community would poise such a standard to be accepted if and when gait analysis enters routine clinical use. As such, the government can fund one a research institution to work on standards setting as part of their gait analysis-related research activities. Such a method could also lead to a more structured method of defining the standard if analysis of other standards used was a stipulation of funding.

The next section summarizes our overall conclusions and policy recommendations

5.7 Part I Concluding Policy Recommendations

Based on our analysis of gait analysis technologies, our hypothesis that the technologies required for gait analysis can be developed through commercial (non-medical) markets was correct. However, our hypothesis that policies should focus on fostering the professional institutions and data standards required for clinical gait analysis to be a practical diagnostic tool was incorrect, as policies cannot directly spur such developments. Only through indirect means, such as funding research into specific topics, can we support the development of organizations around gait analysis and data standards for it. This chapter summarizes the policy recommendations presented in the previous chapters.

5.7.1 Policy Recommendations

The main policy recommendations are summarized below.

Recommendation 1: Don't fund technologies

Public policies should not be used to reimburse gait analysis solely to create a market for further technology development or to support development of such technologies, as advancements and desired performance characteristics of gait analysis-related technologies for non-gait analysis applications are in line with those needed for advancing gait analysis.

Recommendation 2: Improve human body models

On a technical level, public policies should focus on improving the accuracy of biomechanical models used in gait analysis by funding research in this area and in developing technologies that can address this need. These could include cheaper imaging modalities or improved methods to acquire body measurements quickly and cheaply.

Recommendation 3: Research Information Presentation

Gait analysis lacks the "wow" factor of medical MRI or CT images. Public policies should fund further research to link gait analysis technology engineers to clinicians who might find it useful, which might not be limited to physical therapists, physiatrists, and orthopedic surgeons. Specifically, such projects should focus on how such experts want to view the information, and how the technical data could be best presented to them. Such research could be similar to that done in aeronautics regarding human information processing or in computer science regarding user interface development.

Recommendation 4: Fund a Data Standards Research Center

As standards setting is done by non-governmental bodies in the U.S., public policies cannot directly set standards. However, they can spur the development of organizations in charge of standards. One example of this is NIH's SIMBIOS center, which produces OpenSim and defines its data standards for skeletal models. The objective of this collaboration is to create a community and software applications for researchers to share biomechanical models. As gait analysis remains largely in researchers' hands, setting data standards through the research community would poise such a standard to be accepted if and when gait analysis enters routine clinical use. As such, the government can fund one a research institution to work on standards setting as part of their gait analysis-related research activities. Such a method could also lead to a more structured method of defining the standard if analysis of other standards was a stipulation for receiving funding.

5.8 Future Work

Future work could explore mobile gait analysis technologies, which can create a paradigm shift for where and how movement is measured. It could also explore how a database and data standards for movement data could be designed and funded. Detailed workflow analysis of the gait analysis process could also be performed to better understand how to improve its efficiency.

PART II: Body Segment Inertial Parameter Effects on Joint Moment Results

Part II addresses a technical issue in walking gait analysis—specifically, how we can make consistent joint moment calculations given uncertainties in body segment parameters. As explained in Part I, accurate subject-specific body models are required for consistent gait analysis results, and the lack of cheap, efficient methods for acquiring these are a major technical issue. The hypotheses and methodology of this Part II are recapitulated from Chapter 1 below.

Problem

One of the important data outputs from gait analysis is joint moments (or torques). Joint moments are important to know for two reasons. First, they can be correlated to poor biomechanics that lead to degenerative processes. Second, they can be used to compute other variables, such as joint powers and individual muscle and tendon forces (Challis & Kerwin, 1996). But difficulty arises because joint moments are not directly measured variables and must be calculated from experimental data based on additional assumptions, one of these being body segment inertial parameters (BSIPs). BSIPs consist of body segment masses, center-of-mass locations, and inertias. This technical issue limits the use of gait analysis in clinical decision-making. A detailed analysis of uncertainties in joint moment calculations due to differing BSIP values is therefore important for understanding how joint moment calculations may vary for the same subject, which can advance gait analysis's repeatability.

Hypotheses

Based on our literature review, we hypothesize three main findings:

- Joint moment estimates will be significantly different during periods of high force impact, i.e., during heel strike, but not so different at other periods of the gait cycle
- Joint moment variations will be different for different joints.
- Joint variations will be significant at some phases of the gait cycle and less so at others

Methodology

The methodology used involves sensitivity studies of forward dynamics computer simulations as well as analyses of the dynamical equations of motion. 3D forward dynamic simulations are physical simulations that track experimental gait data in order to capture data from instrumented "virtual humans." It is an increasingly popular method for studying human locomotion.

Conclusions

Part II concludes that joint moment variations resulting from different segment inertial parameters are significant at some parts of the gait cycle, particularly heel strike and leg swing. It provides recommendations on which segment inertial parameters one should estimate more accurately depending on which joints and which phases of the gait cycle one is interested in analyzing.

Overview of Proceeding Chapters

Chapter 6 reviews the biomechanics of human walking, while Chapter 7 presents our research methodology in detail. Finally, Chapter 8 presents our results and conclusions.

6 Biomechanics of human locomotion

This chapter summarizes important aspects of walking biomechanics and gait analysis. It also reviews relevant literature. Although this thesis focuses on walking because it is fundamental to physical mobility, running and other forms of gait will be alluded to at times.

Y. C. Fung, a founder of the biomechanics field, defines biomechanics as an interdisciplinary field that applies the principles of mechanics to study and address biological issues (Fung, 1993). The mechanical issues we are interested in regarding human locomotion include energetics, classical dynamics, and stability and control of mechanical systems.

6.1 Biomechanics of Walking

Human walking is marked by two distinct phases: single support and double support. Single support occurs when only one leg supports the body, and it is followed by a double support phase when both feet are in contact with the ground. At the end of the double support phase, body weight is transferred to the front leg and the rear leg swings forward, initiating another single support phase. The cycle then repeats. Walking differs from running because running lacks a double support phase (McMahon, 1984). As walking speed increases, the period of double support for each walking cycle decreases until it reaches zero for running.

Before describing the gait cycle in more detail, we first define the terms "joint flexion" and "joint extension" which are used widely in the field. *Flexion* is a movement that decreases the angle between joints, while *extension* increases the angle between joints. These are shown for the knee and hip in Figure 16.

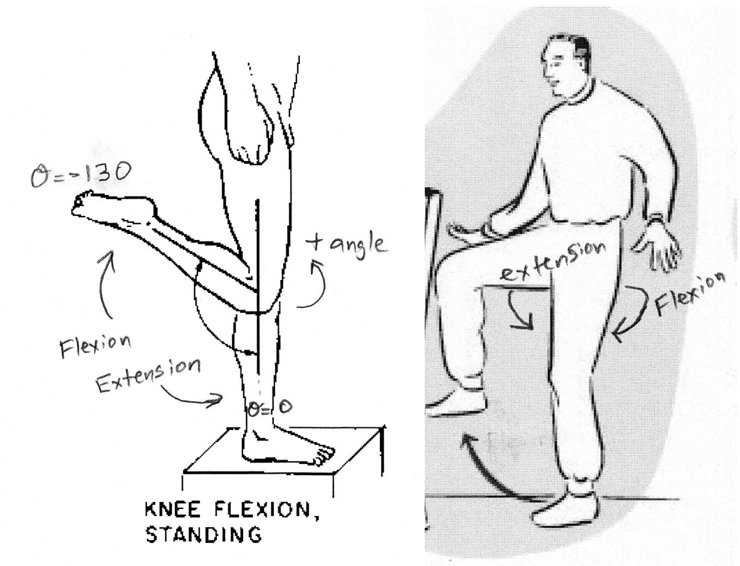

Figure 16: Example of knee flexion and extension (left) and hip flexion and extension (right)

Figure 17 presents a schematic of the walking process normalized by gait cycle. (Remember that a gait cycle is the time required for a leg to undergo both a stance phase and a swing phase.)

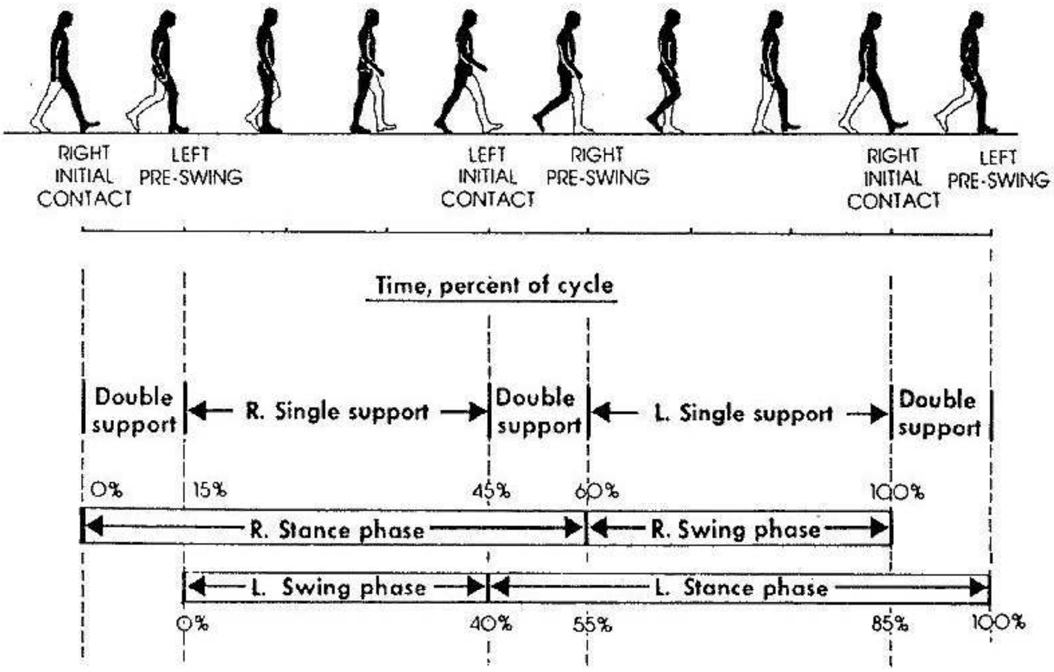

Figure 17: Phases in human walking (Inman *et al.*, 1981)

The cyclic characteristic of walking leads to three readily observable body deviations from progression of the center of mass in a straight line forward: with each step the body (1) speeds up and slows down slightly, (2) oscillates vertically several centimeters (Figure 19), and (3) weaves slightly from side to side (Figure 20) (Inman et al., 1981). Because most movement occurs in the sagittal plane (Figure 18), however, many studies approximate walking as a 2D motion. We use this fact later to justify our analysis of the 2D dynamical equations of motion rather than the 3D equations.

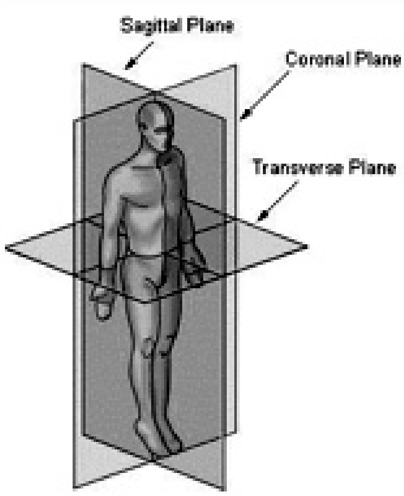

Figure 18: Body Planes (training.seer.cancer.gov)

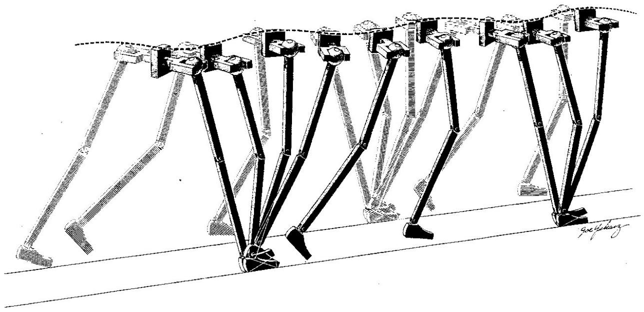

Figure 19: Vertical sinusoidal oscillation of center of mass during walking from Fig 1.12 of (Inman et al., 1981)

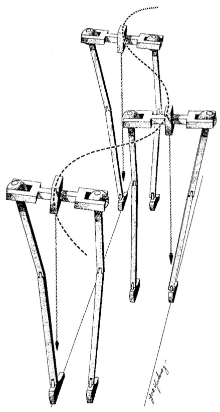

Figure 20: Side-to-side motion of center of mass during walking from Fig. 1.13 of (Inman et al., 1981)

6.2 Gait Analysis Concepts

This section presents concepts important to our analysis of gait analysis errors—specifically, rigid body dynamics, analysis methods used, sources of uncertainty, and reasons for using various body segment inertial parameter models.

6.2.1 Rigid Body Dynamics in Gait Analysis

Gait analysis approximates the body as a rigid body linkage. With this approximation, classical mechanics principles for rigid-body linkages can be used to analyze movement. Two main types of dynamic analyses are performed on gait data depending on the outputs desired: inverse dynamics and forward dynamics.

6.2.1.1 Inverse Dynamics

Inverse dynamics is used to estimate joint torques required to perform measured motions. This analysis feature is included in all commercial clinical gait system software (e.g., Vicon, Motion Analysis). In inverse dynamics, we input kinematic and ground force measurements from a gait analysis session and estimate internal joint forces and moments by summing the forces and torques on each segment. It is hard to determine muscle or tendon forces from inverse dynamics, however, because these forces are time and velocity-dependent.

6.2.1.2 Forward Dynamics Simulations

In recent years, increasing computational power and improved algorithms have popularized the use of forward dynamic simulations for gait analysis. The challenges of modeling locomotion using this method are many, but potential benefits are also great. Forward dynamic simulations allow cause and effect to be better determined, as opposed to empirical measurements in humans, which are limited because of ethical and physiological reasons. Winter states that these simulations allow researchers to ask "What would happen if…" questions (Winter, 2005).

Models can be built from scratch, but most researchers use commercial packages. MATLAB provides a SimMechanics toolbox that can be used to model various mechanical elements represented by Simulink Blocks. Commercial software specifically designed for biomechanics modeling include SIMM by Musculographics and AnyBody by AnyBody Technology. Recently, an open-source version of SIMM was released called OpenSim (Delp et al., 2007). Compared to SIMM, OpenSim has fewer model editing tools but contains features not present in SIMM. One of these is Computed Muscle Control, a control algorithm that allows the simulation model to track gait data.

6.2.2 Uncertainties in Gait Analysis Results

As mentioned in the intro to Part II, the desired outputs from gait analysis, such as joint torques and/or muscle-tendon forces, are not measured directly. Instead, they are calculated from experimental data based on certain assumptions (Simon, 2004). Assumptions made include body segment parameters and locations of joint centers of rotation. Other sources of error include skin motion artifacts, force plate measurement noise, and motion marker noise (Riemer *et al.*, 2008).

Some of these issues have been addressed. The sensitivity of gait analysis results to inaccuracies in joint center locations has been documented, and researchers such as Reinbolt and colleagues have explored using optimization routines to estimate these locations from force and kinematic data (Reinbolt *et al.*, 2007). Optical systems are sufficiently advanced that measuring marker positions is no longer a significant source of error in clinical gait analysis, (Baker, 2006), though skin movement means that marker locations on the body shift during movement, affecting the locating of joint axes. Skin motion artifacts might be addressed by the introduction of markerless motion capture systems, which integrate many visual features from a body rather than a small number of individual markers. Organic Motion recently introduced the first commercial markerless motion capture system, though such a system is still not accurate enough for biomechanical applications. Force plate measurement errors can be reduced by signal processing (Rao *et al.*, 2006). But the effect of body segment inertial parameters (BSIP's) on joint torque estimates is unclear.

6.2.3 Body Segment Inertial Parameters in Gait Analysis

Several methods have been proposed in the literature to improve the accuracy of BSIP estimates, but these methods are generally too time-intensive or costly to be practical (e.g., measuring the whole body with MRI and CT scans, or making hundreds of anatomical measurements). For this reason, researchers still rely on BSIP estimation methods generated from studies performed decades ago. Further, these BSIP estimation methods were originally created for purposes other than 3D gait analysis, such as crash dummy tests. Different BSIP estimates may significantly affect joint torque results.

One study's BSIP model may be better than another's for many reasons, such as the type of motion to be studied, how the body was divided in the study, the size and type of its subject pool, or its measurement method. Often, combinations of models are used because different studies may provide different parameters. Neptune et al.'s forward dynamics model, for example, used a gait model that had BSIPs estimated via two different models, that of Clauser et al. and that of Chandler et al (Neptune *et al.*, 2001).

Another problem with many of the predictive BSIP models proposed in the literature is that they refer to ambiguously defined segment planes, making it difficult to determine exactly how to use them in 3D gait models (Dumas *et al.*, 2007). An analysis of how variations in BSIP estimates affect gait analysis calculations of joint torques would therefore be helpful in determining which joints and which phases of the gait cycle we can be more confident of our joint moment calculations, and whether certain events during gait are associated with larger torque variations due to different BSIP models.

6.3 Literature Review

This section summarizes methods and results from past studies on the effects of body segment inertial parameters (BSIPs) on joint moment results. Studies classify the effects of BSIPs on joint moments in one of two groups: significant and not significant. For walking, however, effects may be significant for some phases of the gait cycle and insignificant at others, which is one of this study's hypotheses.

Significant Effects

Studies by Rao et al. (2006), Riemer et al. (2008), and Kingma et al. (1996) concluded that variations in body segment inertial parameters (BSIPs) had significant effects on joint torque results during inverse dynamics analysis.

Rao et al. compared results based on six different body segment parameter estimation models using a bottom-up 3D inverse dynamics approach (Rao et al., 2006). They found that both joint moment peaks (maximum magnitudes) and joint moment root mean squared values per gait cycle were significantly affected by using different models. However, they did not analyze the physics of gait to understand these effects or provide recommendations on how to address these uncertainties. The range of joint moment results estimated using different BSIP models observed by Rao et al. is reproduced in Figure 21.

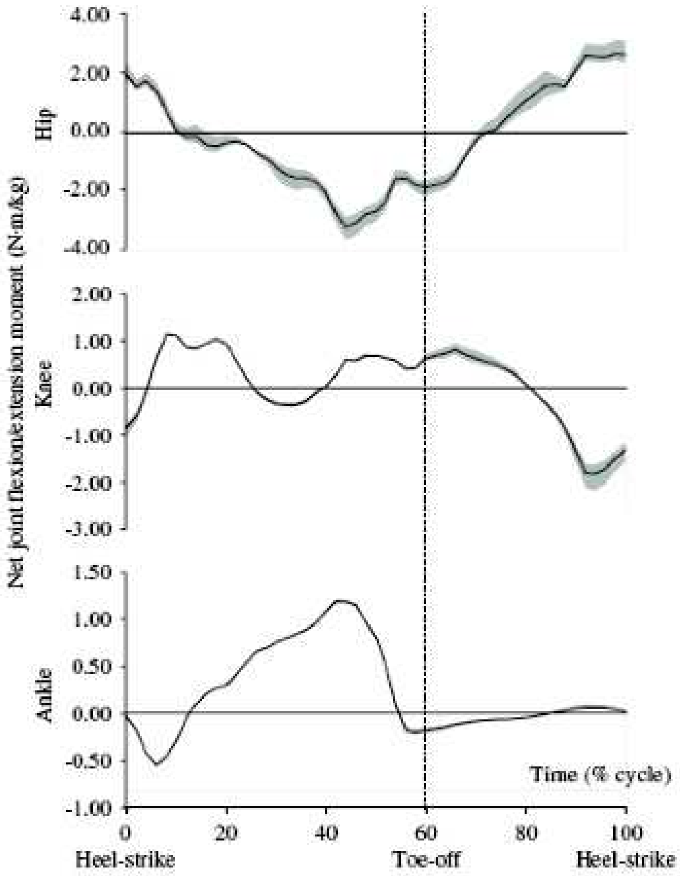

Figure 21: Mean (black line) and range of joint moments (grey) observed by Rao et al. using six different BSIP models to analyze walking gait analysis data.

Riemer et al. analyzed uncertainties in inverse dynamic solutions for one gait cycle due to body segment parameters, segment angles and skin motion artifacts, location of joint center of rotation, force plate measurements, and motion marker noise through an analytical-experimental technique. Using an equation to compute the upper bound on possible error, they analyzed a sagittal-plane model and calculated uncertainty values with respect to a nominal value calculated from De Leva's equations (Riemer et al., 2008). They determined uncertainty values from literature searches, device manuals, and experimental tests on 10 subjects. They concluded that torque uncertainties were significant, ranging from 6% to 232% of maximum torque depending on the joint, and that the major contributors to lower body torque inaccuracies were segment angles, distance from COP to ankle center of rotation, and foot mass.

Kingma et al. analyzed two BSIP models and the difference in joint torque estimations during four sagittal plane (i.e., 2D) lifting movements (Kingma *et al.*, 1996). They also performed sensitivity analyses on individual segment BSIPs to analyze their effects. Their results showed that for lifting motions, the BSIPs with the largest effects were the trunk mass and center-of-mass location, although these results are cannot be generalized to other motions. They also found that joint moments were sensitive to BSIP variations.

Small Effects

Other studies concluded that variations in BSIPs have small effects on joint moment results. However, many of these studies do not analyze gait, analyze only two BSIP models, or did not focus mainly on analyzing BSIP effects.

Andrews and Mish performed a theoretical analysis (i.e., no experimental data) to determine the sensitivity of joint moments to variations in BSIPs (Andrews & Mish, 1996). Comparing results from two sensitivity analysis methods, they concluded that for small variations in BSIPs ($\pm$5%) and smooth movements, joint moment results were not significantly different.

Pearsall and Costigan evaluated the effect of varying body segment parameters (mass, center of mass, and inertia values) on inverse dynamics moments, using the segment parameters predicted by Dempster's equations as the baseline and based on walking data from 15 subjects (Pearsall & Costigan, 1999). They compared six BSIP estimation methods based on three studies: Dempster, Clauser, and Zatsiorsky. The model they used only included leg and thigh segments, with torso modeled as a point mass. Rao et al. point out that the method used by Pearsall and Costigan neglects relationships between BSIP components, namely that masses, inertias, and com's between body segments are not independent (Rao et al., 2006). Pearsall et al.'s results showed that the effects of BSIP variations were small but statistically significant, though they only varied BSIP parameters individually.

Ganley and Powers compared BSIPs measured using dual energy X-ray Absorptiometry (DXA) to those estimated using cadaver-based regression models and analyzed the differences in joint moment results from inverse dynamic analysis of walking (Ganley & Powers, 2004). They concluded the following: (1) net joint moments were qualitatively similar using both BSIP estimates, (2) there were different effects at different joints, and (3) there were different effects at the stance and swing phases of the gait cycle. It is important to realize, however, that the main purpose of their study was to prove the validity of DXA as a way to measure BSIPs, meaning the BSIP estimates they used were similar.

Challis and Kerwin presented a sensitivity analysis procedure for analyzing joint moment estimate uncertainties due to various parameter variations, one of them being BSIPs (Challis & Kerwin, 1996). They then applied this procedure to analyze elbow joint moment estimations for a single subject performing elbow flexion while grasping a 17 kg dumbbell. Using Clauser et al.'s density estimates, they varied the density of the arm model by 5 and 10% and examined the effects on joint moment estimations, concluding that the joint moment estimations about the flexion and supination axes were largely insensitive to BSIP variations. Note that the movement analyzed was not gait and so external forces applied to the body were small.

Silva & Ambrosio investigated the sensitivity of results from inverse dynamic analysis due to imprecision in input data, such as measurement noise, and in the biomechanical model, such as BSIP uncertainties for the legs (Silva & Ambrosio, 2004). Perturbing the masses of the upper and lower legs by 0.01 kg and 1.0 kg, respectively, and applying these models to analyze gait data from one subject, they concluded that joint moments were relatively insensitive to mass variations in the lower and upper leg. However, they did not analyze effects of perturbations in center-of-mass locations or inertias, or alter combinations of BSIPs, which might cause significant changes in joint moments.

Nguyen et al. studied the effects of segment inertial parameter variations on joint moment calculations in inverse dynamics using Monte Carlo simulation and concluded that significant variability in inertial parameters did not necessarily translate into large joint moment variations (Nguyen *et al.*, 2007).

6.4 Summary

This chapter reviewed the biomechanics of human locomotion and previous research that analyzed the effects of body segment inertial parameters on joint torque calculations. The next chapter discusses the methodology used in this study.

7 Methodology for Part II

This chapter explains the methodology used to analyze how joint moments calculated from gait analysis change based on the Body Segment Inertial Parameter (BSIP) model used. Each BSIP model predicts mass, center-of-mass location, and inertia for the body segments.

The research methodology involves two parts: (1) using 3D simulations to track measured 3D gait data and performing a sensitivity analysis by varying BSIP model sets, and (2) analyzing the 2D dynamical equations of motion. The 3D simulation portion involves varying BSIP model sets for an anthropometric 3D walking model that is used to track gait data via forward dynamics simulations to estimate joint torques. Parameter model sets are defined as mass segment relations, center of mass locations, and moment of inertias for the whole body. Modifying a certain parameter (such as the mass of the thigh) alone is not realistic, since the BSIP models denote certain relationships between segment properties. The 2D dynamical equations portion involves deriving the dynamical equations of motion to gain further insight into the effects of BSIPs. 2D equations are derived and used instead of 3D equations because they provide greater clarity into BSIP effects with less complexity while still accurately representing the 3D simulation results.

7.1 Body Segment Inertial Parameter (BSIP) Estimation Models

This section describes the seven BSIP estimation models used and presents the BSIP values calculated from them.

7.1.1 Definitions

We define two key terms used to describe the research method: (1) BSIP model, and (2) model set. We use the term ***BSIP model*** to denote an estimation method such as regression equations or an algorithm used to estimate BSIP’s from body height and mass. These are the most commonly used methods to estimate BSIPs, since more advanced methods such as medical imaging are costly and/or require much greater effort to perform. We define ***model set*** to mean the set of mass, center-of-mass, or inertia relations within each model. For example, if a BSIP Model can predict mass, center-of-mass, and inertia values, then this model contains three Model Sets: a mass model set, a center-of-mass model set, and an inertia model set.

7.1.2 Descriptions of Body Segment Inertial Parameter (BSIP) Models

This study analyzes seven BSIP models. This number includes the scaled model in OpenSim that is widely used in forward dynamics studies of gait. Although other BSIP models are available, these models were chosen because they are applicable to the test subject and are widely used or have been analyzed by other researchers (e.g., (Thelen & Anderson, 2006). (Rao et al., 2006)). For example, Pearsall and Costigan analyze the BSIP model of Jensen and Fletcher (1994), but this BSIP model was created specifically to estimate BSIPs of elderly subjects and so is not applicable to the subject analyzed in this study.

The seven BSIP models represent estimates derived from a variety of study methods, including cadaver and in vivo studies, each of which has advantages and disadvantages. All but one of these models are based on U.S. Air Force studies for human factors applications

Model 1: OpenSim Model

The OpenSim BSIP model has been used in many forward dynamic studies, such as (Arnold *et al.*, 2007), (Thelen & Anderson, 2006), and (Anderson & Pandy, 2001). Inertial properties are based on the data of (McConville *et al.*, 1980) with modifications. McConville used photogrammetry and anthropometric techniques to collect data from 31 living male Caucasian subjects and develop regression equations to predict BSIPs. Photogrammetry is a technique that determines geometric properties about objects from multiple photographs. The algorithm that OpenSim uses to determine BSIPs for the subject is described in Section 7.5.1. This model provides BSIP estimates for the foot, shank, thigh, pelvis, and HAT (head, arms, torso) segments.

Model 2: Dempster (1955)

Dempster performed the first detailed study of BSIP's using cadavers. He used the water volume displacement method to measure segment volumes of living people, which were in turn used to calculate limb segment densities. He determined center-of-mass locations using a balance plate. Finally, he determined segment moments of inertia using the pendulum method, in which the investigator suspends an object from a fixed point, sets it in motion by shifting it several degrees from equilibrium, and measures the time it takes to swing for one oscillation period (Herzog *et al.*, 1999). Although segment inertias for specific subjects are provided in Dempster, no estimation models or methods are presented to allow one to scale these inertias to people of different sizes. Thus, Dempster's inertias values were not used in this study. Model 2 lumps the HAT and pelvis segments together, as opposed to Model 1.

Model 3: Clauser (1969)

Clauser used techniques similar to Dempster's but studied a different subject set. Specifically, all but one of the cadavers used in Dempster's study were unpreserved, while Clauser et al. used only preserved specimens. Clauser et al. also say that they used more "elaborate statistical analysis" than previous studies. Model 3 provides BSIPs for the same segments as Model 2.

Model 4: Chandler (1975)

Chandler et al. used similar methods as Clauser, but again with a different cadaver set. Their main criterion was physical condition, meaning they excluded specimens with such conditions as obesity, major surgery, and other anomalies. Fluoroscopy and X-rays were used to verify bony landmarks. Chandler presents regression equations for estimating moments of inertia in the principal directions (i.e., longitudinally along each segment, and along orthogonal directions to this axis). Model 4 provides BSIPs for the same segments as Models 2 and 3.

Model 5: de Leva (1996, based on Zatsiorsky-Seluyanov, 1983)

de Leva adjusted Zatsiorsky-Seluyanov's data to be relative to joint centers rather than to body landmarks. Zatsiorsky & Seluyanov's study is notable because it analyzes a large sample of living, college age individuals (100 male, 15 female Caucasian subjects). Although no other comprehensive studies have been published about the BSIP's of college age Caucasians, de Leva believes that Zatsiorsky et al.'s data is not generally preferred to cadaver data because it uses bony landmarks as reference points rather than joint centers. This model separates the pelvis and HAT segments, similar to Model 1.

Model 6: Dumas (2007, based on data from McConville, 1980)

Dumas adjusted McConville's data to correspond to conventional segment coordinate systems centered at joints. This model provides estimates for similar segments as in models 1 and 5.

Model 7: GEBOD (GEnerator of BOdy Data software)

GEBOD is a software program developed and used by the U.S. Air Force. Its original purpose was to produce human and dummy body description for the Articulated Total Body model, a software program used to simulate the motion of linked rigid bodies, such as humans in car crashes. When the user inputs subject mass and height, GEBOD outputs estimated segment masses and inertias. Center-of-mass values from GEBOD are not included in our analysis because GEBOD approximates segments as uniform ellipses with center of masses located halfway between joints, which is unrealistic. GEBOD incorporates data from McConville et al. (1980) and from Grunhofer (1975), who synthesized anthropometric data from German Air Force and US Air Force personnel. This model provides estimates for similar segments as models 1, 5, and 6.

These seven models are summarized in Table 7. The notation used to describe each model is M*X_set*, where *X* denotes the model number and *set* denotes whether it is the mass, center-of-mass, or inertia parameter set. The models are formulated such that each parameter set can be calculated independently of the others, although the relationships between members of each set are interdependent. *In theory, this means that one should be able to mix and match any mass, center-of-mass, and inertia parameter set, since they are applicable to the general population of Caucasian males!*

Table 7: Summary of the different estimation models used in this study

BSIP estimation model name	**Model 1 (M1)** M1_mass M1_com M1_inertia	**Model 2 (M2)** M2_mass M2_com	**Model 3 (M3)** M3_mass M3_com M3_inertia	**Model 4 (M4)** M4_mass M4_com	**Model 5 (M5)** M5_mass M5_com M5_inertia	**Model 6 (M6)** M6_mass M6_com M6_inertia	**Model 7 (M7)** M7_mass M7_inertia
Source	Default OpenSim BSIP estimates generated using its scaling algorithm	Dempster BSIP estimates	Chandler BSIP relations	Clauser BSIP estimates	de Leva BSIP estimates (adjusted data from Zatsiorsky-Seluyanov study)	Dumas BSIP estimates (adjusted data from McConville study)	GEBOD (Generator of Body Data software)
Segments defined	HAT Pelvis Thigh Shank Foot	HAT Thigh Shank Foot	HAT Thigh Shank Foot	HAT Thigh Shank Foot	HAT Pelvis Thigh Shank Foot	HAT Pelvis Thigh Shank Foot	HAT Pelvis Thigh Shank Foot
Method	Scaling generic OpenSim model estimated using McConville with modifications	Cadaver study	Cadaver study	Cadaver study	Gamma ray scanning of living subjects	Photogrammetry of living subjects	Algorithm Predicts BSIPs using data from McConville and Grunhofer
Study sample	N/A	8 Caucasian males age 52-83	6 Caucasian males, age 45-65	13 Caucasian males, age 24-78	100 Caucasian males, age 45-65	31 Caucasian males, mean age 27.45 $\pm$ 5.64	U.S. and German Air Force personnel
Country & year of original study	1980 (McConville), USA	1955 (Dempster), USA	1975 (Chandler et al.), USA	1968 (Clauser et al.), USA	1983 (Zatsiorsky et al.), Russia	1980 (McConville), USA	1980 (McConville), 1967-8 (Grunhofer), USA
Source	(Delp et al., 2007)	(Dempster, 1955)	(Chandler *et al.*, 1975)	(Clauser *et al.*, 1969)	(de Leva, 1996); (Zatsiorsky & Seluyanov, 1983)	(Dumas et al., 2007); (McConville et al., 1980)	(Cheng *et al.*, 1994)

7.1.3 Calculations from Models

This study calculates BSIPs using methods provided in each BSIP model. The coordinate systems used are as follows: The principal world coordinate axis is defined as shown in Figure 22, and the orientation of the principal world coordinate axis in the standing position aligns with the local x,y,z axes of each segment. For example, longitudinally along the foot is taken as the x-coordinate in the foot local frame.

Difficulties encountered in using these BSIP models include the following: segments are defined differently in each study, center-of-mass locations are defined relative to different landmarks, and moments of inertia are defined in different directions. For uniformity, all inertias calculated in this study are with respect to segment center-of-mass locations. This is the same definition used in OpenSim, meaning that the value input to the software for a segment's inertia is its inertia about its center-of-mass. Details of the BSIP calculations shown in the following tables are presented in Appendix B. The resulting values are summarized in the following three tables. Note that some models do not calculate total body mass accurately. This is the case for Chandler's regression equations (M4_mass), which calculate total body mass as 78.9 kg, whereas the experimental subject's mass was 72.6 kg.

Table 8: Segment mass estimates in kg for each BSIP model (kg)

	BSIP Model						
Segment	**M1_mass**	**M2_mass**	**M3_mass**	**M4_mass**	**M5_mass**	**M6_mass**	**M7_mass**
HAT (w/o pelvis)	33.068	N/A	N/A	N/A	35.65	35.86	35.58
HAT (including pelvis)	N/A	49.22	49.22	49.54	N/A	N/A	N/A
pelvis	11.38	N/A	N/A	N/A	8.109	10.31	9.728
Thigh	8.984	7.187	7.478	10.78	10.28	8.930	8.984
Shank	3.581	3.340	3.122	2.977	3.144	3.485	3.646
Foot	1.207	1.016	1.089	0.9146	0.9946	0.8712	0.9275

Table 9: Segment center-of-mass location estimates for each BSIP model (m)

Segment	Coordinate in opensim	BSIP Model						
		M1_com	M2_com	M3_com	M4_com	M5_com	M6_com	M7_com
HAT (w/o pelvis)	x	-0.03239	N/A	N/A	N/A	0	0.01414	N/A
relative to torso segment in model	y	0.3455	N/A	N/A	N/A	0.4531	0.4279	N/A
	z	0	N/A	N/A	N/A	0	0.0009791	N/A
HAT (including pelvis)	x	N/A	0	0	0	N/A	N/A	N/A
relative to torso segment in model	y	N/A	0.2970	0.3081	0.3119	N/A	N/A	N/A
	z	N/A	0	0	0	N/A	N/A	N/A
Pelvis	x	-0.07240	N/A	N/A	N/A	0	3.100E-05	N/A
Relative to pelvis segment in model	y	0	N/A	N/A	N/A	-5.800E-4	-0.04140	N/A
	z	0	N/A	N/A	N/A	0	-6.643E-06	N/A
Thigh	x	0	0	0	0	0	-0.01923	N/A
Relative to femur segment	y	-0.1950	-0.2036	-0.1745	-0.1845	-0.1921	-0.2012	N/A
	z	0	0	0	0	0	0.01548	N/A
Shank	x	0	0	0	0	0	-0.02040	N/A
Relative to tibia segment in model	y	-0.1846	-0.1840	-0.1575	-0.1771	-0.1895	-0.1743	N/A
	z	0	0	0	0	0	0.002975	N/A
Foot	x	0.1027	0.1042	0.1067	0.1043	0.1051	0.09092	N/A
Relative to calcn segment in model	y	0.03080	0	0	0	0	-0.03594	N/A
	z	0	0	0	0	0	0.006188	N/A

Table 10: Segment inertia estimates for each BSIP model (kg-m^2)

Segment		BSIP Model						
		M1_inertia	M2_inertia	M3_inertia	M4_inertia	M5_inertia	M6_inetia	M7_inertia
torso (not including head/arms)	Ixx	1.660	N/A	N/A	1.840	1.989	0.7794	1.942
	Iyy	0.8507	N/A	N/A	0.4546	0.5243	0.6682	0.3639
	Izz	1.612	N/A	N/A	1.299	1.731	0.8382	1.812
pelvis	Ixx	0.1042	N/A	N/A	N/A	0.1048	0.1218	0.08130
	Iyy	0.08831	N/A	N/A	N/A	0.09551	0.1341	0.09200
	Izz	0.05870	N/A	N/A	N/A	0.08415	0.1077	0.07330
Thigh	Ixx	0.1702	N/A	N/A	0.1309	0.2449	0.1653	0.1562
	Iyy	0.04462	N/A	N/A	0.02732	0.05022	0.04421	0.03650
	Izz	0.1795	N/A	N/A	0.1356	0.2449	0.1769	0.1634
Shank	Ixx	0.04757	N/A	N/A	0.04368	0.03692	0.04935	0.05970
	Iyy	0.004814	N/A	N/A	0.003590	0.006024	0.006294	0.006200
	Izz	0.04823	N/A	N/A	0.04309	0.03520	0.04935	0.06060
Foot	Ixx	0.001430	N/A	N/A	0.0008306	0.0008663	0.001426	0.0008000
	Iyy	0.003970	N/A	N/A	0.003188	0.003721	0.006756	0.004600
	Izz	0.004180	N/A	N/A	0.003321	0.003382	0.006396	0.004400

The calculated values show that there is little consistency between estimates. For example, thigh mass varies significantly between M3_mass (Chandler et al.) and M5_mass (Zatsiorsky et al.). This difference makes sense, since Chandler analyzed cadavers while Zatsiorsky et al. analyzed live subjects using gamma ray scanning. However, even BSIP models using the same study method have different BSIP estimates. For example, M1_mass and M6_mass are both based on McConville's photogrammetry study, yet they predict masses for the HAT segment that differ by almost 3 kg.

7.2 Human Body Model

The anthropometric model used in this analysis is a 3D, 23 degree of freedom model developed by Thelen, Seth, Anderson, and Delp (Delp et al., 2007). It includes feet, legs, pelvis, and a combined upper body HAT (head, arms, torso) segment and has been used in many forward dynamics gait studies. The world coordinate system is denoted below in Figure 22.

The head, arms, and torso are represented by a single rigid HAT segment that articulates with the pelvis via a ball-and-socket joint located at approximately the third lumbar vertebra. Each hip joint is modeled as a ball-and-socket joint, each knee joint as a hinge joint, each ankle-subtalar joint as a universal joint, and each metatarsal joint as a hinge joint.

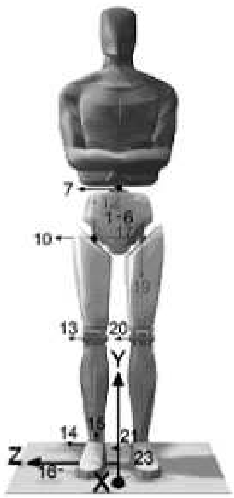

Figure 22: 3D, 23 degree-of-freedom human body model used in the analysis. (Anderson *et al.*, 2006)

7.2.1 Actuator Set

The actuator set used in the model includes torque actuators located at the knee, ankle, hip, and lumbar joints.

Additionally, actuators for "residual forces and moments" are also included to stabilize the model during walking. These are modeled as a 6 degree-of-freedom joint between the pelvis and ground (3 force actuators and 3 moment actuators). The mathematical explanation is presented here. For a perfect model of the human body, the dynamical equations can be represented in the form:

$$\mathbf{M}(q)\ddot{q}+\mathbf{V}(q,\dot{q})+\mathbf{G}(q)=\tau \quad \textbf{(1)}$$

where **M** is the inertia matrix, q is a n-vector of generalized coordinates, **V** is the Coriolis/Centripetal vector, **G** is the gravity vector, and τ are the external generalized forces, which for human gait are ground reaction forces. This equation is derived in for an arbitrary *n*-linkage rigid-body system (Lewis *et al.*, 1993).

However, when one tries to track the gait data using a model, this equation does not hold for many reasons, including measurement errors, model inaccuracies, and unmodeled dynamics such as friction. Therefore, to maintain dynamic consistency, a residual generalized force term $\boldsymbol{\tau_r}$ must be included**:**

$$\mathbf{M}(q)\ddot{q}+\mathbf{V}(q,\dot{q})+\mathbf{G}(q)=\tau+\tau_r \quad \textbf{(2)}$$

Without this residual term, the model becomes unstable and falls over soon after the simulation starts. These residual forces and moments can therefore be a crude metric by which to evaluate the accuracy of our model to the real physical system.

7.3 Gait Data

The gait data used is that of a 1.8 m tall, 72.6 kg (~67.7th percentile) Caucasian male walking at self-selected speed on a Bartec split-belt instrumented treadmill. BSIP studies have been performed most extensively on Caucasian male populations, which makes this data set particularly suitable for analysis.

The gait data includes ground force and motion capture data for approximately 14 seconds of walking and was collected by Chand John of Stanford in the facilities of Prof. Jill Higginson at the University of Delaware. (John *et al.*, 2007). It is included with the OpenSim package. A six-camera motion analysis system was used to record positions of reflective markers placed on the subject according to a modified Cleveland Clinic marker set.

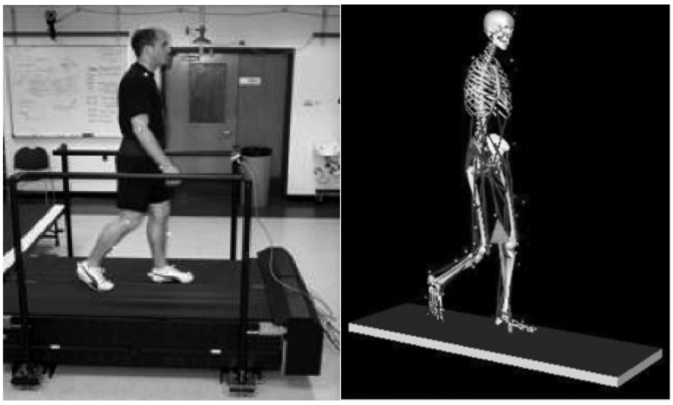

Figure 23: Gait Analysis System used (left) (Neuromuscular Biomechanics Lab, 2008) and gait data representation in OpenSim (right)

7.4 Software

OpenSim is used to create forward dynamic simulations of walking from gait data (Delp et al., 2007). It is a free, open-source equivalent of SIMM (Software for Interactive Musculoskeletal Modeling) developed by Simbios, the NIH center at Stanford University for physics-based simulation of biological structures. SIMM is widely used in biomechanics research, particularly for gait studies, and contains features for easily building musculoskeletal models by modifying anthropometry, muscle attachment points, joints, and muscle mechanical properties. Users can run simulations to track or model certain movements, which allows them to estimate muscle activation patterns and muscle/tendon forces. Physical simulations can be driven by musculotendon actuators or joint moment actuators. OpenSim uses the SimBody engine to perform rigid-body mechanics calculations.

7.5 Simulations

This section discusses the major algorithms used to run the forward dynamics simulations.

7.5.1 Scaling and Inverse Kinematics (IK) Algorithms

OpenSim performs two procedures to match the human body model to the gait data. First, it scales the model to make segment anthropometry match that of the subject, as measured by motion capture marker locations. Next, it calculates joint angles in the model that best match the experimental kinematics of the subject. These two procedures are described in more detail below and summarized in Figure 24. Greater details are provided in the OpenSim user's guide (Anderson et al., 2008).

The scaling algorithm works as follows. It begins with a user-selected generic OpenSim model with joints and BSIP parameters predefined, but not to our specific test subject. This model was discussed in Section 7.2. The generic model is scaled to match the anthropometry of the measured subject using scale factors. Scale factors for each segment are computed by comparing distances between markers on the model and experimental marker positions. Distances between markers are calculated by averaging marker distances across all frames in a user specified time interval. These scale factors can also then be used to scale the generic model's body segment inertial parameters to that of the test subject.

To calculate joint angles for each time step, the Inverse Kinematics (IK) algorithm then determines joint angles that best reproduce the subject's experimental kinematics. This is done by computing the generalized coordinate values that put the model in a configuration that best matches experimental marker and coordinate values at each time step, where the best match is expressed as a weighted least squares problem whose solution minimizes both marker and coordinate errors.

The main setup files for the scaling and IK algorithms are presented in Appendix C.

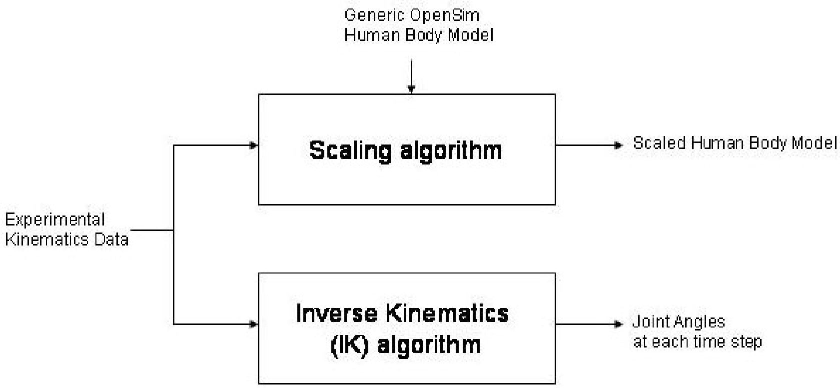

Figure 24: Scaling the generic OpenSim model and determining joint angles to match experimental data

7.5.2 Computed Muscle Control (CMC) Algorithm

After determining model anthropometry and joint angles at each time step, we performed a forward dynamics simulation using the Computed Muscle Control (CMC) algorithm to track joint angles. CMC uses PD control and optimization to find optimal joint torques or muscle activations that track the measured movement (Thelen & Anderson, 2006). Prior to applying CMC, joint angle kinematics were filtered at 6 Hz to remove high frequency noise.

CMC is designed for muscle modeling, which means it takes into account time effects. But since this analysis concerns net joint moments without time-dependent effects, CMC becomes a basic Computed Torque Controller (CTC) (Lewis et al., 1993),. CTC is a standard feedback linearization method for nonlinear systems used in robotics, and is also known as "Inverse dynamics control." The equation for such a controller is

$$\tau = \mathbf{M}(\ddot{q} - u) + \mathbf{N}(q, \dot{q}) \tag{3}$$

where **N** accounts for the Coriolis, friction, and Gravity terms
M is the inertia matrix
q are generalized coordinates
u is an user-selected input

We can represent the error between our desired trajectory and the current trajectory as

$$e = q_d - q \qquad \textbf{(4)}$$

after manipulation of the original dynamical equations for an n-segment linkage, we can represent the errors in Brunovsky canonical form:

$$\frac{d}{dt}\begin{bmatrix} e \\ \dot{e} \end{bmatrix} = \begin{bmatrix} 0 & I \\ 0 & 0 \end{bmatrix}\begin{bmatrix} e \\ \dot{e} \end{bmatrix} + \begin{bmatrix} 0 \\ I \end{bmatrix} u + \begin{bmatrix} 0 \\ I \end{bmatrix} \mathbf{W} \qquad \textbf{(5)}$$

where $\mathbf{W} = \mathbf{M}^{-1}\tau_d$ is the disturbance function.

Since input *u* accounts for the dynamics of the system, as seen from the CTC control law (equation **(3))**, by choosing *u* appropriately we can control the error without explicitly calculating the system dynamics. Control input *u* can be chosen in many ways; the most often used method is PD feedback. CMC uses a combination of PD control and static optimization, where optimization is used when time-dependent actuator behavior is modeled, such as for tendons and muscles. The main setup file used for the CMC algorithm is shown in Appendix C.

7.5.3 Simulation Inputs

Inputs for each forward dynamics simulation include BSIPs, kinematics data to be tracked, ground forces to be applied, and numerical simulations settings such as CMC tracking settings and integration steps. BSIPs were the only inputs that differed between simulation runs. Integration steps were varied to ensure they did not affect results, and kinematics of the runs were compared to ensure they were identical.

Variables, constants, and outputs for the simulations are summarized below in Figure 25. As discussed in this chapter's introduction, different combinations of model sets were used, the rationale being that modifying individual parameters (such as the mass of the thigh) is not realistic, as the BSIP models denote certain relationships between segment properties. At the same time, the model sets for mass, center-of-mass, or inertia are supposed to be generally applicable to the male Caucasian population at large, so combining different model sets is reasonable.

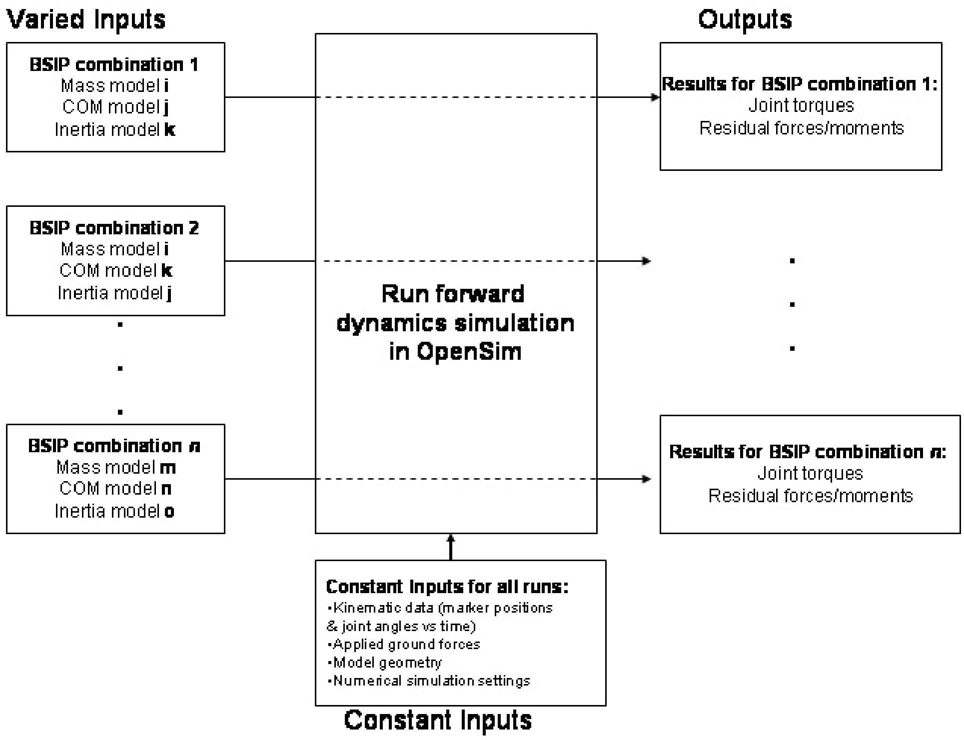

Figure 25: Summary of constant and varied inputs/outputs to simulations

Note that different studies divide up segments differently. For example, McConville separates the pelvis from the torso, while Dempster lumps the pelvis and torso together. Therefore, not all possible combinations of parameter sets are possible. For BSIP models that define parameters for less segments than are defined in the body model, the extra segments have their mass and inertia values set near zero (<1E-5 kg and m^2-kg, respectively). This was done because setting these parameters to zero causes errors, while removing the segment joints interferes with the tracking algorithm.

7.5.4 Summary

The 42 distinct simulations performed are summarized in Table 11. As can be seen from Table 7, BSIP models 2, 3, and 4 lump the pelvis segment with the HAT (head, arms, torso) segment, while models 1, 5, 6, and 7 separate these segments. This means that while the model sets (inertias, masses, center-of-mass location relationships) from Models 1, 5, 6, and 7 can be applied to Models 2, 3, and 4, the reverse is not possible. For example, finding the mass of a lumped pelvis-HAT segment using Model 1 simply involves adding the masses of the pelvis and HAT segments, but calculating the separate masses of the pelvis and of the torso from a lumped segment mass cannot be done. This is reflected in the simulation combinations performed.

Table 11: Simulations performed

Simulation number	Model Set Used		
	Mass	Center-of-Mass location	Inertia
1	M1_mass	M1_com	M1_inertia
2	M1_mass	M1_com	M5_inertia
3	M1_mass	M1_com	M6_inertia
4	M1_mass	M1_com	M7_inertia
5	M2_mass	M2_com	M3_inertia
6	M2_mass	M2_com	M5_inertia
7	M2_mass	M2_com	M6_inertia
8	M2_mass	M2_com	M7_inertia
9	M3_mass	M3_com	M3_inertia
10	M3_mass	M3_com	M5_inertia
11	M3_mass	M3_com	M6_inertia
12	M3_mass	M3_com	M7_inertia
13	M4_mass	M4_com	M3_inertia
14	M4_mass	M4_com	M5_inertia
15	M4_mass	M4_com	M6_inertia
16	M4_mass	M4_com	M7_inertia
17	M5_mass	M5_com	M5_inertia
18	M5_mass	M5_com	M6_inertia
19	M5_mass	M5_com	M7_inertia
20	M6_mass	M6_com	M6_inertia
21	M6_mass	M6_com	M5_inertia
22	M6_mass	M6_com	M7_inertia
23	M2_mass	M3_com	M3_inertia
24	M4_mass	M3_com	M3_inertia
25	M5_mass	M3_com	M3_inertia
26	M6_mass	M3_com	M3_inertia
27	M7_mass	M3_com	M3_inertia
28	M6_mass	M5_com	M5_inertia
29	M7_mass	M5_com	M5_inertia
30	M5_mass	M6_com	M6_inertia
31	M7_mass	M6_com	M6_inertia
32	M7_mass	M1_com	M7_inertia
33	M5_mass	M1_com	M7_inertia
34	M6_mass	M1_com	M7_inertia
35	M3_mass	M2_com	M3_inertia
36	M3_mass	M4_com	M3_inertia
37	M5_mass	M6_com	M5_inertia
38	M5_mass	M1_com	M5_inertia
39	M6_mass	M5_com	M6_inertia
40	M6_mass	M1_com	M6_inertia
41	M1_mass	M5_com	M1_inertia
42	M1_mass	M6_com	M1_inertia

7.6 Rigid Body Dynamics Analysis

To gain insight into the effects of BSIP variations on joint moments, we also derived equations of motion for a model of the human body consisting of Head-Arms-Torso (HAT), pelvis, thigh, shank, and foot segments using the Newton-Euler method. The derivations are shown in Appendix D. Only 2D analysis equations were ultimately desired because these forms are simpler than the 3D representation and can provide better insight into the physics. Section 8.2.1 shows that these 2D equations are well representative of the 3D situation.

The equations were all derived using the world inertial frame rather than local frames for two reasons. First, we are most concerned with joint moments, which are calculated in the absolute frame rather than joint frames. Second, this simplifies the equations greatly, allowing us to gain maximum insight into the physics.

7.6.1 3D Analysis

The 3D equations of motion are presented below:

Forces

Right Leg

$$\vec{F}_{A,R} = m_f(\vec{a}_{f,R} - \vec{g}) - \vec{F}_{Gnd,R} \quad (6)$$
$$\vec{F}_{k,R} = m_{ll}(\vec{a}_{ll,R} - \vec{g}) + \vec{F}_{A,R} \quad (7)$$
$$\vec{F}_{h,R} = m_{ul}(\vec{a}_{ul,R} - \vec{g}) + \vec{F}_{k,R} \quad (8)$$

where,

$\vec{F}_{A,R}$ = reaction force at ankle for right ankle
m_f = mass of foot
$\vec{a}_{f,R}$ = linear acceleration of foot center-of-mass, right foot
$\vec{F}_{Gnd,R}$ = ground reaction force at right foot
$\vec{F}_{k,R}$ = reaction force at knee for right knee
m_{ll} = mass of lower leg
$\vec{a}_{ll,R}$ = linear acceleration of lower leg center-of-mass
$\vec{F}_{h,R}$ = reaction force at hip for right hip
m_{ul} = mass of upper leg
$\vec{a}_{ul,R}$ = linear acceleration of upper leg center-of-mass

Left Leg

$$\vec{F}_{A,L} = m_f(\vec{a}_{f,L} - \vec{g}) - \vec{F}_{Gnd,L} \quad (9)$$
$$\vec{F}_{k,L} = m_{ll}(\vec{a}_{ll,L} - \vec{g}) + \vec{F}_{A,L} \quad (10)$$
$$\vec{F}_{h,L} = m_{ul}(\vec{a}_{ul,L} - \vec{g}) + \vec{F}_{k,L} \quad (11)$$

Lumbar (back)

$$\vec{F}_b = m_{HAT}(\vec{g} - \vec{a}_{HAT}) \quad (12)$$

where,

$\vec{F}_b$ = reaction force at lumbar joint
m_{HAT} = mass of head, arms, torso (HAT) segment
$\vec{a}_{HAT}$ = linear acceleration at HAT center-of-mass

Residual forces

$$\vec{F}_r = m_p(\vec{a}_p - \vec{g}) + \vec{F}_{h,R} + \vec{F}_{h,L} - \vec{F}_b \quad \textbf{(13)}$$

where,

$\vec{F}_r$ = residual force applied at pelvis origin
m_p = mass of pelvis
$\vec{a}_p$ = linear acceleration at pelvis center-of-mass

Moments (for right leg)

Ankle

$$\vec{M}_{A,R} = -(\vec{r}_{Gnd,R} - \vec{r}_{f_{com}}) \times \vec{F}_{Gnd,R} + [I]_f \vec{\alpha}_{f,R} + (\vec{r}_{f_{com},R} \times \vec{F}_{A,R}) \quad \textbf{(14)}$$

Knee

$$\vec{M}_{k,R} = \vec{M}_{A,R} + [I]_{ll} \vec{\alpha}_{ll,R} + (\vec{r}_{ll_{com},R} \times \vec{F}_{k,R}) + [(\vec{L}_{ll,R} - \vec{r}_{ll_{com},R} \times \vec{F}_{A,R}] \quad \textbf{(15)}$$

Hip

$$\vec{M}_{h,R} = \vec{M}_{k,R} + [I]_{ul} \vec{\alpha}_{ul,R} + (\vec{r}_{ul_{com},R} \times \vec{F}_{h,R}) + [(\vec{L}_{ul,R} - \vec{r}_{ul_{com},R}) \times \vec{F}_{k,R}] \quad \textbf{(16)}$$

where,

$\vec{M}_{A,R}$ = ankle joint moment
$\vec{r}_{Gnd,R}$ = distance vector from ankle joint to application point of ground reaction force
$[I]_f$ = inertia matrix of foot about its center-of-mass
$\vec{\alpha}_{f,R}$ = angular acceleration of foot
$\vec{r}_{f_{com},R}$ = distance vector from ankle joint to foot center-of-mass
$\vec{M}_{k,R}$ = knee joint moment
$[I]_{ll}$ = inertia matrix of lower leg about its center-of-mass
$\vec{\alpha}_{ll,R}$ = angular acceleration of lower leg
$\vec{r}_{ll_{com},R}$ = distance vector from knee to lower leg center-of-mass
$\vec{L}_{ll,R}$ = length of lower leg (distance vector from knee to ankle)
$\vec{M}_{h,R}$ = hip joint moment
$[I]_{ul}$ = inertia matrix of upper leg about its center-of-mass
$\vec{\alpha}_{ul,R}$ = angular acceleration of upper leg
$\vec{r}_{ul_{com},R}$ = distance vector from hip to upper leg center-of-mass
$\vec{L}_{ul,R}$ = length of upper leg (distance vector from hip to knee)

and moments for the left leg segments have equivalent forms.

Lumbar (back)

$$\vec{M}_b = (\vec{r}_{HAT_{com}} \times \vec{F}_b) - [I]_{HAT}\vec{\alpha}_{HAT} \quad (17)$$

where,

$\vec{M}_b$ = lumbar joint moment
$\vec{r}_{HAT_{com}}$ = distance vector from lumbar joint to HAT center-of-mass
$[I]_{HAT}$ = moment of inertia of HAT about its center-of-mass
$\vec{\alpha}_{HAT}$ = angular acceleration of HAT segment

Residual Moment

$$\vec{M}_r = \vec{M}_{h,R} + \vec{M}_{h,L} - \vec{M}_b + [I]_p\vec{\alpha}_p + (\vec{r}_{Rh,p_{com}} \times \vec{F}_{h,R}) + (\vec{r}_{Lh,p_{com}} \times \vec{F}_{h,L}) - (\vec{r}_{b,p_{com}} \times \vec{F}_b) - (\vec{r}_{p_{com}} \times \vec{F}_r) + [I]_p\vec{\alpha}_p \quad (18)$$

where,

$\vec{M}_r$ = residual moment applied about pelvis origin
$[I]_p$ = moment of inertia of pelvis about its center-of-mass
$\vec{\alpha}_p$ = angular acceleration of pelvis
$\vec{r}_{Rh,p_{com}}$ = distance vector from pelvis center-of-mass to right hip
$\vec{r}_{Lh,p_{com}}$ = distance vector from pelvis center-of-mass to left hip
$\vec{r}_{b,p_{com}}$ = distance vector from pelvis center-of-mass to lumbar joint

7.6.2 Flexion moment (2D analysis) equations

We then made several simplifying assumptions. First, we assume that the majority of flexion moments occur in the sagittal plane, which remains stationary with respect to the absolute inertial coordinate frame. In the simulation, this was taken as the XY plane (see Figure 22). Accordingly, we approximate the ankle, knee, and hip flexion moments as occurring exclusively in the Z-direction.

Second, we ignore cross products of inertia. In general, this assumption makes sense because the majority of movement occurs in the sagittal plane and because principal moments of inertia tend to lie along directions orthogonal to segment longitudinal directions, as shown by the results of Dempster (1955), Clauser et al.(1969), and other studies.

With these assumptions, the 3D equations simplify into the following scalar equations,

Ankle flexion moment

$$M_A|_z = I_f\alpha_f - m_f g r_{f_{com}} e_{x_f} - r_{Gnd}[e_{x_f}F_{Gnd,y} - e_{y_f}F_{Gnd,x}] + \alpha_f m_f r^2_{f_{com}} + r_{f_{com}} m_f [e_{x_f}a_{ankle,y} - e_{y_f}a_{ankle,x}] \quad (19)$$

Knee flexion moment

$$M_k|_z = M_A|_z + I_{ll}\alpha_{ll} + r_{ll_{com}} m_{ll}[e_{x_{ll}}(a_{knee,y} - g) - e_{y_{ll}} a_{knee,x}] + r^2_{ll_{com}} m_{ll}\alpha_{ll} + m_f L_{ll}(e_{x_{ll}} a_{ankle,y} - e_{y_{ll}} a_{ankle,x} - g) + m_f r_{f_{com}} L_{ll}\alpha_f(e_{x_{ll}} e_{x_f} + e_{y_{ll}} e_{y_f}) + L_{ll}(-e_{x_{ll}} F_{Gnd,y} + e_{y_{ll}} F_{Gnd,x}) \quad \textbf{(20)}$$

Hip flexion moment

$$M_h|_z = M_k|_z + I_{ul}\alpha_{ul} + r_{ul} m_{ul}[e_{x_{ul}}(a_{p,y} - g) - e_{y_{ul}} a_{p,x}] + r^2_{ul} m_{ul}\alpha_{ul} + m_{ll} L_{ul}[e_{x_{ul}}(a_{knee,y} - g) - e_{y_{ul}} a_{knee,x}] + m_f L_{ul}[e_{x_{ul}}(a_{ankle,y} - g) - e_{y_{ul}} a_{knee,x}] + m_{ll} r_{ll} L_{ul}\alpha_{ll}[e_{x_{ul}} e_{x_{ll}} + e_{y_{ul}} e_{y_{ll}}] + m_f r_f L_{ul}\alpha_f[e_{x_{ul}} e_{x_f} + e_{y_{ul}} e_{y_f}] + L_{ul}[-e_{x_{ul}} F_{Gnd,y} + e_{y_{ul}} F_{Gnd,x}] \quad \textbf{(21)}$$

where the e_i*'s* represent the projection of the respective segment's distance vector in direction *i*. In other words, they are trigonometric functions of the joint angle, for example, for the foot,

$$e_{x_f} = sin(\theta_{AF})$$
$$e_{y_f} = -cos(\theta_{AF})$$

where θ_{AF} is the angle of the foot segment from the vertical, as shown in Figure 51 of Appendix D.

Following the approach discussed in (Riemer et al., 2008), we can find an upper bound for the joint moment uncertainties by taking the derivative of the moment equations with respect to all of the body segment inertial parameters:

$$\Delta M_j = \left|\frac{\partial M_j}{\partial x_1}\right| + \left|\frac{\partial M_j}{\partial x_2}\right| + \ldots + \left|\frac{\partial M_j}{\partial x_n}\right| \quad \textbf{(22)}$$

where ΔM_j is the joint moment uncertainty in joint j, M_j is the joint moment equation for joint *j*, and x_i's are the BSIPs. We then get the equations for joint moment uncertainties presented in the next section.

Flexion moment uncertainties

The flexion moment uncertainties represent the maximum uncertainties in joint moments due to variations or uncertainties in the various body segment inertial parameters.

Ankle flexion moment uncertainty

$$\Delta M_A = \alpha_f \Delta I_f + [-m_f g e_{x_f} + 2\alpha_f m_f r_{f_{com}} + m_f(e_{x_f} a_{ankle,y} - e y_f a_{ankle,x})]\Delta r_{f_{com}} + [\alpha_f r^2_{f_{com}} + r_{f_{com}}(e_{x_f} a_{ankle,y} - e_{y_f} a_{ankle,x})]\Delta m_f \quad \textbf{(23)}$$

Knee flexion moment uncertainty

$$\Delta M_k = \Delta M_A + \alpha_{ll}\Delta I_{ll} + [m_{ll}(e_{x_{ll}}(a_{knee,y} - g) - e_{y_{ll}}a_{knee,x}) + 2r_{ll_{com}}m_{ll}\alpha_{ll}]\Delta r_{ll} + [r_{ll}(e_{x_{ll}}(a_{knee,y} - g) - e_{y_{ll}}a_{knee,x}) + r_{ll}^2\alpha_{ll}]\Delta m_{ll} + [L_{ll}(e_{x_{ll}}a_{ankle,y} - e_{y_{ll}}a_{ankle,x} - g) + r_f L_{ll}\alpha_f(e_{x_{ll}}e_{x_f} + e_{y_{ll}}e_{y_f})]\Delta m_f + [m_f L_{ll}\alpha_f(e_{x_{ll}}e_{x_f} + e_{y_{ll}}e_{y_f})]\Delta r_f \quad (24)$$

Hip flexion moment uncertainty

$$\Delta M_h = \Delta M_k + \alpha_{ul}\Delta I_{ul} + [m_u l(e_{x_{ul}}(a_{p,y} - g) - e_{y_{ul}}a_{p,x}) + 2r_{ul}m_{ul}\alpha_{ul}]\Delta r_{ul} + [r_{ul}(e_{x_{ul}}(a_{p,y} - g) - e_{y_{ul}}a_{p,x}) + r_{ul}^2\alpha_{ul}]\Delta m_{ul} + [m_{ll}L_{ul}\alpha_{ll}(e_{x_{ul}}e_{x_{ll}} + e_{y_{ul}}e_{y_{ll}})]\Delta r_{ll} + [L_{ul}(e_{x_{ul}}(a_{knee,y} - g) - e_{y_{ul}}a_{knee,x}) + r_{ll}L_{ul}\alpha_{ll}(e_{x_{ul}}e_{x_{ll}} + e_{y_{ul}}e_{y_{ll}})]\Delta m_l l + [m_f L_{ul}\alpha_f(e_{x_{ul}}e_{x_f} + e_{y_{ul}}e_{y_f})]\Delta r_f + [L_{ul}(e_{x_{ul}}(a_{ankle,y} - g) - e_{y_{ul}}a_{ankle,x}) + r_f L_{ul}\alpha_f(e_{x_{ul}}e_{x_f} + e_{y_{ul}}e_{y_f})]\Delta m_f \quad (25)$$

7.6.3 Moment Sensitivities to individual BSIPs

We calculate the sensitivity of joint moments to variations in the values of individual BSIPs as follows. From the uncertainty equations above ((**23**) through (**25**)), we use 3-4 different values for each parameter while keeping all other parameters constant. These values included the max difference from the mean, the max difference between models, and multiples of the max difference from the mean. The max difference from the mean was taken as the baseline value, and for each time step, the sensitivity $dM / d[BSIP]$ was calculated using the formula,

$$\frac{d\Delta M}{d[BSIP]} = \frac{\Delta M_2 - \Delta M_1}{BSIP_2 - BSIP_1} \quad (26)$$

where ΔM_2 is the uncertainty in joint torque for joint *i* using BSIP value 2, and ΔM_1 is the joint torque uncertainty in joint torque for joint *i* using BSIP value 1 for the specific BSIP of interest. This metric measures how changes in a certain BSIP value affect the uncertainty of our joint torque results.

7.7 Summary

This chapter summarized the methodology used to study the effects of body segment inertial parameter values on joint moments calculated from gait analysis. The next chapter discusses the results and conclusions from our study.

8 Results and Conclusions for Part II

This chapter discusses results from the 3D simulations and the 2D dynamics analysis, concluding with recommendations about how to interpret and improve the accuracy of joint moments calculated from gait data. Figures and tables displaying results from the 3D OpenSim simulations are identified with the label **[3D simulations]**, while results from the 2D dynamics analysis are labeled **[2D dynamics]**. As mentioned in the introduction of Chapter 7, the 3D simulation results are presented because they represent the most accurate representation of how calculated joint torques from walking results vary due to different body segment property models, while the 2D dynamical equation results augment them by providing insight into the physics with less complexity than in a 3D dynamical equation analysis. The 2D results are shown to be an accurate representation of the 3D results.

8.1 3D OpenSim Simulation Results

Because there is no “best” or “ideal” Body Segment Inertial Parameter (BSIP) model or combination of model sets, and because each of the BSIP models are derived from studies limited in significant ways (e.g., very small sample sizes), this study analyzes the average torque estimates of all model sets and their variance through time.

Figure 26 through Figure 29 show the mean +/- variance of joint moments normalized by body weight for the hip, knee, and ankle of the right leg. Variance is defined in the standard statistical sense as the expectation of the squared deviation from the mean. Results are only shown for the right leg, as left leg results would be similar and symmetric.

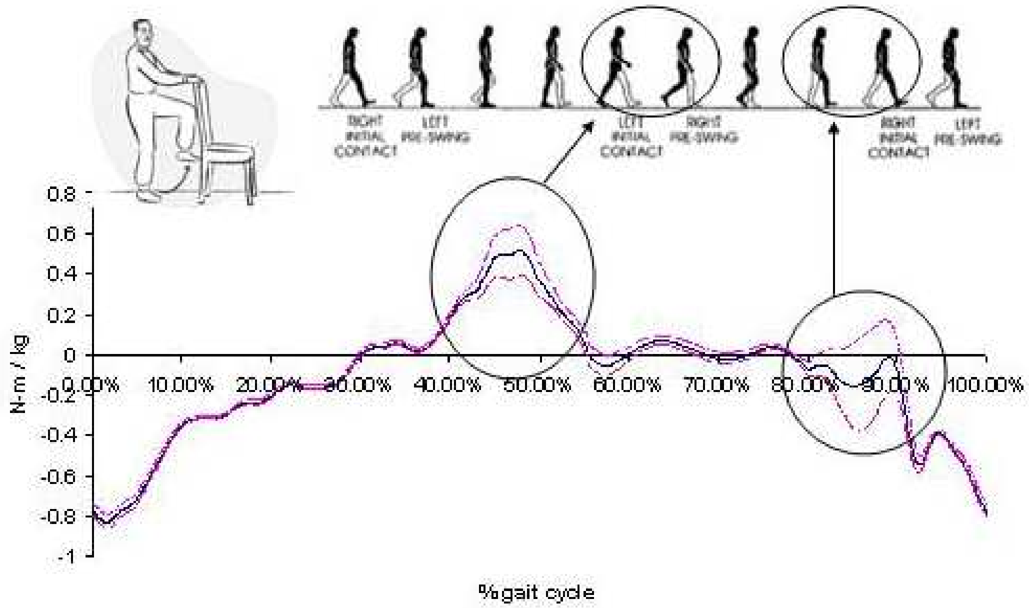

Figure 26: Mean +/- variance for RIGHT LEG HIP FLEXION moment normalized by subject's body mass, where positive moments represent hip flexion, as shown in the drawing [3D simulations] (figure from Inman and weboflife.nasa.gov)

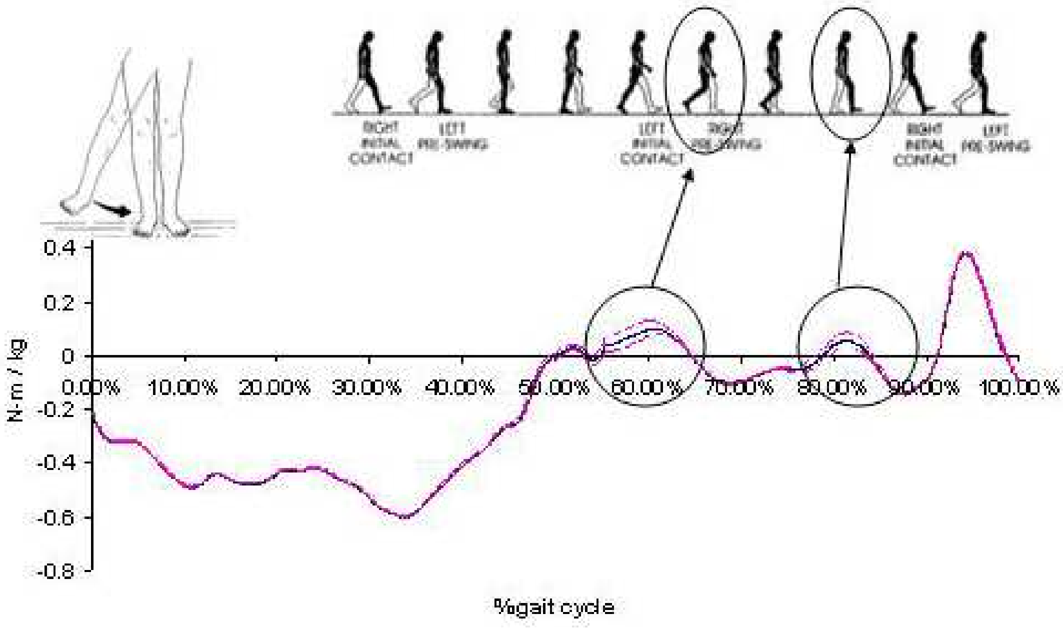

Figure 27: Mean +/- variance for RIGHT LEG HIP ADDUCTION moment normalized by subject's body mass [3D simulations]

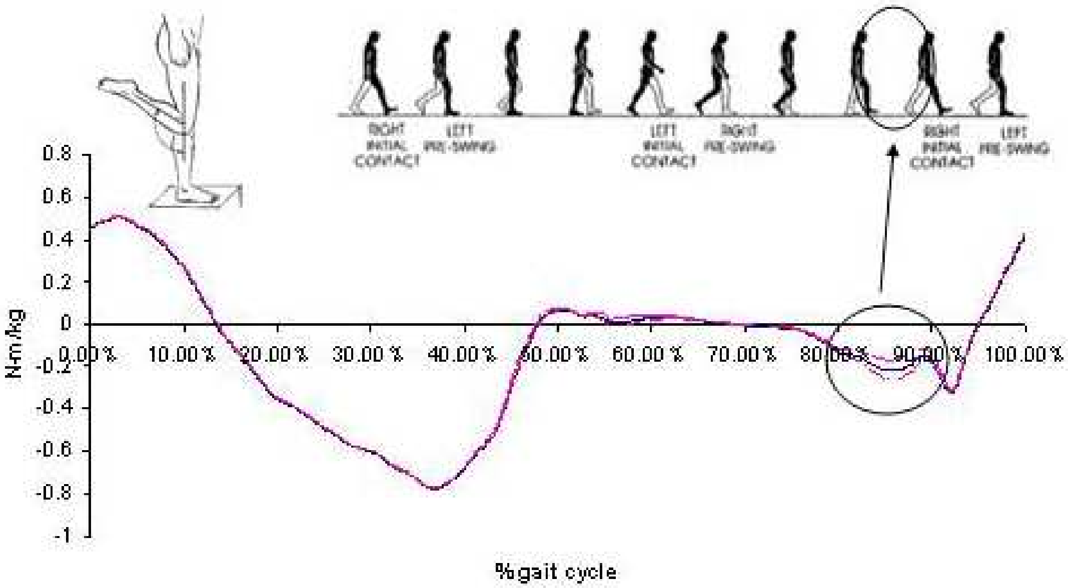

Figure 28: Mean +/- variance for RIGHT LEG KNEE FLEXION moment normalized by subject's body mass, where positive moments represent knee extension [3D simulations] (ovrt.nist.gov)

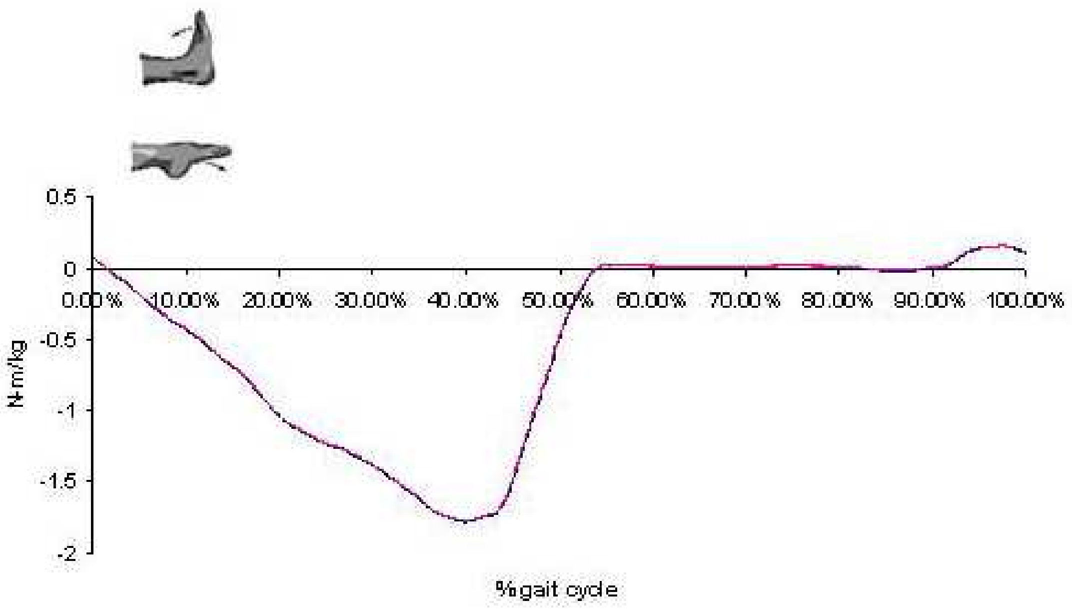

Figure 29: Mean +/- variance for right leg ankle joint flexion moment [3D simulations]

Additionally, Figure 30 through Figure 33 show normalized joint moment variance and maximum differences between BSIP models for the right leg.

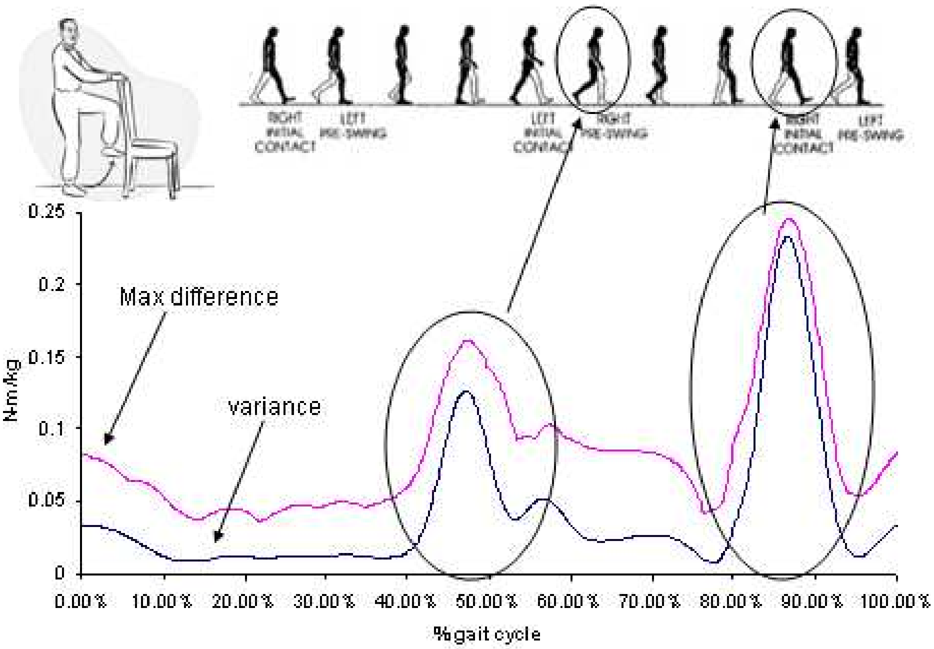

Figure 30: Variance and max difference in RIGHT LEG HIP FLEXION moment calculations between the BSIP models used [3D simulations]

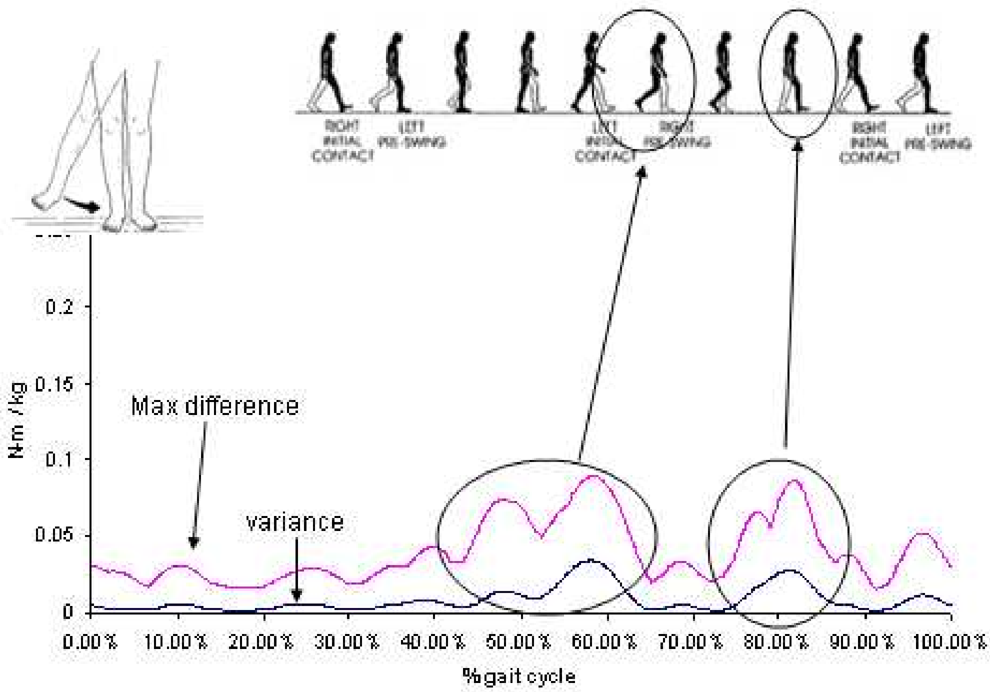

Figure 31: Variance and max difference in RIGHT LEG HIP ADDUCTION moment calculations between the BSIP models used [3D simulations]

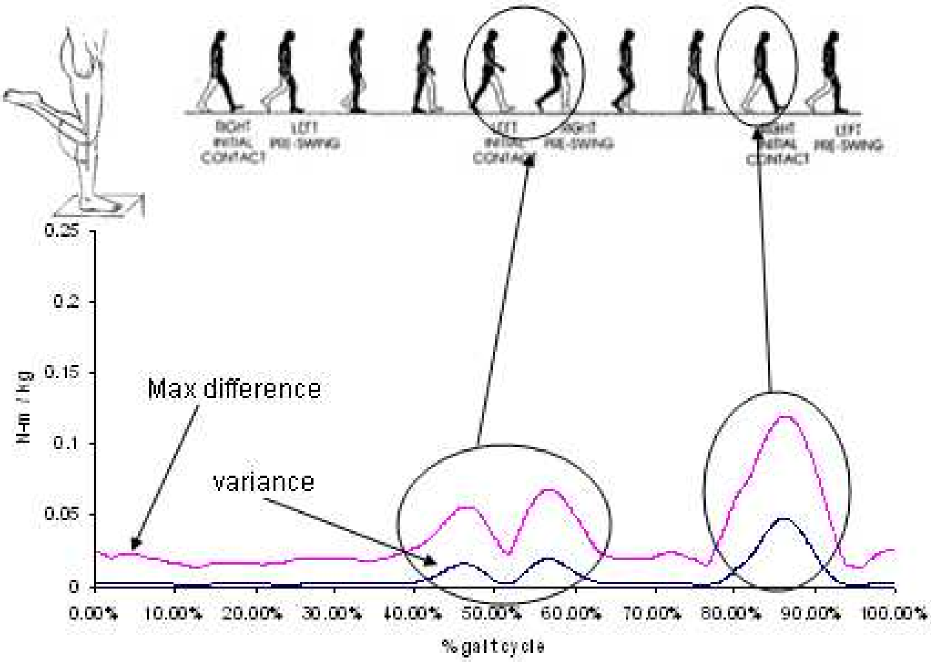

Figure 32: Variance and max difference in RIGHT LEG KNEE FLEXION moment calculations between the BSIP models used [3D simulations]

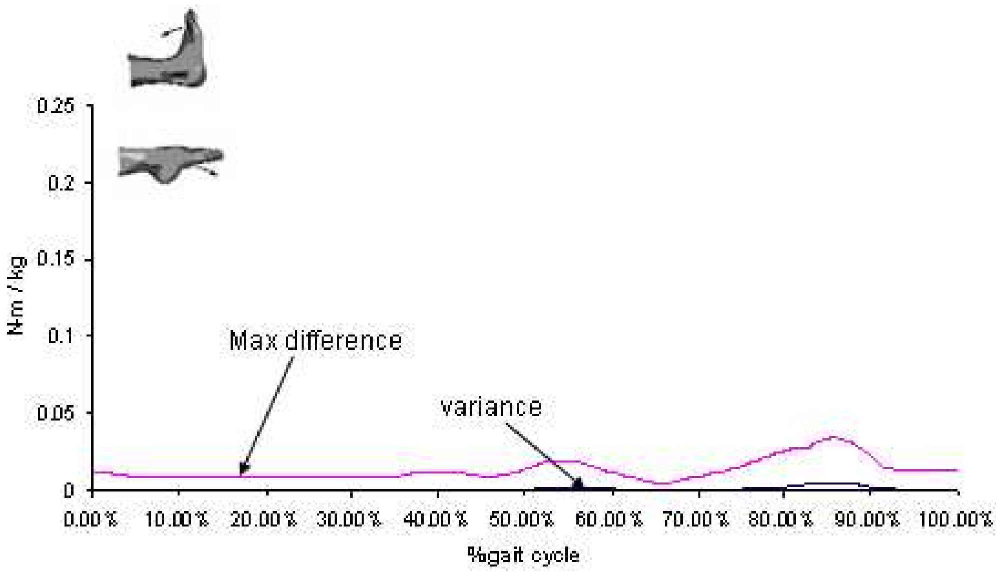

Figure 33: Variance and max difference in RIGHT LEG ANKLE FLEXION moment calculations between the BSIP models used [3D simulations]

From the figures, the following results can be observed:

- For hip flexion moment, the greatest variations occur at 45-50% of the gait cycle (double support/right leg pre-swing), and at 80-90% of the gait cycle (right leg heel strike).
- For hip adduction moment, the greatest variations occur at 55-60% of the gait cycle (beginning of right leg swing phase) and 75-85% (right leg heel strike).
- For knee flexion moment, the greatest variations occur at 45-55% (double support/right leg pre-swing) and 80-90% of the gait cycle (right leg heel strike).
- Variations in ankle flexion are small throughout the gait cycle.
- Joint moment variations are significant compared to average joint moments for some joints at some phases of the gait cycle

These results show that the greatest differences between joint moment results from different BSIP models occur during the start and end of the swing phase. This agrees with Ganley and Powers' results (2004) but is slightly different from Rao et al.'s results (2006), which show that hip joint flexion moment variations are fairly constant throughout the gait cycle (Figure 21). Intuitively, the observation that variations peak at certain points in the gait cycle makes sense because at the start of the swing phase, joint moments accelerate the leg against gravity. The moments required at this phase depends almost entirely on leg segment properties. In contrast, joint moments during stance phase act mainly to lift the body rather than accelerate the leg. There will be less joint moment uncertainty at this phase because total body weight is an accurately measured quantity,. More insight into this relationship is gained by examining the dynamical equations in the 2D Dynamics Analysis section.

The results in Figure 30 through Figure 33 show that joint flexion moment variance decreases as we move down the body (i.e., it is greatest for hip flexion, lower for knee flexion, and lowest for ankle flexion). Other researchers such as Ganley & Powers (2004) have noted this as well, though they did not provide an explanation for this effect. This suggests that we can make better joint moment calculations for lower body joints than upper body joints. Examining the dynamical equations of motion in the next section provides further insight into this result.

Finally, comparing Figures 26 through 29 to Figures 30 through 33 shows that the greatest errors do not always occur where joint torques are greatest in magnitude, particularly during single stance when only the right leg supports the body. This is important because high joint moments suggest high muscle and tendon forces, which are usually what interests clinicians prescribing patient treatment.

Figure 34 shows the average residual forces applied to the model during simulations to maintain its stability. The largest residual force magnitudes occur during heel strike and dual support stage, from 35-50% (left initial contact to right pre-swing) and 80-100% (right initial contact to left-pre-swing). The largest residual moment magnitudes occur just after right leg pre-swing, from 45-55%, and just after left leg pre-swing, at 5% and 95%. Residual forces measure the "model error," since applying any external force besides ground reaction forces to maintain stability is not realistic. However, the contributions of BSIP errors to these forces are unclear, and further studies need to be performed to understand this.

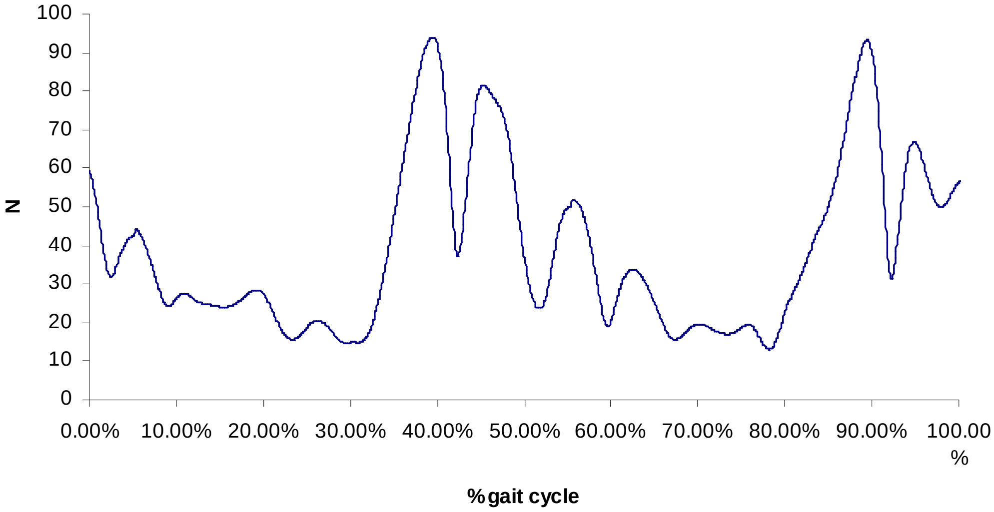

Figure 34: Total mean residual force magnitudes applied to body to maintain simulation model consistency with measurements [3D simulations]

In summary, the results from the 3D simulations suggest that we can have greatest confidence in our hip and knee joint moment results during single stance phase, whereas we can have high confidence in our ankle joint moments throughout the gait cycle.

8.2 2D Dynamics Analysis Results

We next analyze the 2D dynamical equations of motion to gain insights into our simulation observations. As discussed earlier, 2D equations are derived and used instead of 3D equations because they are less complex than the 3D equations, thereby providing more clarity into BSIP effects, while still proving to be accurate representations of the 3D simulation results. The 2D equations only show movement in the sagittal plane as shown in Figure 18, which is reproduced here.

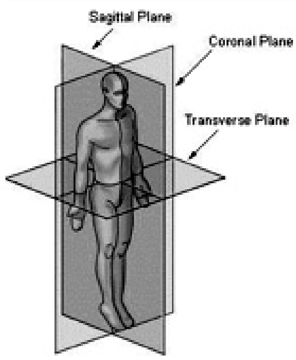

Figure 18: Body Planes

The 2D dynamical equations presented earlier for hip, knee, and ankle flexion torque and their uncertainty analysis equations from Chapter 7 are rewritten below.

Flexion moment (2D analysis) equations

Ankle flexion moment

$$M_A|_z = I_f\alpha_f - m_f g r_{f_{com}} e_{x_f} - r_{Gnd}[e_{x_f} F_{Gnd,y} - e_{y_f} F_{Gnd,x}] + \alpha_f m_f r^2_{f_{com}} + r_{f_{com}} m_f [e_{x_f} a_{ankle,y} - e_{y_f} a_{ankle,x}] \quad \textbf{(19)}$$

Knee flexion moment

$$M_k|_z = M_A|_z + I_{ll}\alpha_{ll} + r_{ll_{com}} m_{ll}[e_{x_{ll}}(a_{knee,y} - g) - e_{y_{ll}} a_{knee,x}] + r^2_{ll_{com}} m_{ll}\alpha_{ll} + m_f L_{ll}(e_{x_{ll}} a_{ankle,y} - e_{y_{ll}} a_{ankle,x} - g) + m_f r_{f_{com}} L_{ll}\alpha_f(e_{x_{ll}} e_{x_f} + e_{y_{ll}} e_{y_f}) + L_{ll}(-e_{x_{ll}} F_{Gnd,y} + e_{y_{ll}} F_{Gnd,x}) \quad \textbf{(20)}$$

Hip flexion moment

$$M_h|_z = M_k|_z + I_{ul}\alpha_{ul} + r_{ul} m_{ul}[e_{x_{ul}}(a_{p,y} - g) - e_{y_{ul}} a_{p,x}] + r^2_{ul} m_{ul}\alpha_{ul} + m_{ll} L_{ul}[e_{x_{ul}}(a_{knee,y} - g) - e_{y_{ul}} a_{knee,x}] + m_f L_{ul}[e_{x_{ul}}(a_{ankle,y} - g) - e_{y_{ul}} a_{knee,x}] + m_{ll} r_{ll} L_{ul}\alpha_{ll}[e_{x_{ul}} e_{x_{ll}} + e_{y_{ul}} e_{y_{ll}}] + m_f r_f L_{ul}\alpha_f[e_{x_{ul}} e_{x_f} + e_{y_{ul}} e_{y_f}] + L_{ul}[-e_{x_{ul}} F_{Gnd,y} + e_{y_{ul}} F_{Gnd,x}] \quad \textbf{(21)}$$

Flexion torque uncertainties

Ankle flexion moment uncertainty

$$\Delta M_A = \alpha_f \Delta I_f + [-m_f g e_{x_f} + 2\alpha_f m_f r_{f_{com}} + m_f(e_{x_f} a_{ankle,y} - e y_f a_{ankle,x})]\Delta r_{f_{com}} + [\alpha_f r^2_{f_{com}} + r_{f_{com}}(e_{x_f} a_{ankle,y} - e_{y_f} a_{ankle,x})]\Delta m_f \quad \textbf{(23)}$$

Knee flexion moment uncertainty

$$\Delta M_k = \Delta M_A + \alpha_{ll}\Delta I_{ll} + [m_{ll}(e_{x_{ll}}(a_{knee,y} - g) - e_{y_{ll}} a_{knee,x}) + 2 r_{ll_{com}} m_{ll}\alpha_{ll}]\Delta r_{ll} + [r_{ll}(e_{x_{ll}}(a_{knee,y} - g) - e_{y_{ll}} a_{knee,x}) + r^2_{ll}\alpha_{ll}]\Delta m_{ll} + [L_{ll}(e_{x_{ll}} a_{ankle,y} - e_{y_{ll}} a_{ankle,x} - g) + r_f L_{ll}\alpha_f(e_{x_{ll}} e_{x_f} + e_{y_{ll}} e_{y_f})]\Delta m_f + [m_f L_{ll}\alpha_f(e_{x_{ll}} e_{x_f} + e_{y_{ll}} e_{y_f})]\Delta r_f \quad \textbf{(24)}$$

Hip flexion moment uncertainty

$$\Delta M_h = \Delta M_k + \alpha_{ul}\Delta I_{ul} + [m_u l(e_{x_{ul}}(a_{p,y} - g) - e_{y_{ul}}a_{p,x}) + 2r_{ul}m_{ul}\alpha_{ul}]\Delta r_{ul} + [r_{ul}(e_{x_{ul}}(a_{p,y} - g) - e_{y_{ul}}a_{p,x}) + r_{ul}^2\alpha_{ul}]\Delta m_{ul} + [m_{ll}L_{ul}\alpha_{ll}(e_{x_{ul}}e_{x_{ll}} + e_{y_{ul}}e_{y_{ll}})]\Delta r_{ll} + [L_{ul}(e_{x_{ul}}(a_{knee,y} - g) - e_{y_{ul}}a_{knee,x}) + r_{ll}L_{ul}\alpha_{ll}(e_{x_{ul}}e_{x_{ll}} + e_{y_{ul}}e_{y_{ll}})]\Delta m_l l + [m_f L_{ul}\alpha_f(e_{x_{ul}}e_{x_f} + e_{y_{ul}}e_{y_f})]\Delta r_f + [L_{ul}(e_{x_{ul}}(a_{ankle,y} - g) - e_{y_{ul}}a_{ankle,x}) + r_f L_{ul}\alpha_f(e_{x_{ul}}e_{x_f} + e_{y_{ul}}e_{y_f})]\Delta m_f \quad (25)$$

These equations were coded in MATLAB for use in analysis. The script is presented in Appendix D.

8.2.1 Comparison with 3D simulation results

We first verify that the 2D approximations match the 3D simulation results well. Figure 35 through Figure 37 show that the 2D sagittal plane approximations match the 3D results fairly well, with increasing accuracy for joints higher in the body. These 2D results were calculated using the mean and maximum variation values from the 3D results as the uncertainty inputs (signified by delta) in equations **(23)** through **(25)**. Here, maximum difference is defined as the maximum difference between joint moments calculated using different BSIP models.

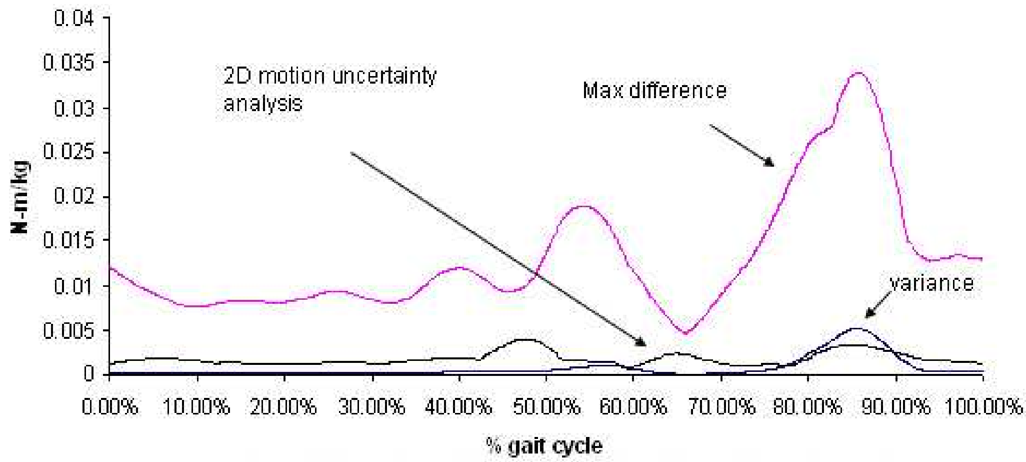

Figure 35: Comparison of 3D simulation variance and maximum difference between BSIP model results and 2D analysis for ANKLE FLEXION moment [3D simulations] [2D Dynamics]

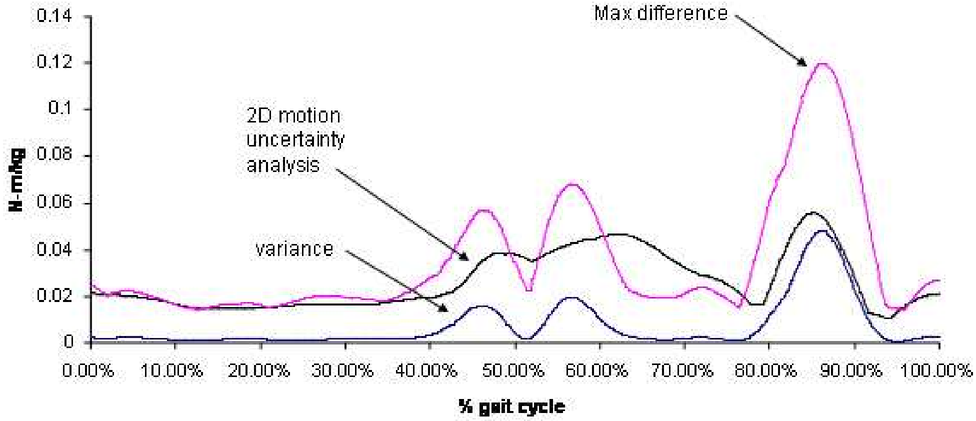

Figure 36: Comparison of 3D simulation variance and maximum difference between BSIP model results and 2D analysis for KNEE FLEXION moment [3D simulations] [2D Dynamics]

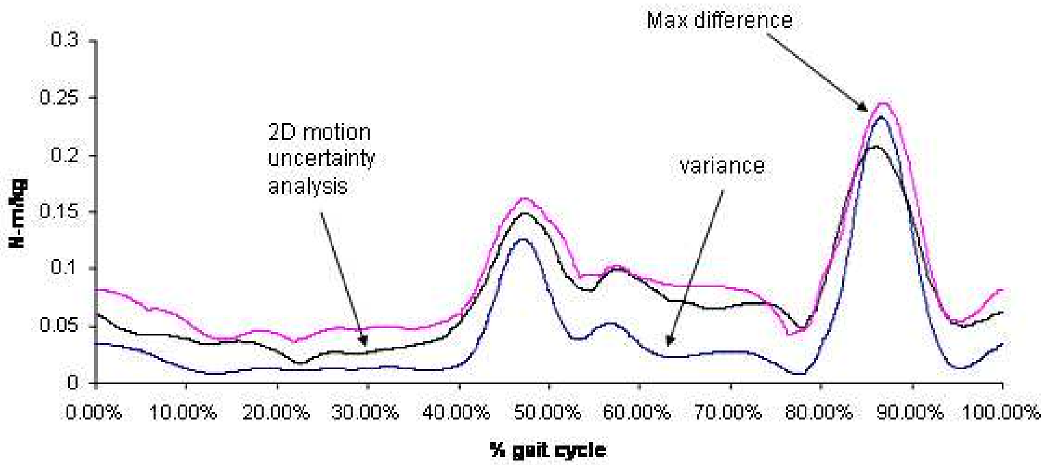

Figure 37: Comparison of 3D simulation variance and maximum difference between BSIP model results and 2D analysis for HIP FLEXION moment [3D simulations] [2D Dynamics]

8.2.2 Discussion

An examination of the rigid body dynamics equations (equations **(23)** through **(25)**) shows several important relationships. First, moment uncertainties for joints located higher in the leg are greater than in lower joints because moment uncertainties from the lower joints cascade up to higher joints. From the free body diagram of the foot, one can see that the foot segment is acted upon by experimentally measured ground reaction forces, which are known, and two estimated forces, the ankle reaction force and the weight of the foot (see in Figure 45 in Appendix D). The only joint moment acting on the foot is the ankle joint moment. In contrast, the thigh and shank segments are acted upon by joint reaction forces, segment weights, and joint moments--all of which are estimated based on body segment inertial parameter (BSIP) assumptions. This can be seen in the joint moment uncertainty equations: uncertainty in ankle joint moment depends only on foot segment inertial parameters, while uncertainty in knee joint moment depends on BSIPs of the lower leg and foot plus uncertainties in ankle joint moment. Similarly, hip flexion moment is dependent on BSIP uncertainties of the thigh, shank, and foot, as well as knee moment, which is in turn dependent on ankle moment. Moment uncertainties therefore cascade up the leg segments because only the foot is acted upon by measured external forces.

Regarding our observation from the 3D simulations that joint moment variations are greater during swing phase than stance phase, we now see mathematically why this occurs. Equations **(23)** through **(25)** (the joint moment uncertainty equations) show that joint flexion moment uncertainties are not functions of ground reaction forces. However, Equations **(19)** through **(21)** (the joint moment equations) show that joint uncertainty as a percentage of joint torque is greater during swing because at stance the joint torques balance out the ground reaction forces, while ground reaction forces are zero during swing. This means that during stance, ground reaction moments dominate the joint movement values, which leads to greater confidence in our joint movement estimates because ground forces are experimental measurements.

Finally, we observe that flexion moment uncertainties in the hip, knee, and ankle are linear with respect to inertia uncertainties, but nonlinear with respect to all other BSIPs. In other words, these flexion moments are linear functions of the inertia. This suggests that joint moments are less sensitive to inertia values than to other BSIPs, a point we will evaluate further in the next section when we isolate the effects of individual BSIPs.

8.2.2.1 Joint moment sensitivities averaged over gait cycle

To evaluate the sensitivity of joint moments to individual BSIPs, we modify one BSIP parameter variation at a time while keeping all others constant in equations **(23)** through **(25)** and calculate the average sensitivity over one gait cycle, as well as the average sensitivity at each point in the gait cycle, as described in section 7.6.3. The MATLAB script used for this analysis is presented in Appendix E.

We first examine the sensitivities averaged over one gait cycle. Table 12 through Table 14 present these results. Note that we can only compare results within each table, and not results between tables, since each table represents normalized joint moment sensitivity for some BSIP model set (mass, center-of-mass location, inertia).

Table 12: Average sensitivity over one gait cycle of joint moment variations to changes in segment mass (N-m/kg^2) [2D dynamics]

	Ankle flexion	Knee flexion	Hip Flexion
	d[ΔM_A normalized] / dΔm	d[ΔM_k normalized] / dΔm	d[ΔM_h normalized] / dΔm
foot	0.000	0.078	0.107
shank	0.000	0.006	0.020
thigh	0.000	0.000	0.005

Table 13: Average sensitivity over one gait cycle of joint moment variations to changes in segment center-of-mass locations (N/kg) [2D dynamics]

	d[ΔM_A normalized] / dΔcom	d[ΔM_k normalized] / dΔcom	d[ΔM_h normalized] / dΔcom
foot	0.103	0.113	0.187
shank	0.000	0.162	0.512
thigh	0.000	0.000	0.410

Table 14: Average sensitivity over one gait cycle of joint moment variations to changes in segment inertias (N/kg) [2D dynamics]

	d[ΔM_A normalized] / dΔIzz	d[ΔM_k normalized] / dΔIzz	d[ΔM_h normalized] / dΔIzz
foot	0.316	0.318	0.318
shank	0.000	0.287	0.287
thigh	0.000	0.000	0.144

From these results, one can see that joint moments are most sensitive to foot mass and inertia, and to shank center-of-mass location. Hip flexion moment sensitivity to foot mass is most pronounced, as this is more than 200 times its sensitivity to thigh mass.

To put these numbers into perspective, we estimate the BSIP uncertainty magnitudes that would be encountered for each segment based on our subject-specific BSIP values from Table 8 through Table 10 of Chapter 7. For our experimentally measured subject (1.8 m, 72.6 kg (160 lbs), ~67th percentile male), the maximum difference in estimates between relevant BSIP models for the foot, shank, and thigh are summarized in Table 15.

Table 15: Maximum differences in BSIP estimations between models

Segment	Mass max difference (kg)	COM max difference (m)	Inertia max difference (kg-m^2)
Thigh	3.741	0.029	0.109
Shank	0.669	0.032	0.025
Foot	0.336	0.016	0.003

For the subject, joint moment uncertainties based on the sensitivity values from Table 12 through Table 14 and the maximum BSIP estimate differences from Table 15 are presented in Table 16 through Table 18

Table 16: Calculated variations in flexion joint moments averaged per gait cycle in experimental subject based on maximum difference in segment mass estimates (N-m) [2D Dynamics]

	M_{ankle}	M_{knee}	M_{hip}
Foot	0.000	1.902	2.609
Shank	0.000	0.291	0.972
Thigh	0.000	0.000	1.358

Table 17: Calculated variations in flexion joint moments averaged per gait cycle in experimental subject based on maximum difference in segment center-of-mass location estimates (N-m) [2D Dynamics]

	M_{ankle}	M_{knee}	M_{hip}
foot	0.118	0.130	0.215
shank	0.000	0.377	1.191
thigh	0.000	0.000	0.867

Table 18: Calculated variations in flexion joint moments averaged per gait cycle in experimental subject based on maximum difference in segment inertia estimates (N-m) [2D Dynamics]

	M_{ankle}	M_{knee}	M_{hip}
foot	0.071	0.071	0.071
shank	0.000	0.529	0.529
thigh	0.000	0.000	1.142

From the 2D dynamical equation analysis results presented, we can conclude the following. First, regarding segment masses, *foot* mass is the most important BSIP to accurately estimate. Second, regarding segment center-of-mass locations, *shank and thigh* center-of-mass locations are the most important BSIPs to accurately estimate. Finally, regarding segment inertias, *shank and thigh* inertias are the most important BSIPs to accurately estimate

8.2.2.2 Joint moment sensitivities at each phase of gait cycle

Though the above averages give us an idea of the joint moment sensitivities throughout the gait cycle, it is also useful to know the sensitivities at each phase in the gait cycle. Important results are plotted in Figure 38 through Figure 41 and discussed.

Figure 38 shows the sensitivity of hip, knee, and ankle flexion moments to foot mass, where moments are again normalized by body mass. One can see that variations in foot mass values have negligible effects on ankle flexion moment uncertainties compared to knee and hip flexion moments. Further, hip flexion moment uncertainty is especially sensitive to foot mass variations during 80-90% of the gait cycle (heel strike). This result agrees with that of Riemer et al. (2008). Figure 39 further highlights this fact by comparing the effects of foot mass on hip flexion moment to those of shank and thigh masses.

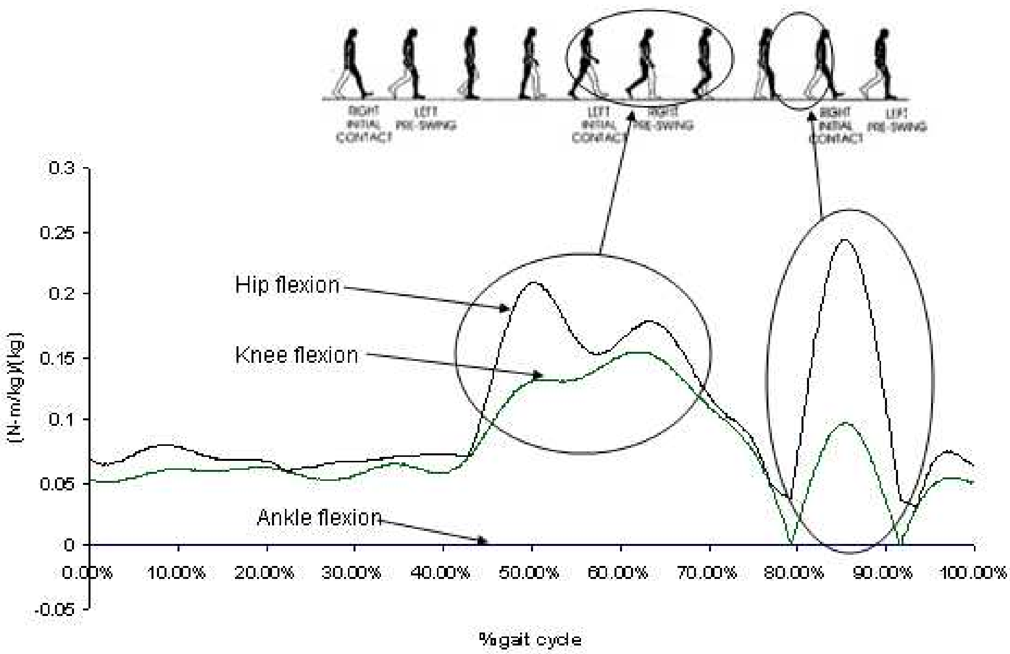

Figure 38: Sensitivity of normalized hip, knee, and ankle flexion moment variations to foot mass [2D Dynamics]

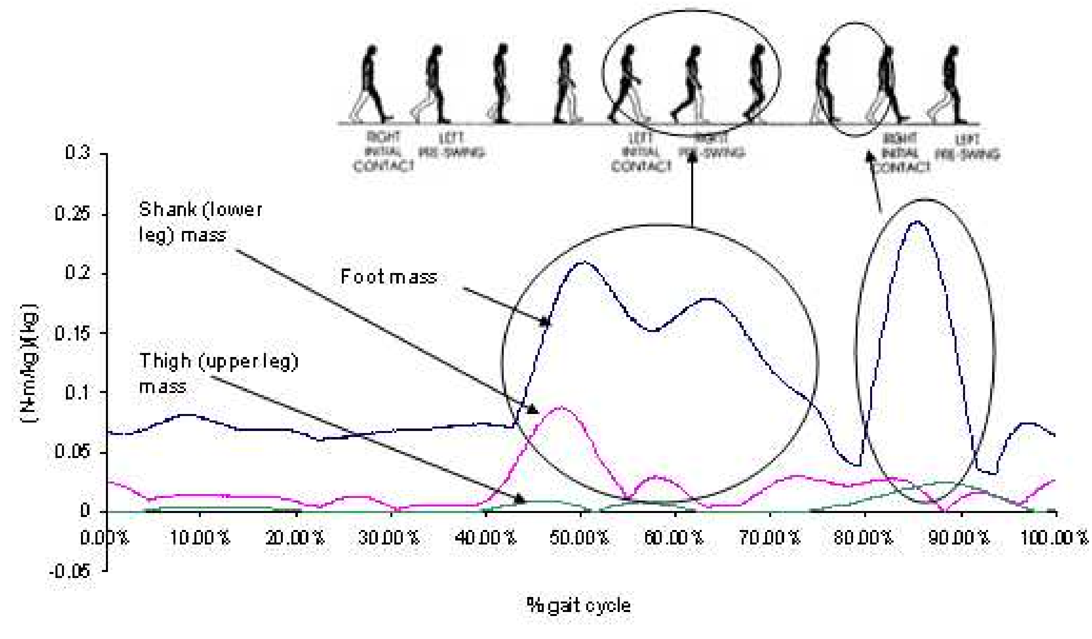

Figure 39: Sensitivity of hip flexion normalized moment variations to foot, shank, and thigh mass [2D Dynamics]

Figure 40 shows the sensitivity of hip flexion moment to variations in foot, shank, and thigh center-of-mass location. It highlights that variations in foot and shank center-of-mass locations have negligible effects on hip flexion torque uncertainty for most of the gait cycle. However, shank-center-of mass location has large effects on hip flexion from 80-90% of the gait cycle (heel strike), while thigh center-of-mass location has moderate effects from 40-50% (double support) and 80-90% of the gait cycle and small effects otherwise.

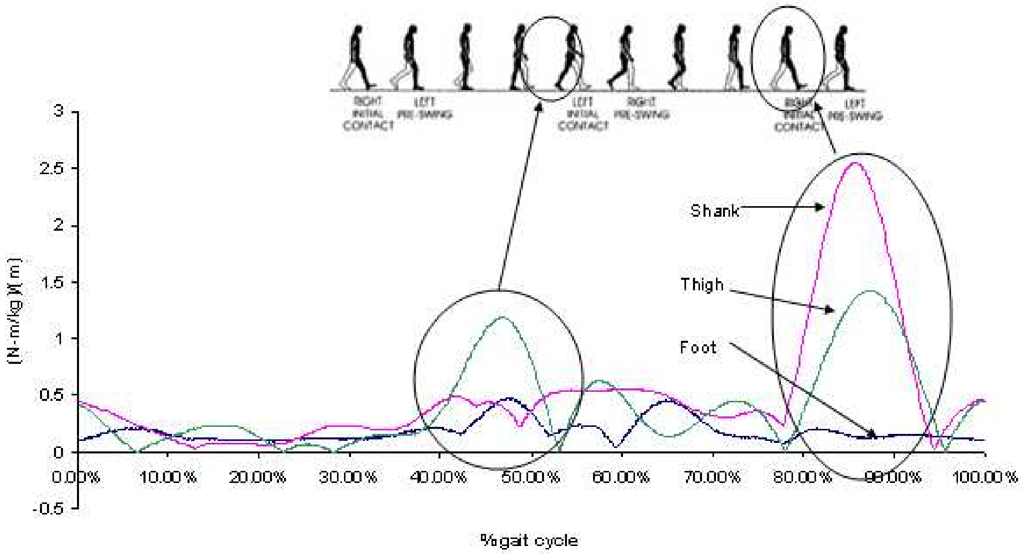

Figure 40: Sensitivity of normalized hip flexion moment to variations in foot, shank, and thigh center-of-mass locations
[2D Dynamics]

Figure 41 shows the sensitivity of normalized hip flexion moment variations to variations in segment inertias.

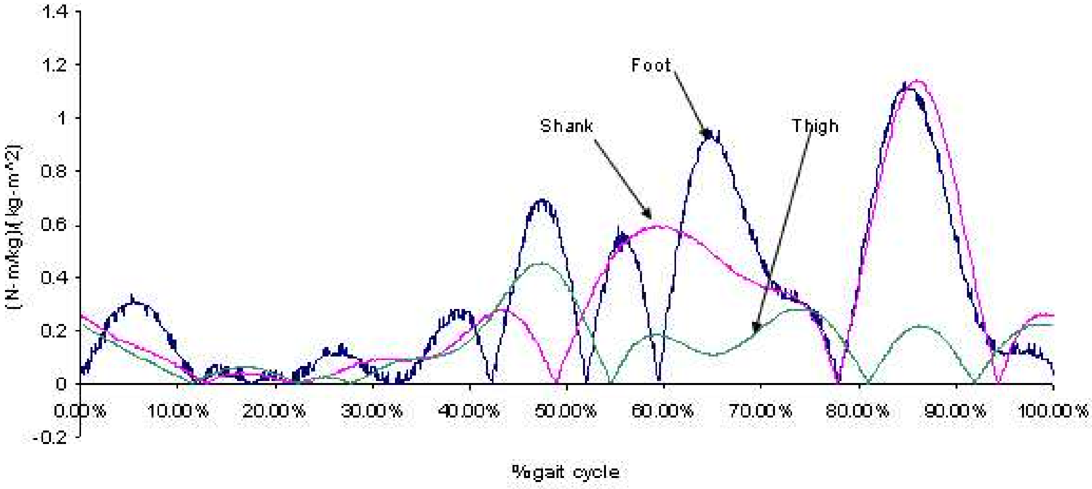

Figure 41: Sensitivity of normalized hip flexion moment variations to inertias [2D Dynamics]

Although hip flexion is highly sensitive to both shank inertia and foot inertia, foot inertia variations are small enough that the overall effects of foot mass are not significant. This can be seen in Table 18 by examining the non-normalized moment sensitivity to the maximum difference in inertia estimations between BSIP models for the experimental subject. However, thigh and shank inertia values do have significant effects. For the measured subject, the sensitivity value from 80-90% of the gait cycle is 1.1 N/(kg^2-m). This corresponds to an absolute moment uncertainty of 8.7 N-m, which is 120% of the joint moment value at that point in the gait cycle!

Performing our analysis BSIP-component-by-BSIP component with a 2D approximation causes some error, but the results are qualitatively similar. For example, for hip flexion the 2D component-by-component analysis predicts a maximum torque variation of 18.5 N-m for the subject at 48% of the gait cycle, while the 3D simulations predict 11.6 N-m. Similarly, at 87% of the gait cycle the 2D analysis predicts a higher value than the 3D simulations (25 N-m vs. 17.8 N-m). For the knee at these gait cycle phases, the 2D analysis vs. 3D simulation results at 48% and 87% of the gait cycle are 4.7 vs. 3.6 N-m and 6.3 vs. 8.7 N-m, respectively.

Table 19: Contributions of each BSIP to hip flexion moment uncertainty from 45-55% of gait cycle for our subject [2D analysis]

Max variation in BSIPs for subject		max Hip sensitivity (N-m/kg per BSIP dimension)	Torque variation (N-m/kg)	Torque variation for subject (N-m)
m_foot (kg)	0.336	0.21	0.07	5.12
m_shank (kg)	0.669	0.087	0.06	4.22
m_thigh (kg)	3.741	0.0097	0.04	2.63
com_foot (m)	0.016	0.48	0.0077	0.56
com_shank (m)	0.032	0.56	0.018	1.30
com_thigh (m)	0.029	1.2	0.035	2.52
I_foot (kg-m^2)	0.003	0.7	0.0021	0.15
I_shank (kg-m2)	0.025	0.49	0.012	0.89
I_thigh (kg-m2)	0.109	0.45	0.049	3.56
			Total (N-m): **Peak mean joint moment:**	20.95 37.03

The above table shows that uncertainty in foot mass contributes the most to hip flexion moment uncertainty, followed by shank mass and thigh inertia. Collectively, these three parameters account for more than half of the joint moment uncertainty, or 12.9 N-m. This seems significant considering that maximum hip flexion in that gait cycle range is approximately 35 N-m. At 80 to 90% of the gait cycle, thigh mass contributes most to moment variation, followed closely by foot mass and shank mass. Collectively, these account for 18.3 N-m of joint moment uncertainty, while peak joint torque in this range is only 11.6 N-m.

8.3 Conclusions and recommendations

Results and findings are now compared against our hypotheses. For convenience, we reiterate our hypotheses from the Part II introduction. First, we hypothesized that joint moment estimates would be significantly different during periods of high force impact, i.e., during heel strike, but not so different at other periods of the gait cycle. Second, we hypothesized that joint moment variations would be different for different joints. Third, we hypothesized that joint variations would be significant at some phases of the gait cycle and less so at others

Our hypothesis that joint moments would vary the most during periods of high force impact was not correct. Although variations were high during heel strike, they were also high during the majority of the swing phase. Our hypothesis that moment variations would be different for different joints was supported, and greater confidence in joint moment results occurs in the lower leg joints such as the ankle.

Our hypothesis that joint uncertainties would be significant at some phases of the gait cycle and less so at others was correct. As a percentage of the maximum joint moments, variations can be considered small, but as a percentage of the joint moment magnitudes at specific phases of the gait cycle, variations due to BSIP estimations can be significant.

The results presented in this chapter show that depending on what phase of the gait cycle and what joints one is interested in analyzing, one should expend extra effort to gather better estimates of different BSIPs. The most important BSIP to measure accurately is foot mass, which significantly affects errors in all lower body joint torques. More accurate measurements of BSIPs might be accomplished using advanced imaging techniques on specific parts of the body, or by taking more manual measurements of segments and using regression equations that take these additional measurements into account. Table 20 summarizes our recommendations regarding BSIP estimations in gait analysis.

Table 20: Recommendations for BSIP estimations

Joint moment of interest	**Phase of gait cycle**	**Recommendations**
Hip adduction	Entire gait cycle	Low variations—can have good confidence in joint moment results
Ankle flexion	Entire gait cycle	Low variations—can have good confidence in joint moment results
Knee flexion	Single support (0-40%)	Low variations—can have good confidence in joint moment results
	Double support (45-55%)	Moderate variations—can address by estimating **foot mass** more accurately.
	Start of swing phase (55-65%)	Moderate variations, but no clear BSIP to be estimated more accurately
	Middle to end of swing phase (65-75%)	Low variations—can have good confidence in joint moment results
	Heel strike (80-90%)	High variations—can address by estimating **foot mass**, **shank inertia**, and **shank center-of-mass** location more accurately
Hip flexion	Single support (0-40%)	Low variations— can have good confidence in joint moment results
	Double support (45-55%)	High variations— can address by estimating **foot mass**, **shank mass**, and **thigh inertia** more accurately.
	Swing phase (55-70%)	Moderate variations—can address by estimating **foot mass** more accurately.
	Heel strike (80-90%)	High variations-- can address by estimating **thigh mass**, **foot mass**, and **shank center-of-mass** location more accurately

8.4 Future work

This study analyzed one subject at one walking speed. Future work would involve analyzing more subjects and different walking speeds to determine how well these conclusions hold. Future work could also be performed to determine how well the equations presented in this study can predict results from faster movements, such as running, which would have greater joint moment variations.

Other work could also focus on comparing model types, such as models that include arms, which might help examine effects on residual forces/moments.

Appendix A: Subject OpenSim Model Anthropometry

OpenSim model scaled to experimental subject

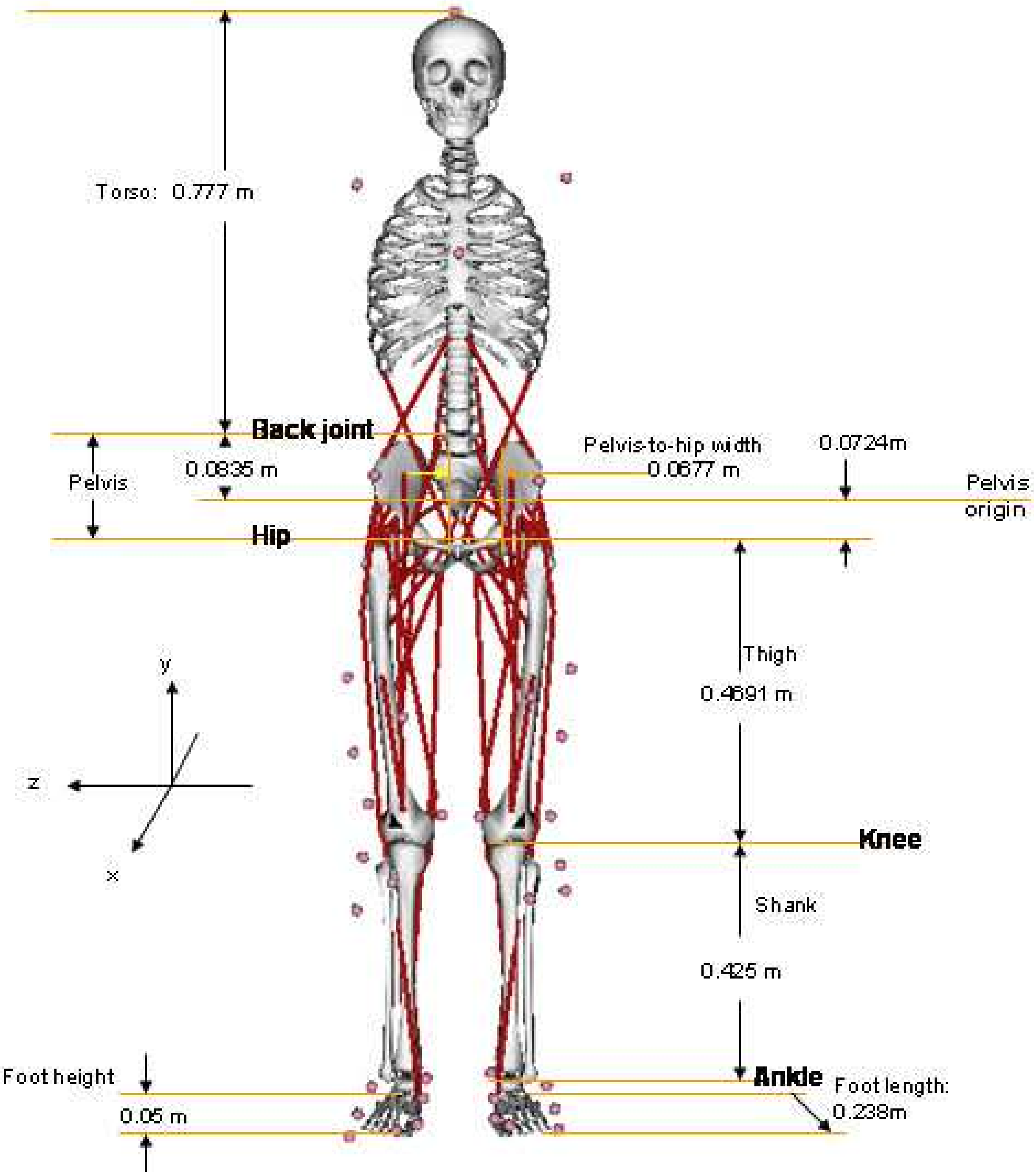

Appendix B: Body Segment Inertial Parameter Calculations

Model 2: Dempster (1955)

Dempster performed a cadaver study of eight male subjects, dividing the body as shown below in Figure 42. His study provides percentage relations to calculate segment masses and center-of-mass locations.

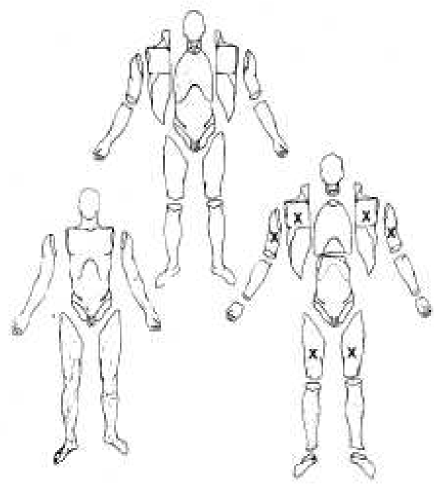

Figure 42: Plan of dismemberment for cadavers (Dempster, 1955)

Segment mass calculations

Dempster provides percentage mass of total body weight for each body segment. Using these equations, HAT segment mass was calculated by adding the masses of the head, torso, and total arms. Total arm is defined in Dempster as comprising the upper arm, forearm, and hand. Torso segment is defined in Dempster as including the pelvis. The results are shown below.

Table 21: Segment masses calculated using Dempster

Segment	Mass as % of total body weight	Mass (kg)
Head	7.9	5.74
Torso	48.6	35.3
Total arm	4.9	3.56
Upper Arm	2.7	1.96
Forearm & hand	2.2	1.60
forearm	1.6	1.16
hand	0.6	0.436
Thigh	9.7	7.04
Shank (calf)	4.5	3.27
Foot	1.4	1.02
HAT		48.1

Segment center-of-mass location calculations

Dempster locates the center-of-masses as described in Table XX. These percentage values were then transferred to be a percentage of the OpenSim scaled model length. Using the OpenSim model lengths shown in Appendix A, an example calculation for the head and trunk segment is shown below.

For the OpenSim model, the distance from the hip to the vertex of the head is

$$0.777 + 0.0835 + 0.0724 = 0.933 \text{ m.}$$

Dempster states that the center of mass is 39.6% of this distance, which is 0.369m. Relative to the torso segment, which has its origin located at the same place as the pelvis, this is

$$0.369 – 0.0724 = 0.297 \text{ m.}$$

Table 22: Center-of-mass locations according to Dempster translated to OpenSim model locations

	Dempster's relations		Transferring Dempster's relations to OpenSim model coordinates		
	COM location				
	% of total segment length		COM location (m)	COM (m) as defined in OpenSim	
Head and trunk minus limbs	39.6	from hip to vertex of head	0.369	0.297	in torso segment (y dir)
Head and neck					
Thorax					
Abdomen plus pelvis	40.0	from hip			
Entire upper extremity (arm, forearm, hand)	51.2	from shoulder			
Thigh	43.4	from hip to knee	0.204	-0.204	in femur segment (y-dir)
Leg	43.3	from knee to ankle	0.184	-0.184	in tibia segment (y-dir)
Foot	43.8	from heel to toe	0.104	0.104	in calcn segment (x-dir)

Model 3: Clauser (1969)

Clauser divides the body similarly to Dempster and provides percentage relations to calculate segment masses and center-of-mass locations.

Segment mass calculations

Clauser, as in Dempster, provides percentage mass of total body weight for each body segment. As before, we calculate HAT segment mass was calculated by adding the masses of the head, torso, and total arms.

Table 23: Segment masses calculated using Clauser

Segment	Mass as % of total body weight	Mass (kg)
Head	7.3	5.30
Torso	50.7	36.8
Total arm	4.9	3.56
Upper Arm	2.6	1.89
Forearm & hand	2.3	1.67
forearm	1.6	1.16
hand	0.7	0.508
Thigh	10.3	7.48
Shank (calf)	4.3	3.12
Foot	1.5	1.09
HAT:		49.2

Segment center-of-mass location calculations

Clauser locates the center-of-masses as described in Table 24. As with Dempster, these percentage values were then transferred to be a percentage of the OpenSim scaled model length.

Table 24: Segment com locations calculated using Clauser

	Clauser's relations		Transferring Clauser's relations to OpenSim model coordinates		
	COM location				
	% of total segment length		COM location (m)	COM location (m) as defined in OpenSim model	
Head + torso	40.79	from hip to head vertex	0.3805	0.3081	in torso segment (y dir)
Thigh	37.19	from trochanterion (near pelvis)	0.1745	-0.1745	in femur segment (y-dir)
Leg	37.05	from tibiale (knee?)	0.1575	-0.1575	in tibia segment (y-dir)
Foot	44.85	from heel	0.1067	0.1067	in calcn segment (x-dir)

Model 4: Chandler (1975)

Chandler performed cadaver studies and divided the body similarly to Dempster and Clauser. However, Chandler provides regression equations that can be used to calculate segment masses and moments of inertia.

Segment mass calculations

Chandler's regression equations and the resulting calculations for the experimental subject's segment masses are shown in Table 25. Note that Chandler provides different estimates for the same segments located on the right and left halves of the body. For our purposes, we take the average of these values and use them for both sides of the body, meaning, for example, that the right thigh is given the same mass as the left thigh.

Table 25: Segment masses calculated using Chandler's regression equations

	Calculation (kg)	regression eqn (gm)
Head	4.229	0.032*body weight + 1,906
Torso	37.92	0.532*body weight - 706
Right upper arm	1.971	0.016*body weight + 809
Left upper arm	2.082	0.022*body weight + 485
Average upper arm mass	*2.026*	
Right forearm	1.234	0.020*body weight - 218
Left forearm	1.190	0.013*body weight + 246
Average forearm mass	*1.212*	
Right hand	0.4782	0.007*body weight - 30
Left hand	0.4390	0.005*body weight + 76
Right thigh	10.84	0.126*body weight - 1,688
Left thigh	10.73	0.127*body weight - 1,511
Average thigh mass	*10.78*	
Right shank	2.938	0.038*body weight + 179
Left shank	3.016	0.044*body weight - 178
Average shank mass	*2.977*	
Right foot	0.9238	0.008*body weight + 343
Left foot	0.9054	0.009*body weight + 252
Average foot mass	*0.9146*	
HAT	49.54	includes pelvis

Segment center-of-mass location calculations

Chandler provides center-of-mass locations for the six cadavers studied. The average of the locations as a percentage of segment length was calculated, and these values were scaled to the OpenSim model lengths, as shown in Table 24. As with the segment mass values, in our study we use the same BSIP values for the left and right halves of the body, which are the average values.

HAT center-of-mass location was found by calculating centroids:

$$C_j = \frac{c_1 m_1 + c_2 m_2 + ... + c_n m_n}{m_1 + m_2 + ... + m_n} \qquad \textbf{Equation 27}$$

where C_j is the center-of-mass location of segment j, which includes segments 1 through n, c_i is the center-of-mass location of segment *i*, and m_i is the mass of segment *i*. In this study, different segment mass model sets are used, which necessitates recalculating the HAT center-of-mass location for each combination. These calculations are also summarized in the table.

Table 26: Segment center-of-mass locations using Chandler's relations

	Segment COM distance (% of length)		COM (m) as defined in osim	
Head	88.4	from hip to head vertex	0.7603	in torso segment (y dir)
Torso	30.4	from hip to head vertex	0.2619	in torso segment (y dir)
Right thigh	38.8	from hip to knee (right)	-0.1822	in femur segment (y dir)
Left thigh	39.8	from hip to knee (left)	-0.1869	in femur segment (y dir)
Right shank	42.0	from knee to ankle (right)	-0.1785	in tibia segment (y dir)
Left shank	41.3	from knee to ankle (left)	-0.1757	in tibia segment (y dir)
Right foot	43.7	from heel (right)	0.1039	in calcn segment (x dir)
Left foot	44.0	from heel (left)	0.1047	in calcn segment (x dir)
HAT			0.3119	in torso segment (y dir)
		Chandler using Dempster's mass:	0.3317	in torso segment (y dir)
		Chandler using Clauser's mass:	0.3246	in torso segment (y dir)
		Chandler using de Leva mass:	0.3305	in torso segment (y dir)
		Chandler using Dumas mass:	0.3235	in torso segment (y dir)
		Chandler using Gebod mass:	0.3280	in torso segment (y dir)

Segment inertia calculations

Chandler provides regression equations to calculate principal moments of inertia along segment longitudinal and orthogonal to the longitudinal directions. These principal moment directions are coincident with the principal moment directions in the OpenSim model, but labeled differently. The resulting OpenSim inertia values are summarized in Table 27. For our study, we use the torso inertia as the HAT inertia.

Table 27: Segment moments of inertia calculated using Chandler's regression equations

(g-cm^2)		Regression equation (g-cm^2)	Value (kg-m^2)	Coordinate in OpenSim
Head	Ixx =	2.129*BW + 32,030	0.01866	Ixx
	Iyy =	1.676*BW + 54,818	0.01765	Izz
	Izz =	3.186*BW - 6,846	0.02245	Iyy

Torso	Ixx =	296.9*BW - 3,156,034	1.840	Ixx
	Iyy =	284.493*BW - 7,664,880	1.299	Izz
	Izz =	102.507*BW - 2,895,524	0.4546	Iyy
Upper right arm	Ixx =	0.535*BW + 98,150	0.01370	
	Iyy =	0.661*BW + 89,662	0.01377	
	Izz =	0.400*BW - 4,018	0.002502	
Upper left arm	Ixx =	2.096*BW + 15,569	0.01677	
	Iyy =	1.352*BW + 49,572	0.01477	
	Izz =	0.567*BW - 14,171	0.002699	
Right forearm	Ixx =	1.508*BW - 31,431	0.007805	
	Iyy =	1.397*BW - 26,562	0.007486	
	Izz =	0.313*BW - 11,645	0.001108	
Left forearm	Ixx =	0.659*BW + 21,806	0.006965	
	Iyy =	0.727*BW + 15,672	0.006845	
	Izz =	0.230*BW - 6,396	0.001030	
Right hand	Ixx =	0.129*BW - 850	0.0008515	
	Iyy =	0.134*BW - 2,599	0.0007129	
	Izz =	0.085*BW - 3,401	0.0002770	
Left hand	Ixx =	0.083*BW + 1,437	0.0007463	
	Iyy =	0.100*BW - 920	0.0006340	
	Izz =	0.028*BW -6	0.0002027	
Right thigh	Ixx =	24.102*BW - 433,522	0.1316	Ixx
	Iyy =	21.186*BW - 222,796	0.1315	Izz
	Izz =	9.262*BW -378,738	0.02937	Iyy
Left thigh	Ixx =	20.310*BW - 172,235	0.1302	Ixx
	Iyy =	23.633*BW - 319,070	0.1397	Izz
	Izz =	5.404*BW - 139,702	0.02526	Iyy
Right shank	Ixx =	5.424*BW + 37,127	0.04309	Ixx
	Iyy =	5.341*BW + 44,749	0.04325	Izz
	Izz =	0.94*BW - 32,220	0.003602	Iyy
Left shank	Ixx =	6.434*BW - 24,410	0.04427	Ixx
	Iyy =	5.350*BW + 40,974	0.04294	Izz
	Izz =	0.969*BW - 34,567	0.003578	Iyy
Right foot	Ixx =	0.433*BW + 5,371	0.003681	Iyy
	Iyy =	0.355*BW + 7,296	0.003307	Izz
	Izz =	0.153*BW - 2,988	0.0008120	Ixx
Left foot	Ixx =	0.371*BW + 8.974	0.002694	Iyy
	Iyy =	0.391*BW + 4,959	0.003335	Izz
	Izz =	0.130*BW - 946	0.0008492	Ixx

Model 5: de Leva (1996, based on Zatsiorsky-Seluyanov, 1983)

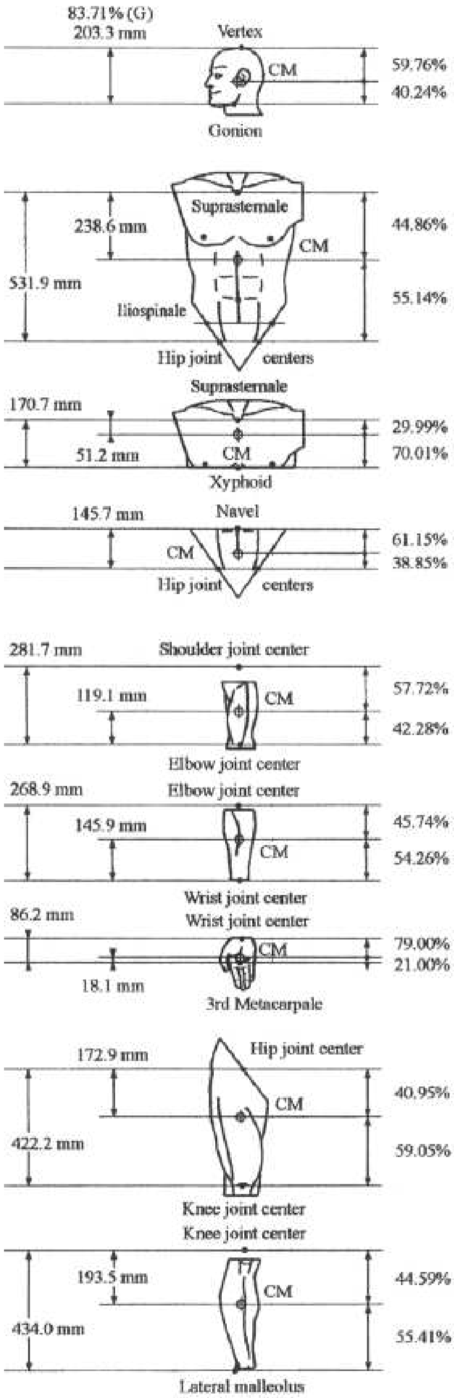

Figure 43: Division of body segments in de Leva

Segment mass calculations
de Leva provides percentage mass of total body weight for each body segment as shown in Table XX. In this study, HAT mass is calculated as the sum of the upper torso, middle torso, head, and arms. The lower torso segment is taken to be the pelvis segment.

Table 28: Segment masses calculated using de Leva's relations

	Segment mass (% of total body mass)	Mass (kg)
Head	6.94	5.038
Trunk	43.46	31.55
UPT (Upper torso)	15.96	11.59
MPT (Middle torso)	16.33	11.86
LPT (Lower torso, or pelvis)	11.17	8.109
Upper arm	2.71	1.967
forearm	1.62	1.176
Hand	0.61	0.4429
Thigh	14.16	10.28
Shank	4.33	3.144
Foot	1.37	0.9946
HAT		35.65

Segment center-of-mass location calculations

Center-of-mass locations as a percentage of specific segment lengths are calculated using the average segment length values presented in de Leva. These values were then converted to OpenSim model lengths.

Table 29: Segment center-of-mass locations calculated using de Leva's relations

COM location (males)	% of segment length		**COM (m) as defined in osim**	
Head	83.47	from hip, with segment length being hips to vertex of head	0.7063	in torso segment (y dir)
Trunk	39.89	from hip, with segment length being hips to vertex of head	0.2998	in torso segment (y dir)
UPT	65.39	from hip, of hip to top of head distance (i.e., pelvis + torso)	0.5376	in torso segment (y dir)
MPT	35.93	from hip, of hip to top of head distance (i.e., pelvis + torso)	0.2628	in torso segment (y dir)
LPT (pelvis)	7.699	from hip, of hip to top of head distance (i.e., pelvis + torso)	-0.0005760	in pelvis segment (y dir)
Thigh	40.95	from hip joint	-0.1921	in femur segment (y dir)
Shank	44.59	from knee	-0.1895	in tibia segment (y dir)
Foot	44.15	from heel	0.1051	in calcn segment (x dir)
HAT (UPT, MPT, head, arms)			0.4531	in torso segment (y dir)
		de Leva HAT using Dumas mass	0.7888	in torso segment (y dir)
		de Leva HAT using Gebod mass	0.3538	in torso segment (y dir)

Segment inertia calculations

de Leva provides radii of gyration for each segment, where radii of gyration values are presented as a percentage of the associated segment's length. The formula to calculate inertia from radius of gyration is,

$$\mathbf{I} = m(rL)^2 \qquad \textbf{Equation 28}$$

where I is the moment of inertia, m is the segment mass, r is the radius of gyration as a percentage of segment length, and L is the segment length Table 30 shows the conversion of de Leva's radius of gyration proportions to OpenSim model proportions, and Table 31 shows the final calculated inertia values.

Table 30: Conversion of de Leva's radii of gyration relations to OpenSim model proportions

	de Leva's values and relations				in Opensim proportions					
		radius of gyration			radius of gyration					
Segment	Longitudinal length (mm)	Sagittal r (%)	Transverse r (%)	Longitudinal r (%)	Sagittal r (%)		Transverse r (%)		Longitudinal r (%)	
Head	203.3	36.2	37.6	31.2	10.01	of hip to head vertex distance	10.40	of hip to head vertex distance	8.63	from hip to head vertex distance
Trunk	531.9	37.2	34.7	19.1	26.91	of hip to head vertex distance	25.10	of hip to head vertex distance	13.82	from hip to head vertex distance
UP Torso	170.7	71.6	45.4	65.9	16.62	of hip to head vertex distance	10.54	of hip to head vertex distance	15.30	from hip to head vertex distance
MP Torso	215.5	48.2	38.3	46.8	14.13	of hip to head vertex distance	11.23	of hip to head vertex distance	13.72	from hip to head vertex distance
LP Torso	145.7	61.5	55.1	58.7	12.19	of hip to head vertex distance	10.92	of hip to head vertex distance	11.63	from hip to head vertex distance
Upper arm	281.7	28.5	26.9	15.8						
forearm	268.9	27.6	26.5	12.1						
hand	86.2	62.8	51.3	40.1						
thigh	422.2	32.9	32.9	14.9	32.9	from hip to knee	32.9	from hip to knee	14.9	from hip to knee
shank	434	25.5	24.9	10.3	25.5	from knee to ankle	24.9	from knee to ankle	10.3	from knee to ankle
foot	258.1	25.7	24.5	12.4	25.7	from heel to toe	24.5	from heel to toe	12.4	from heel to toe

Table 31: Segment inertia values based on de Leva

	Moment of inertia (kg-m^2)					
Segment	**Sagittal I**		**Transverse I**		**Longitudinal I**	
		OpenSim coord		OpenSim coord		OpenSim coord
Head	0.04394		0.04740		0.03264	
Trunk	1.989	Ixx	1.731	Izz	0.5243	Iyy
UP Torso	0.2787		0.1120		0.2361	
MP Torso	0.2060		0.1300		0.1942	
LP Torso	0.1048	Ixx	0.08415	Izz	0.09551	Iyy
Upper arm						
forearm						
hand						
thigh	0.2449	Ixx	0.2449	Izz	0.05022	Iyy
shank	0.03692	Ixx	0.03521	Izz	0.006024	Iyy
foot	0.003721	Iyy	0.003382	Izz	0.0008660	Ixx

Model 5: Dumas (2007, based on data from McConville, 1980)

Segment mass calculations

Dumas provides percentage mass of total body weight for each body segment as shown in Table 32. In this study, HAT mass is calculated as the sum of the head and neck, torso, and arms.

Table 32: Segment masses calculated using Dumas's relations

Segment	Mass as % of total body mass (males)	Mass (kg)
Head & Neck	6.7	4.86
Torso	33.3	24.2
Pelvis	14.2	10.3
Arm	2.4	1.74
Forearm	1.7	1.23
Hand	0.6	0.436
Thigh	12.3	8.93
Shank	4.8	3.48
Foot	1.2	0.871
HAT		35.9

Segment center-of-mass location calculations

Center-of-mass locations as a percentage of specific segment lengths are calculated using the average segment length values presented in Dumas. These values were then converted to OpenSim model lengths

Table 33: Segment com locations calculated using Dumas

Segment		COM dist (% of segment length)		COM (m) as defined in osim	
Head & neck	X	-1.73	from hips to head vertex	-0.0161	in torso segment (x-dir)
	Y	87.6	from hips to head vertex	0.745	in torso segment (y-dir)
	Z	0.0279	from hips to head vertex	0.000260	in torso segment (z-dir)
Torso	X	2.17	from hips to head vertex	0.0202	in torso segment (x-dir)
	Y	46.8	from hips to head vertex	0.364	in torso segment (y-dir)
	Z	0.120	from hips to head vertex	0.00112	in torso segment (z-dir)
pelvis	X	0.00332	from hips to head vertex	3.10E-05	in pelvis segment (x-dir)
	Y	3.32	from hips to head vertex	-0.0414	in pelvis segment (y-dir)
	Z	-0.000712	from hips to head vertex	-6.64E-06	in pelvis segment (z-dir)
Thigh	X	-4.10	from hip	-0.0192	in femur segment (x-dir)
	Y	-42.9	from hip	-0.201	in femur segment (y-dir)
	Z	3.30	from hip	0.0155	in femur segment (z-dir)
Shank	X	-4.80	from knee	-0.0204	in tibia segment (x-dir)
	Y	-41.0	from knee	-0.174	in tibia segment (y-dir)
	Z	0.700	from knee	0.00298	in tibia segment (z-dir)
Foot	X	38.2	ankle joint to toes	0.0909	in calcn segment (x-dir)
	Y	-15.1	ankle joint to toes	-0.0359	in calcn segment (y-dir)
	Z	2.60	ankle joint to toes	0.00619	in calcn segment (z-dir)
HAT	X			0.0141	in torso segment (x-dir)
	Y			0.428	in torso segment (y-dir)
	Z			0.000979	in torso segment (z-dir)
Dumas HAT using de Leva mass:	X			0.0152	in torso segment (x-dir)
	Y			0.417	in torso segment (y-dir)
	Z			0.00100	in torso segment (z-dir)
Dumas HAT using Gebod mass:	X			0.0154	in torso segment (x-dir)
	Y			0.415	in torso segment (y-dir)
	Z			0.00101	in torso segment (z-dir)

Segment inertia calculations

Dumas provides radii of gyration for each segment, where radii of gyration values are presented as a percentage of the associated segment’s length. The conversion of these values to inertia values in the OpenSim model was performed the same way as with de Leva.

Table 34 shows Dumas’s radius of gyration proportions, while Table 35 shows the final OpenSim model inertia values calculated from Dumas’s relations.

Table 34: Segment radii of gyration calculated using Dumas

	Dumas's relations and values				
Segment	**Length (mm)**	**distance (mm)**	**from**		**radii of gyration (% of segment length)**
Head & neck	244	-15.13	neck to top of head	rxx	31
		135.4	neck to top of head	ryy	25
		0.2440	neck to top of head	rzz	33
HAT (torso, head & neck arms)	477	17.17	neck to lumbar	rxx	27
use torso values to calculate inertia		200.3	neck to lumbar	ryy	25
		0.9540	neck to lumbar	rzz	28
pelvis	94	2.632	from lumbar to hip joint (y dir)	rxx	101
		26.32	from lumbar to hip joint (y dir)	ryy	106
		-0.5640	from lumbar to hip joint (y dir)	rzz	95
Thigh				rxx	29
				ryy	15
				rzz	30
Shank				rxx	28
				ryy	10
				rzz	28
Foot				rxx	17
				ryy	37
				rzz	36

Table 35: Segment inertias calculated using Dumas

	Conversion to OpenSim values				
Segment	**radii of gyration (% of Osim segment length)**		radii of gyration (m)	Moment of inertia (kg-m^2)	
Head & neck	9.281	of hip to head vertex length	0.08658	0.03646	Ixx
	7.485	of hip to head vertex length	0.06982	0.02372	Iyy
	9.880	of hip to head vertex length	0.09217	0.04132	Izz
HAT (torso, head & neck arms)	15.80	of hip to head vertex length	0.1474	0.7794	Ixx
use torso values to calculate inertia	14.63	of hip to head vertex length	0.1365	0.6682	Iyy
	16.39	of hip to head vertex length	0.1529	0.8382	Izz
pelvis	11.65	of hip to head vertex length	0.1087	0.1218	Ixx
	12.23	of hip to head vertex length	0.1141	0.1341	Iyy
	10.96	of hip to head vertex length	0.1022	0.1077	Izz
Thigh	29	of hip to knee length	0.1360	0.1653	Ixx
	15	of hip to knee length	0.07037	0.04421	Iyy
	30	of hip to knee length	0.1407	0.1769	Izz
Shank	28	of knee to ankle length	0.1190	0.04935	Ixx
	10	of knee to ankle length	0.04250	0.006294	Iyy
	28	of knee to ankle length	0.119	0.04935	Izz
Foot	17	of heel to toe length	0.04046	0.001426	Ixx
	37	of heel to toe length	0.08806	0.006756	Iyy
	36	of heel to toe length	0.08568	0.006395	Izz

Appendix C: Relevant OpenSim Files

Subject01_Setup_Scale.xml

```
<?xml version="1.0" encoding="UTF-8" ?>
- <ScaleTool name="subject01">
- <!--
Mass of the subject in kg.  Subject-specific model generated by
      scaling step will have this total mass.
  -->
<mass>72.6</mass>
- <!--
Height of the subject in mm.  For informational purposes only (not
      used by scaling).
  -->
<height>1803.4</height>
- <!--
Age of the subject in years.  For informational purposes only (not
      used by scaling).
  -->
<age>99</age>
- <!--
Notes for the subject.
  -->
<notes>This is an example setup file for scale.exe.</notes>
- <!--
Specifies the name of the unscaled model (.osim) and the marker set.
  -->
- <GenericModelMaker name="">
- <!--
Model file (.osim) for the unscaled model.
  -->
<model_file>gait2354_simbody.osim</model_file>
- <!--
Set of model markers used to scale the model. Scaling is done based on
              distances between model markers compared to the same
  distances between
              the corresponding experimental markers.
  -->
<marker_set_file>gait2354_Scale_MarkerSet.xml</marker_set_file>
  </GenericModelMaker>
- <!--
Specifies parameters for scaling the model.
  -->
- <ModelScaler name="">
- <!--
Specifies the scaling method and order. Valid options are
              'measurements', 'manualScale', singly or both in any
  sequence.
  -->
<scaling_order>measurements manualScale</scaling_order>
```

```
- <!--
Scale factors to be used for manual scaling.
  -->
<ScaleSet file="subject01_Scale_ScaleSet.xml" />
- <!--
Specifies the measurements by which body segments are to be scaled.
  -->
<MeasurementSet file="gait2354_Scale_MeasurementSet.xml" />
- <!--
TRC file (.trc) containing the marker positions used for
              measurement-based scaling. This is usually a static trial,
  but doesn't
              need to be.  The marker-pair distances are computed for each
  time step
              in the TRC file and averaged across the time range.
  -->
<marker_file>subject01_static.trc</marker_file>
- <!--
Time range over which to average marker-pair distances in the marker
              file (.trc) for measurement-based scaling.
  -->
<time_range>1 2</time_range>
- <!--
Flag (true or false) indicating whether or not to preserve relative
              mass between segments.
  -->
<preserve_mass_distribution>true</preserve_mass_distribution>
- <!--
Name of SIMM joint file to write when done scaling. If not specified,
              a file will not be written.
          <output_joint_file> subject01_scaledOnly.jnt
  </output_joint_file>
  -->
- <!--
Name of SIMM muscle file to write when done scaling. If not specified,
              a file will not be written.
          <output_muscle_file> subject01_scaledOnly.msl
  </output_muscle_file>
  -->
- <!--
Name of OpenSim model file (.osim) to write when done scaling.
  -->
<output_model_file>subject01_scaledOnly.osim</output_model_file>
- <!--
Name of file to write containing the scale factors that were applied
              to the unscaled model (optional).
  -->
<output_scale_file>subject01_scaleSet_applied.xml</output_scale_file>
  </ModelScaler>
- <!--
Specifies parameters for placing markers on the model once a model is
      scaled.
  -->
```

```
- <MarkerPlacer name="">
  - <!--
  TRC file (.trc) containing the time history of experimental marker
                 positions (usually a static trial).
    -->
  <marker_file>subject01_static.trc</marker_file>
  - <!--
  Task set used to specify weights used in the IK computation of the
                 static pose.
    -->
  <IKTaskSet file="gait2354_Scale_Tasks.xml" />
  - <!--
  Name of file containing the joint angles used to set the initial
                 configuration of the model for the purpose of placing the
    markers.
                 These coordinate values can also be included in the
    optimization
                 problem used to place the markers. Before the model markers
    are
                 placed, a single frame of an inverse kinematics (IK) problem
    is
                 solved. The IK problem can be solved simply by matching
    marker
                 positions, but if the model markers are not in the correct
    locations,
                 the IK solution will not be very good and neither will
    marker
                 placement. Alternatively, coordinate values (specified in
    this file)
                 can be specified and used to influence the IK solution. This
    is
                 valuable particularly if you have high confidence in the
    coordinate
                 values. For example, you know for the static trial the
    subject was
                 standing will all joint angles close to zero. If the
    coordinate set
                 (see the CoordinateSet property) contains non-zero weights
    for
                 coordinates, the IK solution will try to match not only the
    marker
                 positions, but also the coordinates in this file. Least-
    squared error
                 is used to solve the IK problem.
    -->
  <coordinate_file />
  - <!--
  Time range over which the marker positions are averaged.
    -->
  <time_range>1 2</time_range>
  - <!--
  Name of the new SIMM Joint file (.jnt) after scaling and marker
                 placement (optional).
            <output_joint_file> subject01.jnt </output_joint_file>
    -->
```

```
- <!--
Name of the SIMM muscle file (.msl) after scaling and marker placement
              (optional).
          <output_muscle_file> subject01.msl </output_muscle_file>
  -->
- <!--
Output OpenSim model file (.osim) after scaling and maker placement.
  -->
<output_model_file>subject01_simbody.osim</output_model_file>
- <!--
Name of the motion file (.mot) written after marker relocation
              (optional).
  -->
<output_motion_file>subject01_static_output.mot</output_motion_file>
  </MarkerPlacer>
  </ScaleTool>
```

subject01_Setup_IK.xml

```
<?xml version="1.0" encoding="UTF-8" ?>
- <IKTool name="subject01">
- <!--
Name of the .osim file used to construct a model.
  -->
<model_file>subject01_simbody.osim</model_file>
- <!--
Specify which optimizer to use (ipopt or cfsqp).
  -->
<optimizer_algorithm>ipopt</optimizer_algorithm>
- <!--
Task set used to specify IK weights.
  -->
<IKTaskSet file="gait2354_IK_Tasks.xml" />
- <!--
Parameters for solving the IK problem for each trial. Each trial
      should get a seperate SimmIKTril block.
  -->
- <IKTrialSet name="">
- <objects>
- <IKTrial name="first trial">
- <!--
TRC file (.trc) containing the time history of experimental marker
                             positions.
  -->
<marker_file>subject01_walk1.trc</marker_file>
- <!--
Name of file containing the joint angles used to set the initial
                             configuration of the model for the purpose of
  placing the markers.
                             These coordinate values can also be included
  in the optimization
                             problem used to place the markers. Before the
  model markers are
```

```
placed, a single frame of an inverse
kinematics (IK) problem is
solved. The IK problem can be solved simply
by matching marker
positions, but if the model markers are not
in the correct locations,
the IK solution will not be very good and
neither will marker
placement. Alternatively, coordinate values
(specified in this file)
can be specified and used to influence the IK
solution. This is
valuable particularly if you have high
confidence in the coordinate
values. For example, you know for the static
trial the subject was
standing will all joint angles close to zero.
If the coordinate set
(see the CoordinateSet property) contains
non-zero weights for
coordinates, the IK solution will try to
match not only the marker
positions, but also the coordinates in this
file. Least-squared error
is used to solve the IK problem.
  -->
<coordinate_file>subject01_walk1.mot</coordinate_file>
- <!--
Time range over which the IK problem is solved.
  -->
<time_range>0.4 1.60</time_range>
- <!--
Name of the motion file (.mot) to which the results should be written.
  -->
<output_motion_file>subject01_walk1_ik.mot</output_motion_file>
  </IKTrial>
  </objects>
  </IKTrialSet>
  </IKTool>
```

subject01_Setup_RRA.xml

```
<?xml version="1.0" encoding="UTF-8" ?>
- <CMCTool name="subject01_walk1_RRA">
<defaults />
- <!--
Name of the .osim file used to construct a model.
  -->
<model_file>subject01_simbody.osim</model_file>
- <!--
Replace the model's actuator set with sets specified in
      <actuator_set_files>? If false, the actuator set is appended to.
  -->
<replace_actuator_set>true</replace_actuator_set>
```

```
- <!--
List of xml files used to construct an actuator set for the model.
  -->
<actuator_set_files>gait2354_RRA_Actuators.xml</actuator_set_files>
- <!--
Directory used for writing results.
  -->
<results_directory>ResultsRRA/</results_directory>
- <!--
Output precision.  It is 8 by default.
  -->
<output_precision>20</output_precision>
- <!--
Initial time for the simulation.
  -->
<initial_time>0.75</initial_time>
- <!--
Final time for the simulation.
  -->
<final_time>1.25</final_time>
- <!--
Maximum number of integrator steps.
  -->

  <maximum_number_of_integrator_steps>20000</maximum_number_of_integrato
  r_steps>
- <!--
Maximum integration step size.
  -->
<maximum_integrator_step_size>0.001</maximum_integrator_step_size>
- <!--
Integrator error tolerance. When the error is greater, the integrator
      step size is decreased.
  -->
<integrator_error_tolerance>0.0001</integrator_error_tolerance>
- <!--
Integrator fine tolerance. When the error is less, the integrator step
      size is increased.
  -->
<integrator_fine_tolerance>1e-006</integrator_fine_tolerance>
- <!--
Flag (true or false) indicating whether or not to make an adjustment
      in the center of mass of a body to reduced DC offsets in MX and MZ.
  If
      true, a new model is writen out that has altered anthropometry.
  -->
<adjust_com_to_reduce_residuals>true</adjust_com_to_reduce_residuals>
- <!--
Name of the body whose center of mass is adjusted. The heaviest
      segment in the model should normally be chosen. For a gait model,
  the
      torso segment is usually the best choice.
  -->
```

```
<adjusted_com_body>torso</adjusted_com_body>
- <!--
Name of the output model file (.osim) containing adjustments to
      anthropometry made to reduce average residuals. This file is
  written
      if the property adjust_com_to_reduce_residuals is set to true. If a
      name is not specified, the model is written out to a file called
      adjusted_model.osim.
  -->
<output_model_file>subject01_simbody_adjusted.osim</output_model_file>
- <!--
Motion (.mot) or storage (.sto) file containing the desired kinematic
      trajectories.
  -->
<desired_kinematics_file>subject01_walk1_ik_14s.mot</desired_kinematics_file>
- <!--
Low-pass cut-off frequency for filtering the desired kinematics. A
      negative value results in no filtering. The default value is -1.0,
  so
      no filtering.
  -->
<lowpass_cutoff_frequency>6</lowpass_cutoff_frequency>
- <!--
File containing the tracking tasks. Which coordinates are tracked and
      with what weights are specified here.
  -->
<task_set_file>gait2354_RRA_Tasks.xml</task_set_file>
- <!--
File containing the constraints on the controls.
  -->
<constraints_file>gait2354_RRA_ControlConstraints.xml</constraints_file>
- <!--
Motion file (.mot) or storage file (.sto) containing the external
      loads applied to the model.
  -->
<external_loads_file>subject01_walk1_grf.mot</external_loads_file>
- <!--
Motion file (.mot) or storage file (.sto) containing the model
      kinematics corresponding to the external loads.
  -->

  <external_loads_model_kinematics_file>subject01_walk1_ik.mot</external_load
  s_model_kinematics_file>
- <!--
Name of the body to which the first set of external loads should be
      applied (e.g., the name of the right foot).
  -->
<external_loads_body1>calcn_r</external_loads_body1>
- <!--
Name of the body to which the second set of external loads should be
      applied (e.g., the name of the left foot).
  -->
<external_loads_body2>calcn_l</external_loads_body2>
```

```xml
- <!--
Low-pass cut-off frequency for filtering the model kinematics
      corresponding to the external loads. A negative value results in no
      filtering. The default value is -1.0, so no filtering.
  -->
  <lowpass_cutoff_frequency_for_load_kinematics>6</lowpass_cutoff_frequency_for_
  load_kinematics>
- <!--
Flag (true or false) indicating whether to use the fast CMC
      optimization target. The fast target requires the desired
      accelerations to be met. The optimizer fails if the acclerations
      constraints cannot be met, so the fast target can be less robust.
  The
      regular target does not require the acceleration constraints to be
      met; it meets them as well as it can, but it is slower and less
      accurate.
  -->
<use_fast_optimization_target>false</use_fast_optimization_target>
- <!--
Perturbation size used by the optimizer to compute numerical
      derivatives. A value between 1.0e-4 and 1.0e-8 is usually
      approprieate.
  -->
<optimizer_derivative_dx>0.0001</optimizer_derivative_dx>
- <!--
Convergence criterion for the optimizer. The smaller this value, the
      deeper the convergence. Decreasing this number can improve a
  solution,
      but will also likely increase computation time.
  -->
<optimizer_convergence_criterion>1e-006</optimizer_convergence_criterion>
- <!--
Maximum number of iterations for the optimizer.
  -->
<optimizer_max_iterations>2000</optimizer_max_iterations>
- <!--
Print level for the optimizer, 0 - 3. 0=no printing, 3=detailed
      printing, 2=in between
  -->
<optimizer_print_level>0</optimizer_print_level>
- <!--
Specify which optimizer to use (ipopt or cfsqp).
  -->
<optimizer_algorithm>ipopt</optimizer_algorithm>
- <!--
Time window over which the desired actuator forces are achieved.
      Muscles forces cannot change instantaneously, so a finite time
  window
      must be allowed. The recommended time window for RRA is about 0.001
      sec, and for CMC is about 0.010 sec.
  -->
<cmc_time_window>0.001</cmc_time_window>
- <!--
```

```
Flag (true or false) indicating whether or not to use the curvature
      filter. Setting this flag to true can reduce oscillations in the
      computed muscle excitations.
  -->
<use_curvature_filter>false</use_curvature_filter>
- <!--
Flag (true or false) indicating whether or not to compute average
      residuals. No actions are taken based on this flag other than
  printing
      the average residuals, which can be useful for seeing if the
  solution
      is good.  Average residuals should be be close to 0.0.  If not,
  there
      is likely problem in the experimental data, in the model, or both.
  -->
<compute_average_residuals>true</compute_average_residuals>
- <!--
Flag (true or false) indicating whether or not to make an adjustment
      in the center of mass of a body to reduced DC offsets in MX and MZ.
  If
      true, a new model is writen out that has altered anthropometry.
  -->
  </CMCTool>
```

Appendix D: Rigid-Body Dynamics Derivations

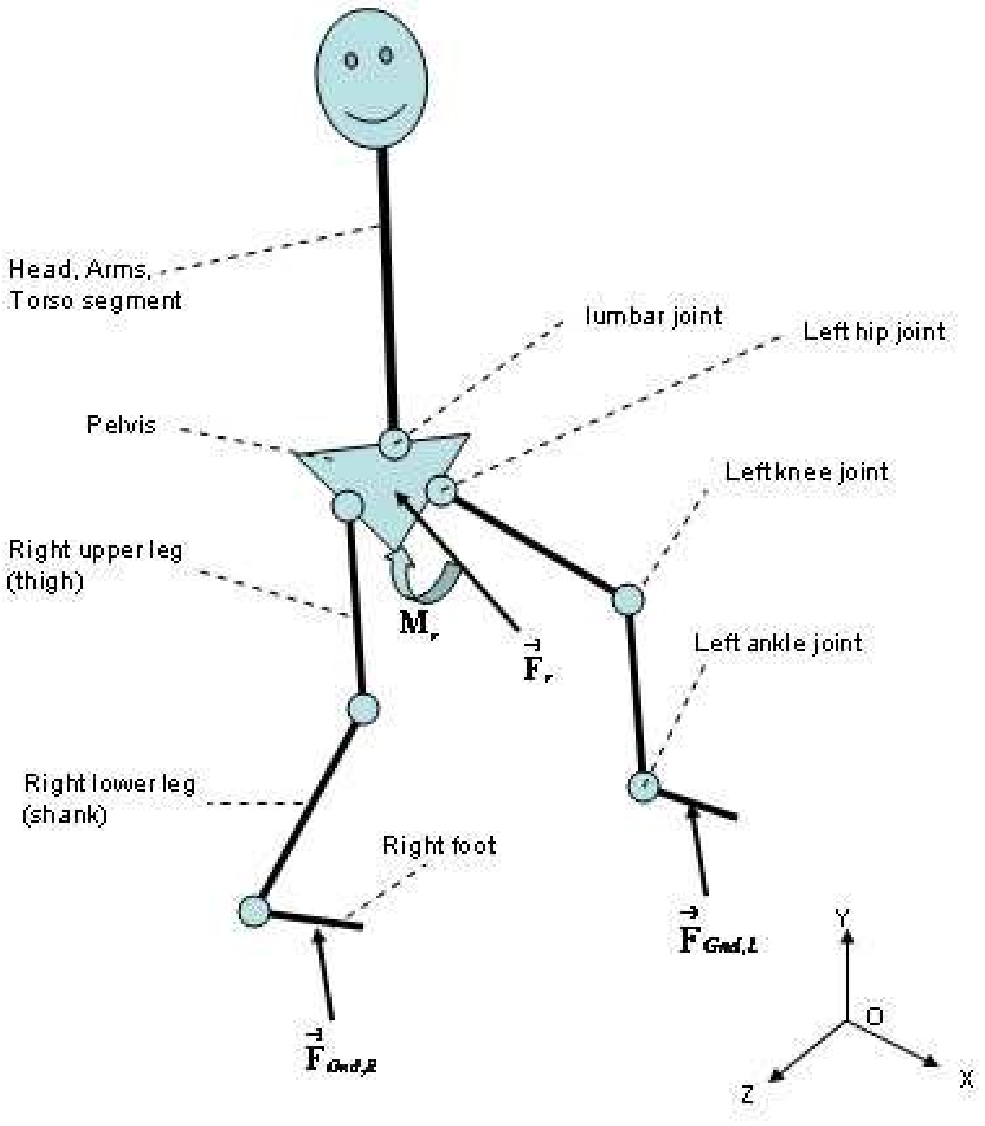

Figure 44: Schematic of 2D dynamic analysis body model

A schematic of the body with external ground and residual forces and moments applied is shown above. Equations were then derived using the Newton-Euler method.

Foot

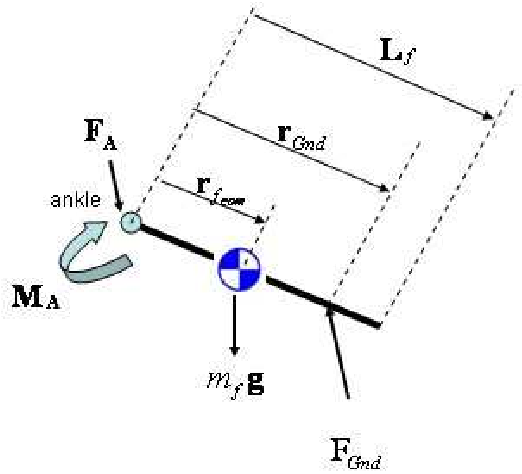

Figure 45: Free body diagram of foot

Vectors shown in the free body diagram above are all with respect to the world coordinate frame and are defined as follows:

$\vec{F}_A$ = reaction force at ankle
$\vec{M}_A$ = ankle joint moment
$\vec{F}_Gnd$ = ground reaction force
m_f = mass of foot
$\vec{a}_f$ = linear acceleration at foot center-of-mass
$[I]_f$ = moment of inertia matrix at foot center-of-mass
$\vec{r}_{f_{com}}$ = distance from ankle to foot center-of-mass
$\vec{r}_{Gnd}$ = distance from ankle to application point of ground reaction force
$\vec{L}_f$ = foot length vector

Summing forces about the foot, we have

$$\sum F : \vec{F}_A + m_f\vec{g} + \vec{F}_{Gnd} = m_f\vec{a}_f \tag{29}$$

Rearranging to solve for $\boldsymbol{F_A}$***:***

$$\vec{F}_A = m_f(\vec{a}_f - \vec{g}) - \vec{F}_{Gnd} \tag{30}$$

Summing torques about the center-of-mass, we have

$$\sum \tau_{com} : \vec{M}_A + (-\vec{r}_{f_{com},r} \times \vec{F}_A) + [(\vec{r}_{Gnd} - \vec{r}_{f_{com}} \times \vec{F}_{Gnd}] = [I]_f\vec{\alpha}_f \tag{31}$$

Rearranging to solve for ankle joint moment,

$$\vec{M}_{A,R} = -(\vec{r}_{Gnd,R} - \vec{r}_{f_{com},R}) \times \vec{F}_{Gnd,R} + [I]_f \vec{\alpha}_{f,R} + (\vec{r}_{f_{com},R} \times \vec{F}_{A,R}) \quad \textbf{(32)}$$

Lower Leg (Shank)

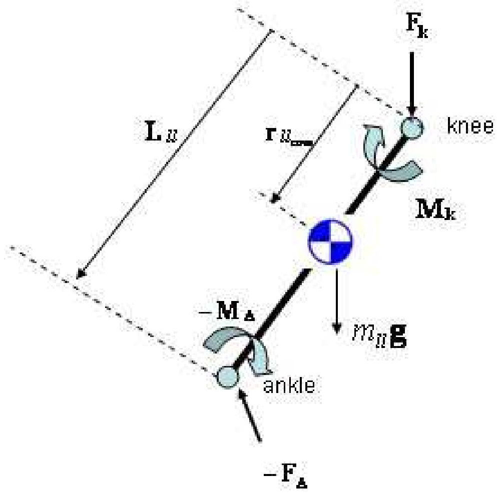

Figure 46: Free body diagram of lower leg

Vectors shown in the free body diagram above are all with respect to the world coordinate frame and are defined as follows:

$\vec{M}_k$ = knee joint moment
$\vec{F}_k$ = reaction force at knee
m_{ll} = mass of lower leg (shank) segment
$\vec{a}_{ll}$ = linear acceleration at shank center-of-mass
$[I]_{ll}$ = moment of inertia matrix at shank center-of-mass
$\vec{r}_{ll_{com}}$ = distance vector from knee to lower leg center-of-mass
$\vec{L}_{ll}$ = length vector from knee to ankle

Summing forces on the segment, we have

$$\sum F : -\vec{F}_A + \vec{F}_k + m_{ll}\vec{g} = m_{ll}\vec{a}_{ll} \tag{33}$$

Solving for knee joint moment and substituting equation XX,

$$\vec{F}_k = m_{ll}(\vec{a}_{ll} - \vec{g}) + m_f(\vec{a}_f - \vec{g}) - \vec{F}_{Gnd} \tag{34}$$

Summing torques about the center-of-mass and solving for knee joint moment,

$$\vec{M}_k = \vec{M}_A + [I]_{ll}\vec{\alpha}_{ll} + (\vec{r}_{ll_{com}} \times \vec{F}_k) + [(\vec{L}_{ll} - \vec{r}_{ll_{com}} \times \vec{F}_A] \tag{35}$$

Upper Leg (Thigh)

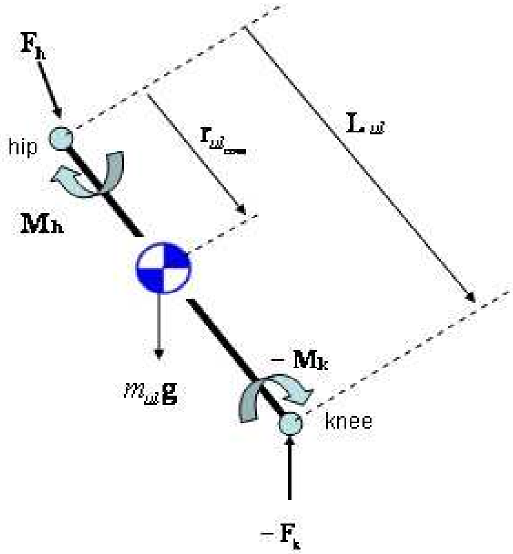

Figure 47: Free body diagram of upper leg

Vectors shown in the free body diagram above are all with respect to the world coordinate frame and are defined as follows:

$\vec{F}_h$ = hip reaction force
$\vec{M}_h$ = hip joint moment
m_{ul} = mass of upper leg (thigh) segment
$\vec{a}_{ul}$ = linear acceleration at thigh center-of-mass
$[I]_{ul}$ = moment of inertia matrix at thigh center-of-mass
$\vec{r}_{ul_{com}}$ = distance vector from hip joint to thigh center-of-mass
$\vec{L}_{ul}$ = length vector from hip to knee

Summing forces on the segment, we have

$$\sum F : -\vec{F}_k + \vec{F}_h + m_{ul}\vec{g} = m_{ul}\vec{a}_{ul} \quad \textbf{(36)}$$

Solving for hip joint moment and substituting equations XX and XX,

$$\vec{F}_h = m_{ul}(\vec{a}_{ul} - \vec{g}) + m_{ll}(\vec{a}_{ll} - \vec{g}) + m_f(\vec{a}_f - \vec{g}) - \vec{F}_{Gnd} \quad \textbf{(37)}$$

Summing torques about the center-of-mass and solving for hip joint moment,

$$\vec{M}_h = \vec{M}_k + [I]_{ul}\vec{\alpha}_{ul} + (\vec{r}_{ul_{com}} \times \vec{F}_h) + [(\vec{L}_{ul} - \vec{r}_{ul_{com}}) \times \vec{F}_k] \quad \textbf{(38)}$$

Head, Arms, Torso (HAT) segment

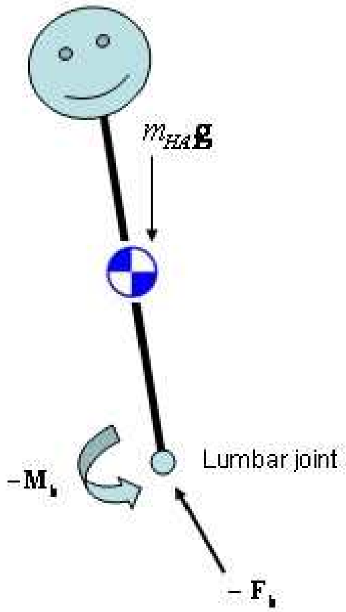

Figure 48: Free body diagram of HAT segment

Definition of variables:
$\vec{F_b}$ = reaction force at lumbar joint
$\vec{M_b}$ = lumbar joint moment
m_{HAT} = mass of head,arms,torso segment
r_{HAT} = distance vector from lumbar joint to HAT center-of-mass
$[I]_{HAT}$ = moment of inertia matrix for HAT segment
$\vec{a}_{HAT}$ = linear acceleration at HAT center-of-mass

Summing forces on the segment and solving for lumbar joint reaction force,

$$\vec{F_b} = m_{HAT}(\vec{g} - \vec{a}_{HAT}) \tag{39}$$

Summing moments about center-of-mass and solving for lumbar joint moment,

$$\vec{M_b} = (\vec{r}_{HAT_{com}} \times \vec{F_b}) - [I]_{HAT}\vec{\alpha}_{HAT} \tag{40}$$

Pelvis

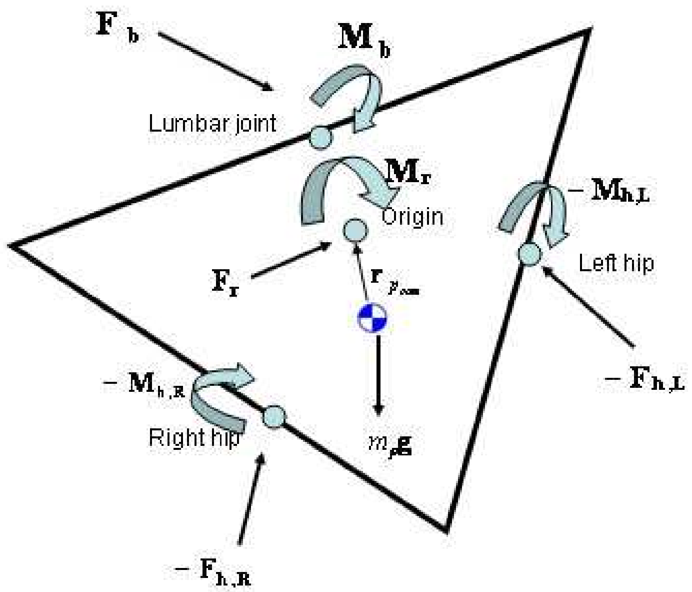

Figure 49: Free body diagram of pelvis

Vectors shown in the free body diagram above are all with respect to the world coordinate frame and are defined as follows:

$\vec{F}_r$ = residual external force applied to maintain bipedal stability
$\vec{M}_r$ = residual exeternal moment applied to maintain bipedal stability
$\vec{r}_{p_{com}}$ = distance vector from pelvis center-of-mass to origin, where residual forces/moments are applied
$\vec{a}_p$ = linear acceleration of pelvis center-of-mass
$[I]_p$ = moment of inertia matrix at pelvis center-of-mass
m_p = mass of pelvis
$\vec{F}_{h,R}$ = reaction force at right hip joint
$\vec{M}_{h,R}$ = right hip joint moment
$\vec{F}_{h,L}$ = reaction force at left hip joint
$\vec{M}_{h,L}$ = left hip joint moment
$\vec{r}_{Rh,p_{com}}$ = distance vector from pelvis com to right hip
$\vec{r}_{Lh,p_{com}}$ = distance vector from pelvis com to left hip
$\vec{r}_{b,p_{com}}$ = distance vector from pelvis com to lumbar joint
α_p = angular acceleration of pelvis segment

Summing forces on segment and solving for residual force,

$$\vec{F}_r = m_p(\vec{a}_p - \vec{g}) + \vec{F}_{h,R} + \vec{F}_{h,L} - \vec{F}_b \quad \textbf{(41)}$$

Summing torques about center-of-mass and solving for residual moment,

$$\vec{M}_r = \vec{M}_{h,R} + \vec{M}_{h,L} - \vec{M}_b + [I]_p\vec{\alpha}_p + (\vec{r}_{rh,p_{com}} \times \vec{F}_{u,R}) + (\vec{r}_{lh,p_{com}} \times \vec{F}_{h,L}) - (\vec{r}_{b,p_{com}} \times \vec{F}_b) - (\vec{r}_{p_{com}} \times \vec{F}_r) + [I]_p\vec{\alpha}_p \quad (42)$$

2D flexion approximations

For the 2D approximations, we assume all motion occurs in the sagittal plane. The sagittal plane is defined as shown in Figure 50. With this assumption, we are interested in joint moments in the world z-axis as shown in Figure 44. We also assume the principal moment of inertia is aligned with the z-axis and ignore cross products of inertia.

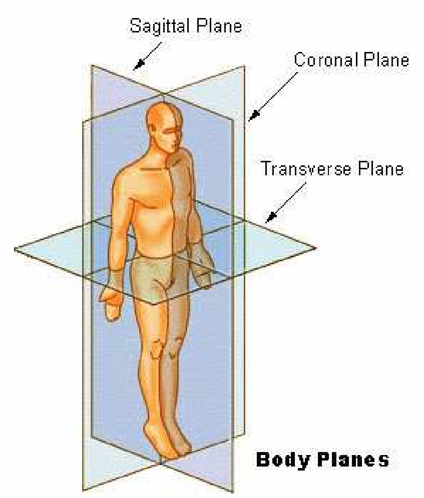

Figure 50: Definitions of body planes

OpenSim defines joint angles in local frames. We begin by converting these to angles in the world frame with respect to the vertical (y-axis). These world angle definitions are shown in Figure 51 and are the angles used in our derivations.

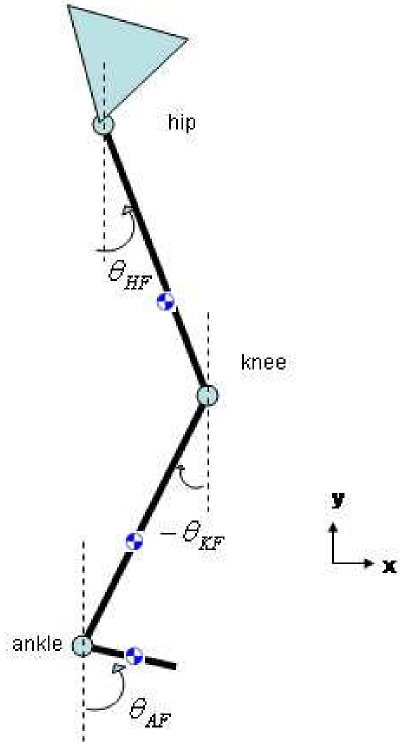

Figure 51: Definition of joint angles in world frame with respect to vertical (y-axis)

2D Ankle Flexion Moment

We begin by converting the 3D dynamical equation for the foot to its 2D approximation. From earlier, the 3D equation for ankle joint moment is,

$$\vec{M}_{A,R} = -(\vec{r}_{Gnd,R} - \vec{r}_{f_{com},R}) \times \vec{F}_{Gnd,R} + [I]_f \vec{\alpha}_{f,R} + (\vec{r}_{f_{com},R} \times \vec{F}_{A,R}) \tag{32}$$

Here, we will ignore the subscripts *R* that denote this is for the right leg, and take this analysis to be for any leg. The cross and dot products in this equation are evaluated as follows,

$$(\vec{r}_{f_{com}} \times \vec{F}_A) = r_{f_{com}} \begin{bmatrix} e_{x_f} \\ e_{y_f} \\ e_{z_f} \end{bmatrix} \times \begin{bmatrix} m_f a_{f,x} - F_{Gnd,x} \\ m_f(a_{f,y} - g) - F_{Gnd,y} \\ m_f a_{f,z} - F_{Gnd,z} \end{bmatrix} \tag{43}$$

$$[I]_f \vec{\alpha}_f = \begin{bmatrix} I_{xx,f} & 0 & 0 \\ 0 & I_{yy,f} & 0 \\ 0 & 0 & I_{zz,f} \end{bmatrix} \begin{bmatrix} \alpha_{f,x} \\ \alpha_{f,y} \\ \alpha_{f,z} \end{bmatrix} = I_{xx,f}\alpha_{f,x}\hat{x} + I_{yy,f}\alpha_{f,y}\hat{y} + I_{zz,f}\alpha_{f,z}\hat{z} \tag{44}$$

$$[(\vec{r}_{Gnd}-\vec{r}_{f_{com}})\times\vec{F}_{Gnd}) = \begin{bmatrix} r_{Gnd,x}-r_{f_{com},x} \\ r_{Gnd,y}-r_{f_{com},y} \\ r_{Gnd,z}-r_{f_{com},z} \end{bmatrix} \times \begin{bmatrix} F_{Gnd,x} \\ F_{Gnd,y} \\ F_{Gnd,z} \end{bmatrix} \tag{45}$$

We now substitute equations (43), (44), and (45) into (42). The ankle flexion moment in the sagittal plane (z-direction) is therefore,

$$M_A|_z = I_f\alpha_f + r_{f_{com}}m_f[e_{x_f}(a_{f,y}-g) - e_{y_f}a_{f,x}] + r_{Gnd}[-e_{x_f}F_{Gnd,y} + e_{y_f}F_{Gnd,x} \tag{46}$$

Where,

$$e_{x_f} = sin(\theta_{AF}) \text{ is the component of } r_{f_{com}} \text{ in the x-direction}$$
$$e_{y_f} = -cos(\theta_{AF}) \text{ is the component of } r_{f_{com}} \text{ in the y-direction}$$

with θ_{AF} being the angle from the vertical as shown in Figure 51. Further, we made the following notational simplifications:

$$I_f = I_{zz,f}$$
$$\alpha_f = \alpha_{z,f}$$

Since the linear acceleration of the foot segment at its center-of-mass (com) is a function of the com location and not determined directly from measurements, we write this term in terms of the linear acceleration of the ankle, which is known from measurements:

$$\begin{aligned} a_{f,x} &= a_{ankle,x} - r_{f_{com}}e_{y_f}\alpha_f \\ a_{f,y} &= a_{ankle,y} + r_{f_{com}}e_{x_f}\alpha_f \end{aligned} \tag{47}$$

The equation for 2D ankle flexion moment then becomes,

$$\begin{aligned} M_A|_z = {} & I_f\alpha_f - m_f g r_{f_{com}}e_{x_f} - r_{Gnd}[e_{x_f}F_{Gnd,y} - e_{y_f}F_{Gnd,x}] + \alpha_f m_f r^2_{f_{com}} + \\ & r_{f_{com}}m_f[e_{x_f}a_{ankle,y} - e_{y_f}a_{ankle,x}] \end{aligned} \tag{19}$$

2D Knee Flexion Moment

From earlier, the 3D knee flexion moment equation was determined to be,

$$\vec{M}_k = \vec{M}_A + [I]_{ll}\vec{\alpha}_{ll} + (\vec{r}_{ll_{com}} \times \vec{F}_k) + [(\vec{L}_{ll} - \vec{r}_{ll_{com}} \times \vec{F}_A] \tag{35}$$

As with the 2D ankle flexion moment derivation, we first evaluate the cross and dot products and simplify. We make similar notational similar notational simplifications and write linear acceleration of the lower leg center-of-mass in terms of linear acceleration of the knee. The resulting equation for 2D knee flexion moment then becomes,

$$\begin{aligned} M_k|_z = {} & M_A|_z + I_{ll}\alpha_{ll} + r_{ll_{com}} m_{ll}[e_{x_{ll}}(a_{knee,y} - g) - e_{y_{ll}} a_{knee,x}] + r_{ll_{com}}^2 m_{ll}\alpha_{ll} + \\ & m_f L_{ll}(e_{x_{ll}} a_{ankle,y} - e_{y_{ll}} a_{ankle,x} - g) + m_f r_{f_{com}} L_{ll}\alpha_f(e_{x_{ll}} e_{x_f} + e_{y_{ll}} e_{y_f}) + \\ & L_{ll}(-e_{x_{ll}} F_{Gnd,y} + e_{y_{ll}} F_{Gnd,x}) \end{aligned} \tag{20}$$

2D Hip Flexion Moment

We derive the 2D hip flexion moment using the same method as with 2D ankle and knee flexion moments. This equation becomes,

$$\begin{aligned} M_h|_z = {} & M_k|_z + I_{ul}\alpha_{ul} + r_{ul} m_{ul}[e_{x_{ul}}(a_{p,y} - g) - e_{y_{ul}} a_{p,x}] + r_{ul}^2 m_{ul}\alpha_{ul} + \\ & m_{ll} L_{ul}[e_{x_{ul}}(a_{knee,y} - g) - e_{y_{ul}} a_{knee,x}] + m_f L_{ul}[e_{x_{ul}}(a_{ankle,y} - g) - e_{y_{ul}} a_{knee,x}] + \\ & m_{ll} r_{ll} L_{ul}\alpha_{ll}[e_{x_{ul}} e_{x_{ll}} + e_{y_{ul}} e_{y_{ll}}] + m_f r_f L_{ul}\alpha_f[e_{x_{ul}} e_{x_f} + e_{y_{ul}} e_{y_f}] + \\ & L_{ul}[-e_{x_{ul}} F_{Gnd,y} + e_{y_{ul}} F_{Gnd,x}] \end{aligned} \tag{21}$$

Appendix E: MATLAB script for 2D Dynamics analysis

```
%This m-file analyzes uncertainties in joint moments caused by
%uncertainties in body segment inertial parameters
%By JunJay Tan

clear

%Load .mat data file
load gait_data

%constants
m = 72.6;   %mass of test subject in kg
g = -9.81;

%mean parameters
m_f = 1;
com_f = 0.011;
Izz_f = 0.0043;
m_ll = 3.32;
com_ll = 0.1778;    %use positive values, since sin/cos already takes
care of direction
Izz_ll = 0.0473;
m_ul = 8.709;
com_ul = 0.192;
Izz_ul = 0.18;

%longitudinal length of segments in m
L_ll = 0.425;
L_ul = 0.4691;

%initializing vectors
dM_ankle = []; %ankle joint moment uncertainty
dM_knee =[];
dM_hip = [];
dM_ankle_norm = [];
dM_knee_norm = [];
dM_hip_norm = [];

%User defined parameters
dm_f = 0.202;   %foot mass uncertainty
dm_ll = 0.343;   %shank mass uncertainty
dm_ul = 2.07;   %thigh mass uncertainty

dcom_f = 0.011;
dcom_ll = 0.02;
dcom_ul = 0.017;

dIzz_f = 0.002;  %foot inertia uncertainty
dIzz_ll = 0.013;
dIzz_ul = 0.195;
```

```
%-------Description of vectors-----------------------
%   gait_cycle = % of gait cycle
%   ax_ankle = linear accel in x-dir of ankle in m/s^2
%   ay_ankle = linear accel in y-dir of ankle in m/s^2
%   ax_knee = linear accel in x-dir of knee in m/s^2
%   ay_knee = linear accel in y-dir of knee in m/s^2
%   ax_p = linear accel in x-dir of pelvis in m/s^2
%   ay_p = ...
%   alpha_f = angular accel of foot in rad/s^2, i.e., ankle ang accel
%   alpha_ll = angular accel of lower leg (shank) in rad/s^2, i.e.,
knee
%               ang accel
%   alpha_ul = ang accel of upper leg (thigh)in rad/s^2, i.e., hip
flexion
%               ang accel
%   theta_HF = hip flexion angle wrt vertical, starting from downward
pos
%               (in radians)
%   theta_KF = knee flexion angle wrt vertical (rad)
%   theta_AF = ankle flexion angle wrt vertical "       "
%   F_gndx = ground force on right foot in N, x-component
%   F_gndy = ground force on right foot in N, y (vertical) component
% Note: all vectors are wrt to world inertial frame
%-------------------------------------------------------

%conversion factors between radians and degrees
rad2deg=180/pi;
deg2rad=1/rad2deg;

%Calculate joint moment uncertainties

%Calculate ANKLE MOMENT uncertainty
dM_ankle = abs([alpha_f])*dIzz_f + abs([-m_f*g*sin(theta_AF) +
2*alpha_f*m_f*com_f + m_f*(sin(theta_AF).*ay_ankle - (-
cos(theta_AF).*ax_ankle))])*dcom_f...
            + abs([alpha_f*com_f^2 + com_f*(sin(theta_AF).*ay_ankle +
cos(theta_AF).*ax_ankle)])*dm_f;



%Calculate KNEE MOMENT UNCERTAINTY
dM_knee = dM_ankle + abs(alpha_ll)*dIzz_ll +...
          abs([m_ll*(sin(theta_KF).*(ay_knee-g) +
cos(theta_KF).*ax_knee) + 2*com_ll*m_ll*alpha_ll])*dcom_ll +...
          abs([com_ll*(sin(theta_KF).*(ay_knee-g) +
cos(theta_KF).*ax_knee) + com_ll^2*alpha_ll])*dm_ll + ...
          abs([L_ll*(sin(theta_KF).*ay_ankle + cos(theta_KF).*ax_ankle
- g) + com_f*L_ll*alpha_f.*(sin(theta_KF).*sin(theta_AF) + ...
          cos(theta_KF).*cos(theta_AF))])*dm_f + ...
          abs([m_f*L_ll*alpha_f.*(sin(theta_KF).*sin(theta_AF) +
cos(theta_KF).*cos(theta_AF))])*dcom_f;


%Calculate HIP MOMENT UNCERTAINTY
dM_hip = dM_knee + abs(alpha_ul)*dIzz_ul +...
```

```
        abs([m_ul*[sin(theta_HF).*(ay_p-g)+ cos(theta_HF).*ax_p] +
2*com_ul*m_ul*alpha_ul])*dcom_ul +...
        abs([com_ul*[sin(theta_HF).*(ay_p-g) + cos(theta_HF).*ax_p] +
com_ul^2*alpha_ul])*dm_ul + ...
        abs([m_ll*L_ul*alpha_ll.*(sin(theta_HF).*sin(theta_KF) +
cos(theta_HF).*cos(theta_KF))])*dcom_ll + ...
        abs([L_ul*[sin(theta_HF).*(ay_knee-g) + cos(theta_HF).*ax_knee]
+
com_ll*L_ul*alpha_ll.*(sin(theta_HF).*sin(theta_KF)+cos(theta_HF).*cos(
theta_KF))])*dm_ll +...
        abs([m_f*L_ul*alpha_f.*[sin(theta_HF).*sin(theta_AF) +
cos(theta_HF).*cos(theta_AF)]])*dcom_f + ...
        abs([L_ul*(sin(theta_HF).*(ay_ankle-g) +
cos(theta_HF).*ax_ankle) +
com_f*L_ul*alpha_f.*[sin(theta_HF).*sin(theta_AF)+cos(theta_HF).*cos(th
eta_AF)]])*dm_f;

%normalize moments by body weight
dM_ankle_norm = dM_ankle/m;
dM_knee_norm = dM_knee/m;
dM_hip_norm = dM_hip/m;

figure, plot(gait_cycle,abs(dM_ankle_norm)), title('normalized ankle
flex moment'),xlabel('% gait cycle'),ylabel('N-m/kg')
figure, plot(gait_cycle,abs(dM_knee_norm)), title('normalized knee flex
moment'),xlabel('% gait cycle'),ylabel('N-m/kg')
figure, plot(gait_cycle,abs(dM_hip_norm)), title('normalized hip flex
moment'),xlabel('% gait cycle'),ylabel('N-m/kg')
```

References

Abelson, R. (2004, 13 Mar.). An m.R.I. Machine for every doctor? Someone has to pay. *The New York Times*.

Aetna. (2008, 30 May 2008). Clinical policy bulletin: Gait analysis and electrocardiogram. Retrieved 1 Aug., 2008, from http://www.aetna.com/cpb/medical/data/200_299/0263.html

Anderson, F. C., Arnold, A. S., Pandy, M. G., Goldberg, S. R., & Delp, S. L. (2006). Simulation of walking. In *Human walking* (3rd ed.): Williams and Wilkins.

Anderson, F. C., Guendelman, E., Habib, A., Hamner, S., Holzbaur, K., John, C. T., et al. (2008). *Opensim user's guide*. Palo Alto: Stanford University.

Anderson, F. C., & Pandy, M. (2001). Dynamic optimization of human walking. *Journal of Biomechanical Engineering, 123*, 381-390.

Andrews, J. G., & Mish, S. P. (1996). Methods for investigating the sensitivity of joint resultants to body segment parameter variations. *Journal of Biomechanics, 29*(5), 651-654.

Appleby, J. (2008). The case of ct angiography: How americans view and embrace new technology. *Health Affairs, 27*(6), 1515-1521.

Arnold, A. S., Thelen, D. G., Schwartz, M. H., Anderson, F. C., & Delp, S. L. (2007). Muscular coordination of knee motion during the terminal-swing phase of normal gait. *Journal of Biomechanics, 40*, 3314-3324.

Ashruf, C. M. A. (2002). Thin flexible pressure sensors. *Sensor Review, 22*, 322-327.

Baker, R. (2006). Gait analysis methods in rehabilitation. *Journal of NeuroEngineering and Rehabilitation*.

Berenson, A., & Abelson, R. (2008, 29 Jun). Weighing the costs of a ct scan's look inside the heart. *The New York Times*.

Blue Cross & Blue Shield of Mississippi. (2008, 2008). Medical policy search: Gait (motion) analysis. Retrieved 1 Aug., 2008, from http://www.bcbsms.com/index.php?id=200&action=viewPolicy&path=/policy/emed/Gait_Analysis.html

Bonato, P. (2005). Advances in wearable technology and applications in physical medicine and rehabilitation. *Journal of NeuroEngineering and Rehabilitation, 2*(2).

Bonato, P. (2009). Phone conversation (Motion Analysis Lab, Spaulding Rehabilitation Hospital ed.). Boston.

Brenner, D. J., & Hall, E. J. (2007). Computed tomography-- an increasing source of radiation exposure. *The New England Journal of Medicine, 357*(22), 2277-2284.

Challis, J. H., & Kerwin, D. G. (1996). Quantification of the uncertainties in resultant joint moments computed in a dynamic activity. *Journal of Sports Sciences, 14*(3), 219-231.

Chandler, R. F., Clauser, C. E., McConville, J. T., Reynolds, H. M., & Young, J. W. (1975). *Investigation of inertial properties of the human body*. Ohio: Aerospace Medical Research Laboratory, Wright-Patterson Air Force Base, U.S. Air Force.

Cheng, H., Obergefell, L., & Rizer, A. (1994). *Generator of body data (gebod) manual*. Ohio: Armstrong Laboratory, Wright-Patterson Air Force Base, U.S. Air Force.

Clauser, C. E., McConville, J. T., & Young, J. W. (1969). *Weight, volume, and center of mass of segments of the human body*. Ohio: Aerospace Medical Research Laboratory, Aerospace Medical Division, Wright-Patterson Air Force Base.

Coyne, K. E. (2009). Mri: A guided tour. Retrieved 31 Dec, 2008, from http://www.magnet.fsu.edu/education/tutorials/magnetacademy/mri/fullarticle.html

de Leva, P. (1996). Adjustments to zatsiorsky-seluyanov's segment inertia parameters. *Journal of Biomechanics, 29*(9), 1223-1230.

Delp, S. L., Anderson, F. C., Arnold, A. S., Loan, P., Habib, A., John, C. T., et al. (2007). Opensim: Open-source software to create and analyze dynamic simulations of movement. *IEEE Transactions on Biomedical Engineering, 54*(11), 1940-1950.

Dempster, W. T. (1955). *Space requirements of the seated operator*. Ohio: Aero Medical Laboratory, Wright Air Development Center, Wright-Patterson Air Force Base, U.S. Air Force.

Dolmatch, B. L. (2005, July). The history of ct angiography. *Endovascular Today*, 23-30.

Dumas, R., Cheze, L., & Verriest, J.-P. (2007). Adjustments to mcconville et al. And young et al. Body segment inertial parameters. *Journal of Biomechanics, 40*, 543-553.

Eddy, D. M. (2005). Evidence-based medicine: A unified approach. *Health Affairs, 24*(1), 9-17.

Edginton, K. A., Guler, H. C., Ober, J. J., & Berme, N. (2007). *Instrumented treadmills: Reducing the need for gait labs*: Bertec Corporation.

Finch, L. (2001, Dec/Jan). Gait analysis comes out ahead. *Rehab Management*.

Fung, Y. C. (1993). *Biomechanics: Mechanical properties of living tissues* (Second ed.). New York: Springer-Verlag.

Gait & Clinical Movement Analysis Society. (2008, 2008). Research committee. Retrieved 28 Dec., 2008, from http://www.gcmas.org/research_committee

Ganley, K. J., & Powers, C. M. (2004). Determination of lower extremity anthropometric parameters using dual energy x-ray absorptiometry: The influence on net joint moements during gait. *Clinical Biomechanics, 19*, 50-56.

Gazelle, G. S., McMahon, P. M., Siebert, U., & Bienfeld, M. T. (2005). Cost-effective analysis in the assessment of diagnostic imaging technologies. *Radiology, 235*, 361-370.

Gleicher, M. (1999, 3/3/1999). Cs838 - topics in computer animation. Retrieved 2 Jan., 2009, from http://www.cs.wisc.edu/graphics/Courses/cs-838-1999/Jeff/MoCapTOC.html

Herzog, W., Guimaraes, A. C. S., & Zhang, Y. T. (1999). Measuring techniques. In B. M. Nigg & W. Herzog (Eds.), *Biomechanics of the musculoskeletal system* (second ed., pp. 245-422). New York: John Wiley & Sons.

Hillman, B. J. (1986). Government health policy and the diffusion of new medical devices. *Health Services Research, 21*(5), 681-711.

Iezzoni, L. I. (2003). *When walking fails: Mobility problems of adults with chronic conditions*. Berkeley: University of California Press.

Iezzoni, L. I., & O'Day, B. (2005). *More than ramps: A guide to improving health care quality and access for people with disabilities*. Oxford: Oxford University Press.

Iezzoni, L. I., & O'Day, B. L. (2006). *More than ramps: A guide to improving health care quality and access for people with disabilities*. Oxford: Oxford University Press.
Inman, V. T., Ralston, H. J., & Todd, F. (1981). *Human walking*. Baltimore: Williams & Wilkins.
John, C. T., Anderson, F. C., Guendelman, E., Higginson, J. S., & Delp, S. L. (2007). Long-duration muscle actuated simulations of walking at multiple speeds, *American Society of Biomechanics Conference*. Stanford University, Palo Alto, CA.
Joyce, K. A. (2008). *Magnetic appeal*. Ithaca: Cornell University Press.
Kingma, I., Toussaint, H. M., De Looze, M. P., & Van Dieen, J. H. (1996). Segment inertial parameter evaluation in two anthropometric models by application of a dynamic linked segment model. *Journal of Biomechanics, 29*(5), 693-704.
Kitagawa, M., & Windsor, B. (2008). *Mocap for artists: Workflow and techniques for motion capture*. Burlington, MA: Focal Press/Elsevier.
Kowalczyk, L. (2004, 28 Sep.). Rush for medical scans raises concerns on cost. *The Boston Globe*.
Lewis, F. L., Abdallah, C. T., & Dawson, D. M. (1993). *Control of robot manipulators*. New York: Macmillan.
Mallet, R. L. (1998). Why standards matter. *Issues in Science and Technology, 15*.
McConville, J. T., Churchill, T. D., Kaleps, I., Clauser, C. E., & Cuzzi, J. (1980). *Anthropometric relationships of body and body segment moments of inertia*. Ohio: Air Force Aerospace Medical Research Laboratory, Wright-Patterson Air Force Base, U.S. Air Force.
McMahon, T. A. (1984). *Muscles, reflexes, and locomotion*. Princeton: Princeton University Press.
Motion Lab Systems. (2008). *The c3d file format users guide*. Baton Rouge: Motion Lab Systems, Inc.
Neptune, R. R., Kautz, S. A., & Zajac, F. E. (2001). Contributions of the individual ankle plantar flexors to support, forward progression and swing initiation during walking. *Journal of Biomechanics, 34*, 1387-1398.
Neuromuscular Biomechanics Lab. (2008). Facilities and equipment. Retrieved 30 July 2008, from http://research.me.udel.edu/higginson/facilitiesequipment.html
Nguyen, T. C., Baker, R., & Pandy, M. (2007). Effect of the variability in segment inertial parameters on joint moment using monte carlo simulation. *Journal of Biomechanics, 40*(Supplement 2), S348.
Olson, E. (2008). High-tech devices keep elderly safe from afar. *The New York Times*.
Pearsall, D. J., & Costigan, P. A. (1999). The effect of segment parameter error on gait analysis results. *Gait and Posture, 9*, 173-183.
Pearson, S. D., Knudsen, A. B., Scherer, R. W., Weissberg, J., & Gazelle, G. S. (2008). Assessing the comparative effectiveness of a diagnostic technology: Ct colonography. *Health Affairs, 27*(6), 1503-1514.
Pianykh, O. S. (2008). *Digital imaging and communications in medicine (dicom): A practical introduction and survival guide*. Berlin: Springer.
Piazza, S. J. (2006). Muscle-driven forward dynamic simulations for the study of normal and pathological gait. *Journal of NeuroEngineering and Rehabilitation, 3*(5).

Rao, G., Amarantini, D., Berton, E., & Favier, D. (2006). Influence of body segments' parameters estimation models on inverse dynamics solutions during gait. *Journal of Biomechanics, 39*(8), 1531-1536.
Redberg, R. F. (2007). Evidence, appropriateness, and technology assessment in cardiology: A case study of computed tomography. *Health Affairs, 26*(1), 86-95.
Reinbolt, J. A., Haftka, R. T., Chmielewski, T. L., & Fregly, B. J. (2007). Are patient-specific joint and inertial parameters necessary for accurate inverse dynamics *IEEE Transactions on Biomedical Engineering, 54*(5), 782-793.
Riemer, R., Hsiao-Wecksler, E. T., & Zhang, X. (2008). Uncertainties in inverse dynamics solutions: A comprehensive analysis and an application to gait. *Gait & Posture, 27*, 578-588.
Roan, S. (2007, 1 Jan. 2007). Ok, let's take a closer look at that stride. *The Los Angeles Times*.
Ruiz, K. (2002). Experimental motion capture systems development. Retrieved 7 Jan., 2009, from http://www.rpi.edu/~ruiz/research/research2/krmkmocap.htm
Sackett, D. L. (1996). Evidence based medicine: What it is and what it isn't. *BMJ, 312*, 71-72.
Shapiro, C. (2001). Setting compatibility standards: Cooperation or collusion? In R. Dreyfuss (Ed.), *Expanding the boundaries of intellectual property: Innovation policy for the knowledge society*. Oxford: Oxford University Press.
Silva, M. P. T., & Ambrosio, J. A. C. (2004). Sensitivity of the results produced by the inverse dynamic analysis of a human stride to perturbed input data. *Gait & Posture, 19*, 35-49.
Simon, S. R. (2004). Quantification of human motion: Gait analysis--benefits and limitations to its application to clinical problems. *Journal of Biomechanics, 37*, 1869-1880.
Stanford School of Medicine Human Performance Lab. (2008). 2d and 3d motion analysis. Retrieved 28 Jul. 2008, 2008, from http://humanperformance.stanford.edu/PDFs/2D_and_3D_Motion_Analysis.pdf
Sutherland, D. H. (2001). The evolution of clinical gait analysis part 1: Kinesiological emg. *Gait and Posture, 24*, 61-70.
Sutherland, D. H. (2002). The evoution of clinical gait analysis part ii kinematics. *Gait and Posture, 16*, 159-179.
Sutherland, D. H. (2005). The evolution of clinical gait anaysis part iii -- kinetics and energy assessment. *Gait & Posture, 21*, 447-461.
Thelen, D. G., & Anderson, F. C. (2006). Using computed muscle control to generate forward dynamic simulations of human walking from experimental data. *Journal of Biomechanics, 39*, 1107-1115.
U.S. Food and Drug Administration. (2006). Premarket notification 510(k). Retrieved 15 Jul., 2008, from http://www.fda.gov/cdrh/devadvice/314.html
U.S. Food and Drug Administration. (2009, 1/6/09). Product classification database. Retrieved 10 Jan., 2009, from http://www.accessdata.fda.gov/scripts/cdrh/cfdocs/cfpcd/classification.cfm
Vlasic, D., Adelsberger, R., Vannucci, G., Barnwell, J., Gross, M., Matusik, W., et al. (2007). Practical motion capture in everyday surroundings. *ACM Transactions on Graphics, 26*(3).

Whittle, M. (1996). Clinical gait analysis: A review. *Human Movement Science, 15*, 369-387.

Whittle, M. (2002). *Gait analysis: An introduction*. Philadelphia: Elsevier Health Sciences.

Winter, D. A. (2005). *Biomechanics and motor control of human movement* (Third ed.). Hoboken: John Wiley & Sons.

Yin, R. K. (2003). *Case study research: Design and methods* (Vol. 5). Thousand Oaks: SAGE.

Zatsiorsky, V., & Seluyanov, V. (1983). The mass and inertia characteristics of the main segments of the human body. In H. Matsui & K. Kobayashi (Eds.), *Biomechanics viii-b*. Illinois: Human Kinetic.